INDC(JPN)-162/U

NOT FOR PUBLICATION

PROGRESS REPORT

(July 1991 to June 1992 inclusive)

August 1992

Editor

S. Kikuchi

Japanese Nuclear Data Committee

Japan Atomic Energy Research Institute
Tokai Research Establishment
Tokai-mura, Ibaraki-ken, Japan

Editor's Note

This is a collection of reports which have been submitted to the Japanese Nuclear Data Committee at the committee's request. The request was addressed to the following individuals who might represent or be in touch with groups doing researches related to the nuclear data of interest to the development of the nuclear energy program.

Although the editor tried not to miss any appropriate addressees, there may have been some oversight. Meanwhile, contribution of a report rested with discretion of its author. The coverage of this document, therefore, may not be uniform over the related field or research.

In this progress report, each individual report is generally reproduced as it was received by the JNDC secretariat, and editor also let pass some simple obvious errors in the manuscripts if any.

This edition covers a period of July 1, 1991 to June 30, 1992. The information herein contained is of a nature of "Private Communication". Data contained in this report should not be quoted without the author's permission.

Table of Contents

ELEMENT S	A	QUANTITY	ENERGY MIN	MAX	LAB	TYPE	DOCUMENTATION REF VOL PAGE	DATE	COMMENTS
H	2	(N,GAMMA)	1.0+4	9.0+4	TIT	EXPT-PROG	INDC(JPN)162/U	AUG 92	IGASHIRA+.P143,NDG
LI	7	(N,GAMMA)	1.0+4	8.0+4	TIT	EXPT-PROG	INDC(JPN)162/U	AUG 92	IGASHIRA+.P143,PARTIAL CAPT SIG,NGD
BE	9	(N,GAMMA)	1.0+4	9.0+4	TIT	EXPT-PROG	INDC(JPN)162/U	AUG 92	IGASHIRA+.P142,PARTIAL CAPT SIG,NGD
BE	9	RESON PARAMS	6.2+5		TIT	EXPT-PROG	INDC(JPN)162/U	AUG 92	KITAZAWA+.142,PARTIAL WG,CFD MDL CAL
C	13	(GAMMA,N)	2.0+7	7.0+7	TOH	EXPT-PROG	INDC(JPN)162/U	AUG 92	ITO+.P135,DIFF SIG,NDG
MG	24	RESON PARAMS	6.6+5		TIT	EXPT-PROG	INDC(JPN)162/U	AUG 92	KITAZAWA+.141,PARTIAL WG,CFD MDL CAL
SI	28	RESON PARAMS	1.8+5		TIT	EXPT-PROG	INDC(JPN)162/U	AUG 92	KITAZAWA+.141,PARTIAL WG,CFD MDL CAL
S	32	RESON PARAMS	1.0+5		TIT	EXPT-PROG	INDC(JPN)162/U	AUG 92	KITAZAWA+.141,PARTIAL WG,CFD MDL CAL
TI	48	(N,P)	9.1+6		JAE	EXPT-PROG	INDC(JPN)162/U	AUG 92	IKEDA+,P24,B11+H NEUT,ACT SIG IN TBL
V	51	(N,ALPHA)	9.1+6	1.1+7	JAE	EXPT-PROG	INDC(JPN)162/U	AUG 92	IKEDA+,P24,B11+H NEUT,ACT SIG IN TBL
FE		NONELA GAMMA		3.3+7	KTO	EXPT-PROG	INDC(JPN)162/U	AUG 92	TANABE+.P55,P+BE NEUT,DA/DE,SIG,FIGS
FE		N EMISSION	1.4+7		TOH	EXPT-PROG	INDC(JPN)162/U	AUG 92	BABA+.P125,DA/DE, NDG
FE		(N,ALPHA)	4.2+6	1.4+7	TOH	EXPT-PROG	INDC(JPN)162/U	AUG 92	BABA+.P128,DA/DE, NDG
FE	56	(N,P)	9.1+6	1.1+7	JAE	EXPT-PROG	INDC(JPN)162/U	AUG 92	IKEDA+,P24,B11+H NEUT,ACT SIG IN TBL
FE	56	(GAMMA,N)	2.0+7	7.0+7	TOH	EXPT-PROG	INDC(JPN)162/U	AUG 92	ITO+.P135,DIFF SIG,NDG
CO	59	(N,ALPHA)	9.1+6	1.1+7	JAE	EXPT-PROG	INDC(JPN)162/U	AUG 92	IKEDA+,P24,B11+H NEUT,ACT SIG IN TBL
NI		(N,ALPHA)	4.2+6	1.4+7	TOH	EXPT-PROG	INDC(JPN)162/U	AUG 92	BABA+.P128,DA/DE IN FIG
ZN	64	(N,P)	9.1+6	1.1+7	JAE	EXPT-PROG	INDC(JPN)162/U	AUG 92	IKEDA+,P24,B11+H NEUT,ACT SIG IN TBL
ZR	90	(N,P)	9.1+6	1.1+7	JAE	EXPT-PROG	INDC(JPN)162/U	AUG 92	IKEDA+,P24,B11+H N,ACT SIG(META),TBL
NB	93	DIFF INELAST	1.4+7	1.5+7	JAE	EXPT-PROG	INDC(JPN)162/U	AUG 92	IKEDA+,P16,ACT SIG IN TBL AND FIG

CONTENTS OF JAPANESE PROGRESS REPORT INDC(JPN) 162/U

ELEMENT S	A	QUANTITY	ENERGY MIN	MAX	LAB	TYPE	DOCUMENTATION REF VOL PAGE	DATE	COMMENTS
NB	93	(N,2N)	1.1+7		JAE	EXPT-PROG	INDC(JPN)162/U	AUG 92	IKEDA+,P24,B11+H N,ACT SIG(META),TBL
NB	93	N EMISSION	1.4+7	1.8+7	TOH	EXPT-PROG	INDC(JPN)162/U	AUG 92	BABA+.P125,DA/DE, NDG
NB	93	(N,ALPHA)	9.1+6	1.1+7	JAE	EXPT-PROG	INDC(JPN)162/U	AUG 92	IKEDA+,P24,B11+H N,ACT SIG(META),TBL
MO		N EMISSION	1.4+7		TOH	EXPT-PROG	INDC(JPN)162/U	AUG 92	BABA+.P125,DA/DE, NDG
TC	99	DIFF INELAST	1.4+7	1.5+7	JAE	EXPT-PROG	INDC(JPN)162/U	AUG 92	IKEDA+,P21,ACT SIG IN TBL
TC	99	(N,P)	1.4+7	1.5+7	JAE	EXPT-PROG	INDC(JPN)162/U	AUG 92	IKEDA+,P21,ACT SIG IN TBL
TC	99	(N,ALPHA)	1.4+7	1.5+7	JAE	EXPT-PROG	INDC(JPN)162/U	AUG 92	IKEDA+,P21,ACT SIG IN TBL
TC	99	(N,NA)	1.5+7		JAE	EXPT-PROG	INDC(JPN)162/U	AUG 92	IKEDA+,P21,ACT SIG IN TBL
RU	101	(N,P)	1.3+7	1.5+7	NAG	EXPT-PROG	INDC(JPN)162/U	AUG 92	KATOH+.P100,ACT SIG IN FIG
RU	102	(N,P)	1.3+7	1.5+7	NAG	EXPT-PROG	INDC(JPN)162/U	AUG 92	KATOH+.P100,ACT SIG TO ISOMER IN FIG
RU	102	(N,NP)	1.3+7	1.5+7	NAG	EXPT-PROG	INDC(JPN)162/U	AUG 92	KATOH+.P100,ACT SIG IN FIG
RU	104	(N,P)	1.3+7	1.5+7	NAG	EXPT-PROG	INDC(JPN)162/U	AUG 92	KATOH+.P100,ACT SIG IN FIG
RU	104	(N,ALPHA)	1.3+7	1.5+7	NAG	EXPT-PROG	INDC(JPN)162/U	AUG 92	KATOH+.P100,ACT SIG IN FIG
PD	104	(N,P)	1.3+7	1.5+7	NAG	EXPT-PROG	INDC(JPN)162/U	AUG 92	KATOH+.P100,ACT SIG TO ISOMER IN FIG
PD	105	(N,P)	1.3+7	1.5+7	NAG	EXPT-PROG	INDC(JPN)162/U	AUG 92	KATOH+.P100,ACT SIG TO ISOMER IN FIG
PD	105	(N,NP)	1.3+7	1.5+7	NAG	EXPT-PROG	INDC(JPN)162/U	AUG 92	KATOH+.P100,ACT SIG TO ISOMER IN FIG
PD	106	(N,NP)	1.3+7	1.5+7	NAG	EXPT-PROG	INDC(JPN)162/U	AUG 92	KATOH+.P100,ACT SIG TO ISOMER IN FIG
PD	108	(N,2N)	1.3+7	1.5+7	NAG	EXPT-PROG	INDC(JPN)162/U	AUG 92	KATOH+.P100,ACT SIG TO ISOMER IN FIG
PD	108	(N,P)	1.3+7	1.5+7	NAG	EXPT-PROG	INDC(JPN)162/U	AUG 92	KATOH+.P100,ACT SIG IN FIG
PD	108	(N,NP)	1.3+7	1.5+7	NAG	EXPT-PROG	INDC(JPN)162/U	AUG 92	KATOH+.P100,ACT SIG IN FIG

ELEMENT S A	QUANTITY	ENERGY MIN	MAX	LAB	TYPE	DOCUMENTATION REF VOL PAGE	DATE	COMMENTS
CD 112	(N,ALPHA)	1.3+7	1.5+7	NAG	EXPT-PROG	INDC(JPN)162/U	AUG 92	KATOH+.P100,ACT SIG TO ISOMER IN FIG
CD 116	(N,P)	1.3+7	1.5+7	NAG	EXPT-PROG	INDC(JPN)162/U	AUG 92	KATOH+.P100,ACT SIG IN FIG
SN 119	(N,P)	1.3+7	1.5+7	NAG	EXPT-PROG	INDC(JPN)162/U	AUG 92	KATOH+.P100,ACT SIG TO GND/META,FIGS
SN 120	(N,P)	1.3+7	1.5+7	NAG	EXPT-PROG	INDC(JPN)162/U	AUG 92	KATOH+.P100,ACT SIG TO ISOMER IN FIG
TA 181	N EMISSION	1.4+7		TOH	EXPT-PROG	INDC(JPN)162/U	AUG 92	BABA+.P125,DA/DE, NDG
AU 197	(N,2N)	9.1+6	1.1+7	JAE	EXPT-PROG	INDC(JPN)162/U	AUG 92	IKEDA+,P24,B11+H NEUT,ACT SIG IN TBL
PB 208	EVALUATION	2.0+7	1.0+9	JAE	EVAL-PROG	INDC(JPN)162/U	AUG 92	FUKAHORI.P37,CALC. WITH ALICE-F,NDG
BI 209	EVALUATION	2.0+7	1.0+9	JAE	EVAL-PROG	INDC(JPN)162/U	AUG 92	FUKAHORI.P37,CALC. WITH ALICE-F,NDG
BI 209	N EMISSION	1.4+7	1.8+7	TOH	EXPT-PROG	INDC(JPN)162/U	AUG 92	BABA+.P125,DA/DE, NDG
BI 209	(GAMMA,N)		1.0+8	JPN	EVAL-PROG	INDC(JPN)162/U	AUG 92	IGARASI.P109,GDR+QUASI-D MDL,FIG
NP 237	FISSION	3.0+0	1.0+4	KTO	EXPT-PROG	INDC(JPN)162/U	AUG 92	KIMURA+.P53,LINAC,PB-SPECTMETER,FIG
PU 239	TOTAL	1.0+3	5.0+5	JAE	EVAL-PROG	INDC(JPN)162/U	AUG 92	DERRIEN.P34,PUBLISHED IN NST,29
PU 239	TOTAL	1.0+3	2.5+3	JAE	EVAL-PROG	INDC(JPN)162/U	AUG 92	DERRIEN.P30,R-M ANAL,AV SIG IN TBL
PU 239	(N,GAMMA)	1.0+3	2.5+3	JAE	EVAL-PROG	INDC(JPN)162/U	AUG 92	DERRIEN.P30,R-M ANAL,AV SIG IN TBL
PU 239	FISSION	1.0-2	2.5+3	JAE	EVAL-PROG	INDC(JPN)162/U	AUG 92	DERRIEN.P30,R-M ANAL,AV SIG IN TBL
PU 239	RESON PARAMS		2.5+3	JAE	EVAL-PROG	INDC(JPN)162/U	AUG 92	DERRIEN.P30,REICH-MOORE ANAL,NDG
MANY	EVALUATION	1.0-5	2.0+7	JAE	EVAL-PROG	INDC(JPN)162/U	AUG 92	KAWAI+,P39,172 FP,PUBL IN NST,29,195
MANY	EVALUATION	NDG		KNK	EVAL-PROG	INDC(JPN)162/U	AUG 92	OHSAWA+.P47,FOR TH CYCLE,NDG
MANY	SCATTERING	NDG		JAE	REVW-PROG	INDC(JPN)162/U	AUG 92	CHIBA+.P42,OPTMDL ANAL FOR FP,NDG
MANY	N EMISSION	1.4+7		JAE	EVAL-PROG	INDC(JPN)162/U	AUG 92	YU+.P38,DA/DE FOR JENDL FUSION FILE

CONTENTS OF JAPANESE PROGRESS REPORT INDC(JPN) 162/U

ELEMENT S A	QUANTITY	ENERGY MIN	ENERGY MAX	LAB	TYPE	DOCUMENTATION REF VOL PAGE	DATE	COMMENTS
MANY	N EMISSION	1.4+7		JAE	EVAL-PROG	INDC(JPN)162/U	AUG 92	CHIBA+.P38,FOR JENDL FUSION FILE,NDG
MANY	N EMISSION	1.4+7		JAE	EVAL-PROG	INDC(JPN)162/U	AUG 92	CHIBA+.P40,FOR JENDL FUSION FILE,NDG
MANY	N EMISSION	4.2+6	1.8+7	JAE	REVW-PROG	INDC(JPN)162/U	AUG 92	FUKAHORI+.P37,DA/DE,JENDL-3 CFD OTHS
MANY	SPECT FISS N	NDG		KNK	REVW-PROG	INDC(JPN)162/U	AUG 92	OHSAWA.P48,REVIEW OF RECENT THEORIES

The content table in the CINDA format was compiled by the JNDC CINDA group: S. Chiba (JAERI), M. Kawai (Toshiba), H. Kitazawa (Tokyo Inst. of Tech.), T. Nakagawa (JAERI), R. Nakasima (Hosei Univ.), M. Sakamoto (JAERI).

I. Electrotechnical Laboratory

A. Quantum Radiation Division

I-A-1

The Effect of Secondary Neutrons on Energy Distribution of Reference 2.413MeV and 14.00MeV Neutron Fields

K. Kudo, N. Takeda, X. Yang*, Matiullah** and A. Fukuda

Monoenergetic neutrons play very important roles for accurate determination of reaction cross sections and precise calibration of neutron spectrometers. But it sometimes happens that neutron energies differ in some cases by amounts which are several times the uncertainties quoted for the energy determinations. Such errors in neutron energy result from uncertainties in the energy of the bombarding charged particles incident on the neutron producing target and in the properties of the target. Adding to the preciseness of neutron energy, much narrower width of energy is highly required to improve the quality of these measuremnets. In our earlier papers, we reported techniques for production of the reference monoenergetic neutrons of 2.413MeV using a $D(d,n)^3He$ reaction and 14.00MeV using a $T(d,n)^4He$ reaction respectively. Therein, it was concluded that these neutrons emitted at a chosen angle of 100 deg. or 96 deg. for each reaction to the direction of incident deuteron beam have energy of 2.413MeV or 14.00MeV with very narrow width of energy respectively, regardless of the target thickness, its irradiation history and the deuteron energy incident on the target[1),2)]. Furthermore, an attempt was made to investigate the angular straggling effect of the incident deuterons in a Ti−D target on the emitted neutron energy distribution at the reference angle of 100 deg. The results indicated the angular straggling of deuterons in a target material is inevitable for the energy spread of the emitted neutrons. However, this energy spread does not significantly affect the actual energy calibration for existed neutron spectrometers like ^3He ion chambers and proportional counters, which have energy resolution better than 3%.

The another inevitable problem on the energy reference field is the contamination of unwanted secondary neutrons produced in a target assembly and in surroundings of an experimental room. The contribution of the room scattered neutrons can be estimated experimentally by using a inverse−square law technique. On the other hand,

* Present Address: China Institute of Atomic Energy, Beijing, P.R. of China
**Present Address: Center for Nuclear Studies, Islamabad, Pakistan

the secondary neutrons from the target assembly can not be separated from the primary neutrons from the source, even if the inverse-square law technique is adopted.

It would be very informative to determine the quantity of secondary neutrons contaminated in the reference field. The effect of this secondary neutrons on the distribution of the neutrons emitted at the special angle can be calculated by three dimensional MCNP (Monte Carlo Neutron and Photon Transport Code) computer code[3]. Figure 1 shows a schematic diagram of our target assembly including an associated particle counting system which was used in the calculations of the MCNP code. It consists of a neutron producing target (a copper backing of diameter 36.8mm and thickness 0.25mm) and aluminum pipes of thickness 0.5mm. The MCNP code is a general-purpose, continuous-energy, generalized-geometry and coupled neutron-photon Monte Carlo code system, and therefore it can treat an arbitrary three-dimensional configuration of the target assembly. The angular distribution of primary neutrons produced by the $D(d,n)^3He$ reaction or the $T(d,n)^4He$ reaction was taken from Liskien's data[4] under the conditions that 130keV deuterons induce the neutron producing reaction. The neutron spectra were calculated based on the differential elastic, inelastic and other reaction cross sections given in ENDF/B-IV[5].

Figure 2 shows MCNP code calculated spectrum in terms of fluences per energy in MeV per source neutron as a function of neutron energy at a distance of 50 cm from the point source of primary neutrons which have an energy distribution depending on the emission angle. The secondary neutrons from the target assembly have a continuous and smooth energy spectrum below 2.9MeV. The energy component higher than the primary neutrons of 2.413MeV results from the scattering of the higher energy neutrons originally emitted at smaller angles and interacted with the copper backing and the aluminum wall. The total yields of secondary neutrons compared to the primary neutrons are summarized in Table 1. The contribution of secondary neutrons in the energy range of (2.413 ± 0.05)MeV was about 0.6% from the table.

The energy spectrum at 14.00MeV reference field was similarly calculated by using the MCNP code under the similar computational conditions described above. The results are shown in Fig.3 and also summarized in Table 1.

To summarize, in the foregoing, we have described our work concerning the effect of secondary neutrons produced in the target assembly on the reference energy field, by using the MCNP Monte Carlo code. The results show that the secondary neutrons do not affect the energy spread of the reference energy, although such a backward angle as 100 deg. or 96 deg. is used as the reference energy field. These reference fields would mainly be used for the calibration of precise neutron spectrometers which are used especially in fusion diagnostics concerning the DD and DT plasma.

References:
1)K.Kudo and T.Kinoshita, Nucl. Eng. & Design/Fusion 10,145(1989).
2)K.Kudo, N.Takeda, Matiullah and A.Fukuda, Proc. on Nucl. Data for Sci. & Eng., held in Jülich, FRG(1991).
3)Documentation for CCC-200/MCNP Code Package, ORNL, CCC-200(1983).
4)H.Liskien and A.Paulsen, Nucl. Data Table, 11, 569(1973).
5)Evaluated Nuclear Data File ENDF/B-IV, BNL, Upton, New York(1973).

Table 1 Contribution of secondary neutrons in the energy range of $E_n \pm \Delta E_n$ produced in a target assembly respect to the primary neutrons of E_n

ratio of secondary neutrons to the primary neutrons			
$2.413MeV \pm \Delta E_n$		$14.00MeV \pm \Delta E_n$	
ΔE_n=0.05MeV	0.6%	ΔE_n=0.1MeV	0.3%
ΔE_n=0.1 MeV	0.8%	ΔE_n=0.2MeV	0.5%
ΔE_n=0.2 MeV	2.5%	ΔE_n=0.3MeV	0.6%
ΔE_n=0.3MeV	4.6%	ΔE_n=0.5MeV	0.8%

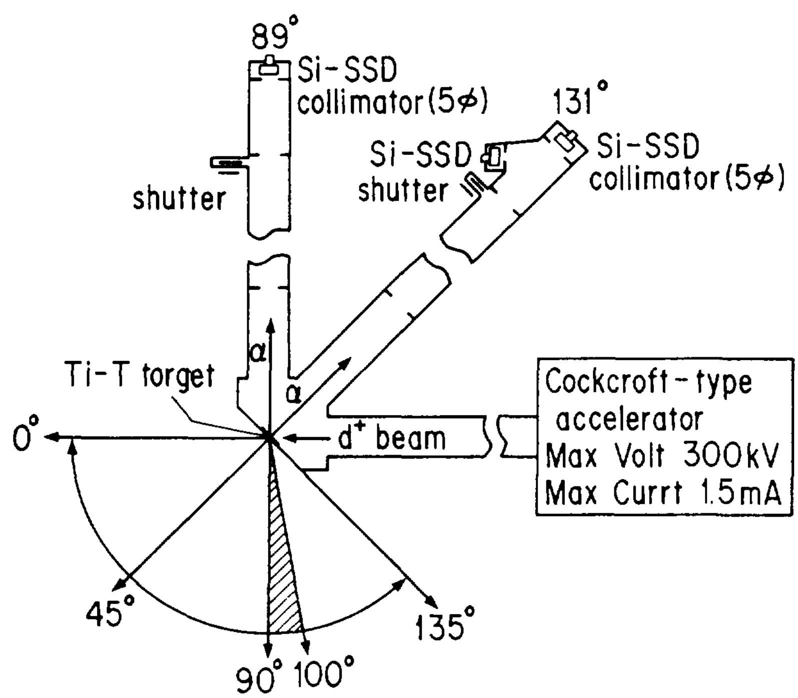

Figure 1. Layout of ETL reference energy field including an associated particle counting system which was used in the calculations of MCNP code

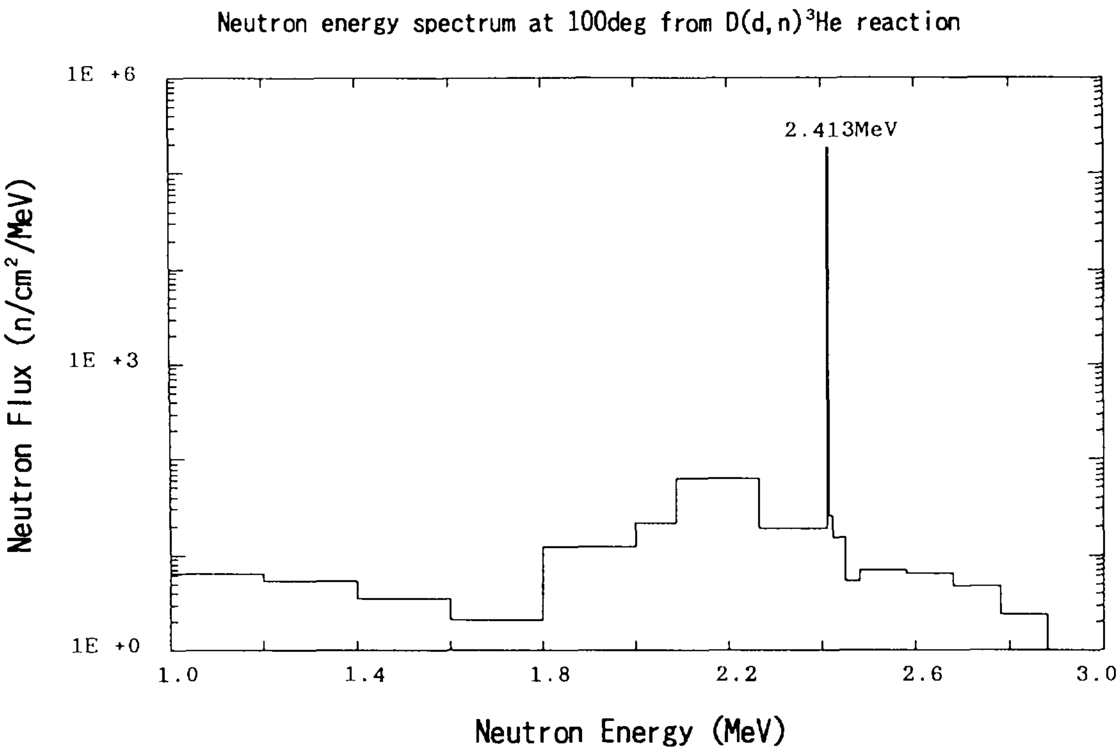

Figure 2. Neutron energy distribution in the case of 2.413MeV reference field at the emission angle of 100 deg. calculated by MCNP code.

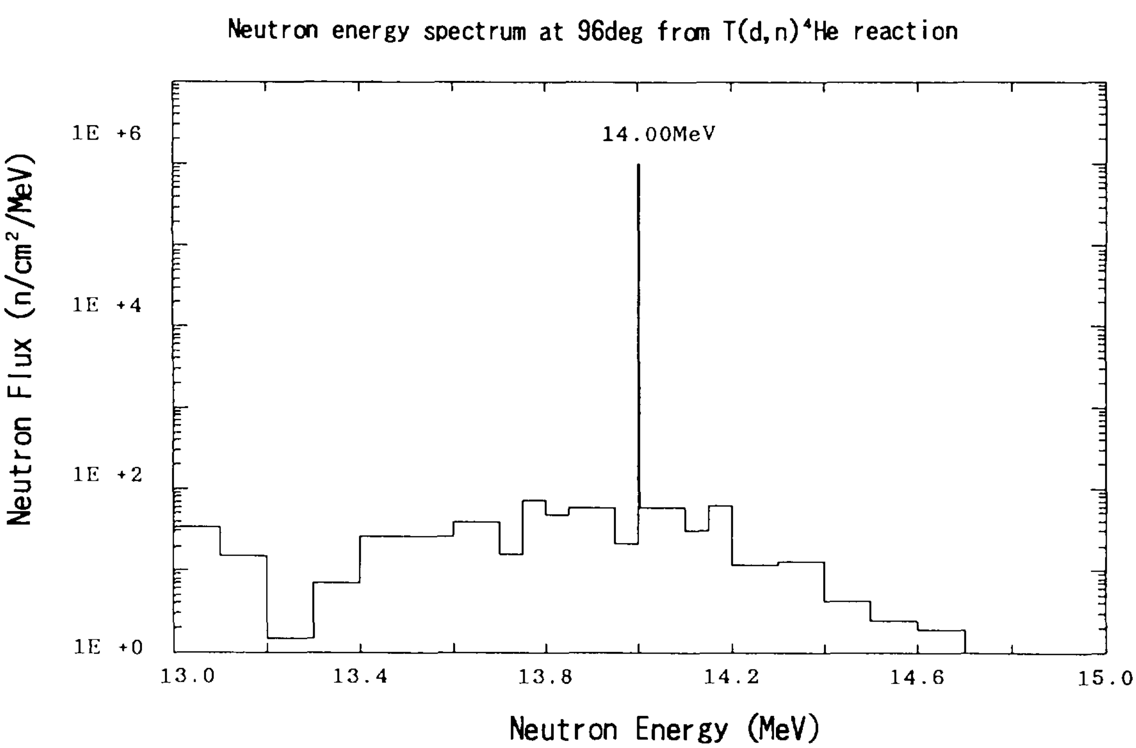

Figure 3. Neutron energy distribution in the case of 14.00MeV reference field at the emission angle of 96 deg. calculated by MCNP code.

II. Japan Atomic Energy Research Institute

II-A-1

Measurement of Production Cross Sections of ^{56}Co, ^{65}Zn and ^{48}Sc via (p,n) Sequential Reaction Process in Fe, Cu and Ti, Associated with 14 MeV Neutron Irradiation

Y. Ikeda and C. Konno

Importance of radioactivities produced in structural materials by higher order reactions with both neutrons and charged particles increases as the fusion reactor operation lasts for long period. The sequential reaction is defined as a reaction which is caused by charged particles emitted from the primary neutron reaction with the materials. This reaction process has been overlooked in the radioactivity calculation so far. Recently, Cierjacks and Hino investigated the contribution of the sequential reaction to the induced radioactivities in D-T fusion reactor component and showed that the reactions can not be neglected for the long-lived radioactivity estimation.[1,2] The code system, FISPACT, has been developed by Forrest to treat all possible reaction passes.[3,4] However, the code has to rely on the available data base in terms of charged particle energy distribution, cross section for the charged particle reaction and stopping powers in the materials. Moreover, strong current of 14 MeV neutron forced three-dimensional treatment considering multiple element in a mixture. It is worthwhile to provide experimental data for verifying code system with use of the radioactivity production rate due to 14 MeV neutron irradiation.

In the present study, we focused on the measurement of proton induced sequential reactions associated with 14 MeV neutron irradiation in iron, copper and titanium, namely, (1) Fe(n,xp) - ^{56}Fe(p,n)^{56}Co [$T_{1/2}$=78 day], (2) Cu(n,xp) - ^{65}Cu(p,n)^{65}Zn [$T_{1/2}$=270 day] and (3) Ti(n,xp) -^{48}Ti(p,n)^{48}V [$T_{1/2}$=16 day]. Three identical foils of same material attached each other were placed in front of the D-T neutron source at FNS and irradiated for 4 to 6 hours. Neutron fluxes at positions of Fe, Cu and Ti samples were determined from the associated activation reaction rates of ^{54}Fe(n,p)^{54}Mn, ^{63}Cu(n,α)^{60}Co and ^{48}Ti(n,p)^{48}Sc, respectively. They ranged 2 - 6 x 10^{10} /cm^2/s. After appropriated cooling of short-lived activities, γ-ray spectrum was measured with a Ge detector. The foil in the middle of three was used as the sample in order to eliminate unexpected background due to the proton produced in the surrounding materials. There was clear difference in the activation rate among the three foils for the (p,n) reaction production.

The ^{56}Co in the iron sample was identified by the γ-ray energies and their intensity relationship. Figure 1 shows the γ-ray spectrum measured after three month cooling time. Clear

γ-ray peaks corresponding to the lines of ^{56}Co were observed. Careful background subtraction was needed to identify the γ-line at 1115 keV of the ^{65}Zn, because of strong background due to ^{60}Co which is produced in the Cu sample by the reaction of $^{63}Cu(n,\alpha)^{60}Co$ [$T_{1/2}$=5.27 year] with longer half-life than that of ^{65}Zn. For the Ti sample, the target activity of ^{48}V emits the same γ-ray as ^{48}Sc, product of $^{48}Ti(n,p)^{48}Sc$ [$T_{1/2}$=1.9 day]. The radioactivities was identified by the difference in half-lives, which was obtained from numbers of consecutive measurements following the decay. The decay curves of γ-ray lines of Ti sample are given in Fig. 2.

Table 1 summarizes the result for the production cross sections investigated along with the estimated cross sections (ECS) based on the data available. The ECS is derived from the definition given by,

$$ECS = \sigma_n * \int_0^{Ep\text{-}Max} P(E_p)*\sigma_p(E_p)*N*(\frac{dE}{dx})^{-1}dE,$$

where, σ_n is the cross section for (n,xp) reaction, $P(E_p)$ normalized proton spectrum, σ_p denotes the cross section for (p,n) reaction, N number of target nuclei in unit volume and dE/dx corresponds to stopping power of proton in the target material. It is shown that the ECSs are in good agreements with the measured value even through there are large uncertainties in the $P(E_p)$ and (p,n) cross sections assumed in the calculation. It is proved that the treatment for the sequential reaction process is valid from the present results.

It is found that the cross sections for the sequential reactions investigated are considerably small in comparison with the primary reaction cross sections with neutrons. However, this reaction concerns the target nuclides of major components so that comparable amount of inventory is expected due to primary reactions on minor compositions or impurities in the order of a few % to ppm with cross sections from mb to b . For the long-lived radioactivity consideration, investigation has stressed on the low activation materials in which all possible long-lived radioactivities should be subjected. The current study for the induced activity are treating the material in ppm or less. In this view, the reaction pass of the sequential reaction, in particular, for the light mass materials, increase importance.

References

1) Cierjacks S. and Hino Y., " The role of Sequential (x,n) Reactions on Element Activation of Fusion Reactor Materials and Related Nuclear Data Needs", Proc. of a Specialists' Meeting on Neutron Activation Cross Sections for Fission and Fusion Energy Applications, September 13-15, 1989, Argonne National Laboratory, USA (1990) 19-28.
2) Cierjacks S. and Hino Y., J. Nucl. Material, 170 134 (1990).
3) Forrest R. A. and Endacott D. A. J., "FISPACT-User Manual", AERE M 3654 (1988).
4) Forrest R. A.,Sowerby M. G., Partric B. H. and Endacott D. A. J., "The Data Library UKACT1 and Inventory Code FISPACT", Proc. Nucl. Data for Sci. and Technol, Mito, Japan, (1988) 1061.

Table 1 Measured and estimated cross sections

Target	Reaction	Product	Half-life	Cross Section (μb) Measured	Estimated
Fe	Fe(n,xp) --->^{56}Fe(p,n)	^{56}Co	78.76 d	4.6 ± 0.3	6.2
Cu	Cu(n,xp) --->^{65}Cu(p,n)	^{65}Zn	244.1 d	11.4 ± 1.9	12.2
Ti	Ti(n,xp) --->^{48}Ti(p,n)	^{48}V	15.97 d	14.7 ± 1.9	14.3

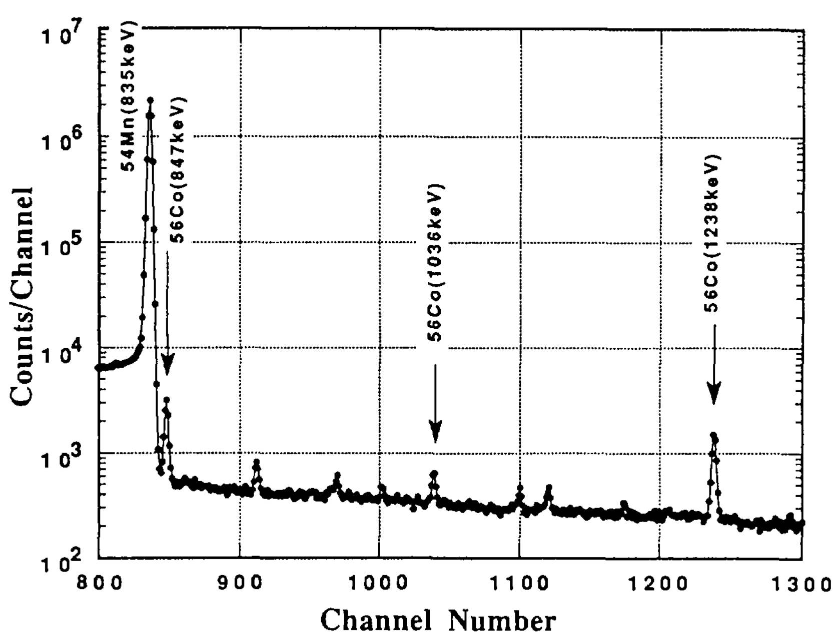

Fig. 1 Gamma-ray spectrum for the Fe sample measured at 3 months after irradiation.

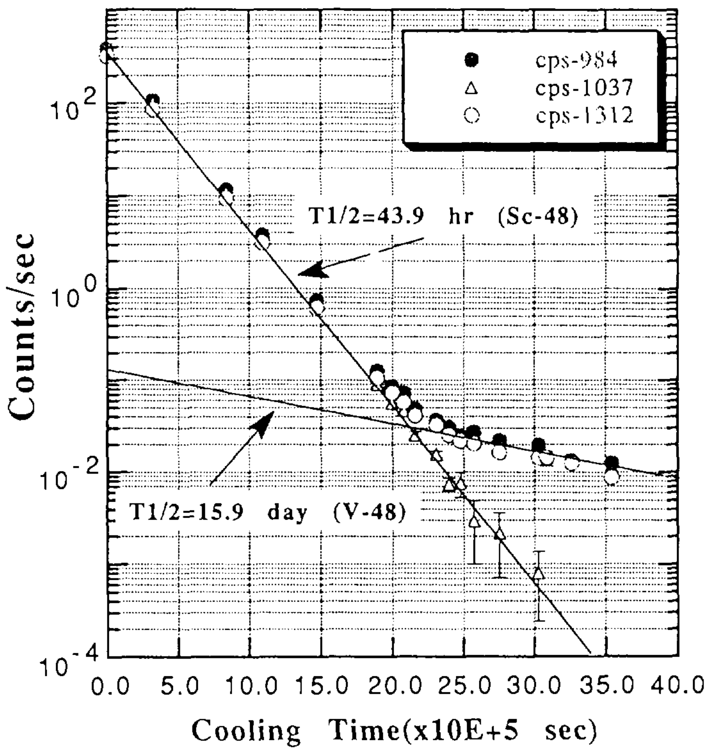

Fig. 2 Decay curves of γ-rays from Ti sample irradiated with D-T neutrons.

II-A-2

Measurement of Radioactivities of ^{24}Na and ^{92m}Nb Recoiled from Al and Nb via Reactions of with 14.9 MeV Neutrons

Y. Ikeda and C. Konno

Fast neutron reactions with materials yield energetic atoms release from the material surface. This phenomenon is defined as "neutron sputtering". In the fusion reactor development, importance of "neutron sputtering" has been recognized in terms of increase of impurity in a plasma degrading the plasma temperature as well as erosion of plasma facing materials giving a limit of life time. It also assumed importance due to that the sputtering process is identical to that for the displacement damage in the structural materials. In a decade in 1970, many material scientists had investigated extensively "neutron sputtering yield" (Sn) by both experimental and theoretical approaches.[1-10)] Materials subjected, however, were rather limited to be particular materials on niobium and gold, and some other structural materials. Furthermore the data reported by different authors were in poor agreements each other. Major reason for the deficiency is attributable to the lack of appropriate neutron source and no progress in the measuring technique to be sensitive to provide better statistics of deposited atoms. From the view point of fusion reactor design, a critical problem concerning the induced radioactivity has been pointed out[11-13)]; the neutron sputtering bring a serious increase of radioactivity level in the cooling media for the first wall and relevant structure near the plasma D-T source. As for the erosion of plasma facing materials and associated impurities, it has been considered not serious based on the available data so far reported. However, in light of potential use of low Z materials such as graphite and Be-Cu alloy as armors, we must say there is large uncertainty because that, as mentioned, the investigation had been focused on the relatively high Z materials and no data for low Z has been available. It is generally understandable that recoiled atoms receive higher energy and stopping power decreases in low Z materials relative to high Z materials, resulting in higher Sn. In particular, the on-going project of ITER requires more comprehensive data base through the Engineering Design Activity (EDA). Therefore, strong needs have been addressed in terms of systematic experimental data for fusion material development as well as fusion reactor safety. In this regard, we have initiated a program to measure the neutron sputtering ratio for a variety materials. This paper reports experimental procedure and preliminary results.

The D-T neutrons were generated by bombarding tritium target with deuterium with 20 mA and 350 keV, at the FNS facility. The cold work foils of aluminum and niobium with thickness of 5 μm and 12.5 μm, respectively, were used as the target materials. The collector materials of scotch tape were palced in both front and back sides of the target foils at the distance of 0.2 mm for Al and 0.2, 1.0 and 2.0 mm for Nb. A schematic arrangement of target sample is given in Fig.1. They were placed at distances of 10 to 15 mm from the neutron source in a direction of 0^o with respect to d^+ beam and were irradiated with neutrons for 4,500 sec. The mean energy of D-T neutron was estimated 14.8 MeV. After irradiation, the activities in the collectors were measured with a Ge detector. The numbers of radioactive recoil atom were determined from their activation rates. The D-T neutron fluence at foils of Al and Nb were determined from the activation-rates for ^{27}Al(n,α)^{24}Na and ^{93}Nb(n,2n)^{92m}Nb reaction assuming the cross sections of 112 mb and 455 mb, respectively. To extract the deposition rate of radioactivity, we assumed the 100 % collection efficiency. Background activity due to impurity was examined by irradiating the sample by inserting a mask with different materials between the target and collectors. As a result, no corresponding activity was detected in the collector.

Radioactivities detected were ^{24}Na from ^{27}Al(n,α)^{24}Na reaction for Al target, and

^{92m}Nb and ^{90m}Y from $^{93}Nb(n,2n)^{92m}Nb$ and $^{93}Nb(n,\alpha)^{90m}Y$, respectively, for Nb target. Concerning ^{24}Na and ^{90m}Y, Sns have been measured for the first time. The present configuration for the irradiation in air gave smaller number than actual Sn due to the attenuation in the air. The data are plotted in Fig. 2 along with data of ^{92m}Nb reported by Behrich[12] and Thomas[13]. The data for ^{92m}Nb presented relation of $\ln(Sn(r))=A*\ln(r)+B$. It indicated that the number of recoil atom decreased rapidly as the distance increased. The Sn was deduced by extrapolating the data at different distance to the point of zero distance. The data ranged 0.8 x 10^{-7} to 1.5 x 10^{-7}, resulting in good agreement with data reported in Refs. 12,13). For the ^{90m}Y, Sn at 1 mm distance is 20 times smaller than that of ^{92m}Nb. This is simply due to the small reaction cross section for $^{93}Nb(n,\alpha)^{90m}Y$ is 5 mb at 14.8 MeV, while the cross section for $^{93}Nb(n,2n)^{92m}Nb$ is 455 mb. The Sn of ^{24}Na is 6 times higher than that of ^{92m}Nb at 0.2 mm. The cross section of 113 mb at 14.6 MeV for $^{27}Al(n,\alpha)^{24}Na$ is 4 times lower than that for $^{93}Nb(n,2n)^{92m}Nb$. However, it is explained by that larger momentum transfer and low stopping power for ^{24}Na in Al enhanced the Sn to this order of magnitude. The Sn is estimated by using extrapolation as employed for ^{92m}Nb, where the same inclination of the attenuation curve is assumed.

There is clear difference in Sn for forward and backward direction with respect to the neutron current. For ^{24}Na and ^{92m}Nb, the ratios of Sn: forward and backward are found to be 20 and 32.1, respectively. These values are simply obtained from the activity ratios in the collectors attached on both side of Al and Nb targets of 10 mm in diameter. The value of 32.1 for Nb is much less than the ratio of 139 reported by Thomas[13]. This difference could be attributable to the difference in the experimental geometrical configuration. A theoretical prediction for Nb sputtered by 15 MeV incident neutron indicates value of 22[3], being consistent with the present data.

References

1) Behrisch R., J. Nucl. Mat. 108 & 109 73 (1982).
2) Nishizawa K., Morita Y., Sensui Y. and Matsuura T., J. Nucl. Sci. and Technol. 16 684 (1979).
3) Andersen H. H., J. Nucl. Mat. 76 & 77 190 (1978).
4) Jenkins L. H., Smith G. J., Wendelken J. F. and Saltmarsh M. J., J. Nucl. Mat. 63 438 (1967).
5) Harling O. K., Thomas M. T., Bradzinski R. L. and Rancitelli L. A., J. Nucl. Mat. 63 422 (1976).
6) Kaminsky M., Peavey J. H. and Das S. K., Phys. Rev. Lett. 32, 11 599 (1974).
7) Roberto J. B., Robinson M. T. and Fu C. Y., J. Nucl. Mat. 63 460 (1976)
8) Harling O. K., Thomas M. T., Brodzinski R. L. and Rancitelli L. A., Phys. Rev. Lett. 34, 21 1340 (1975).
9) Keller K., Plasma Physics, Vol 10 195 (1968).
10) Kaminsky M. and Das S. K., J. Nucl. Mat. 53 162 (1974).
11) Kulcinski G. L. and Emmert G. A., J. Nucl. Mat. 53 31 (1974).
12) Behrisch R., Gahler R. and Kalus J., J. Nucl. Mat. 53 183 (1974).
13) Thomas M. T., Harrling O. K., Brodzinski R. L. and Rancitelli L. A., J. Nucl. Mat. 63 448 (1976) .

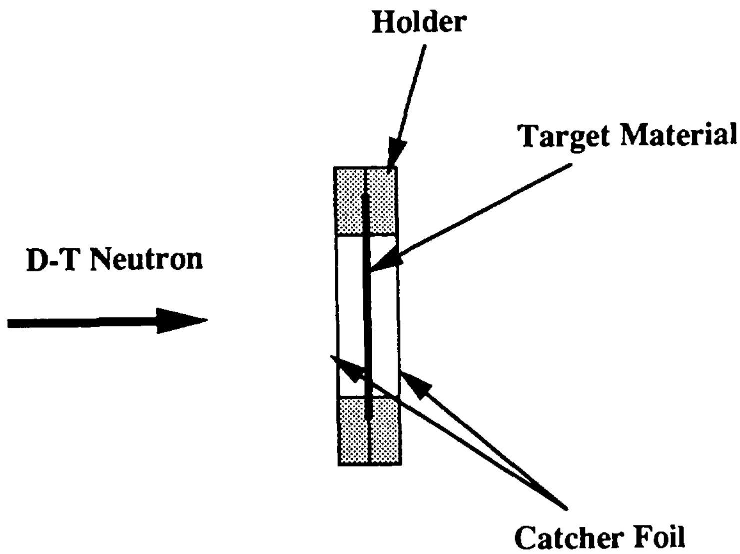

Fig. 1 Schematic configuration for the measurement of recoil radioactivities.

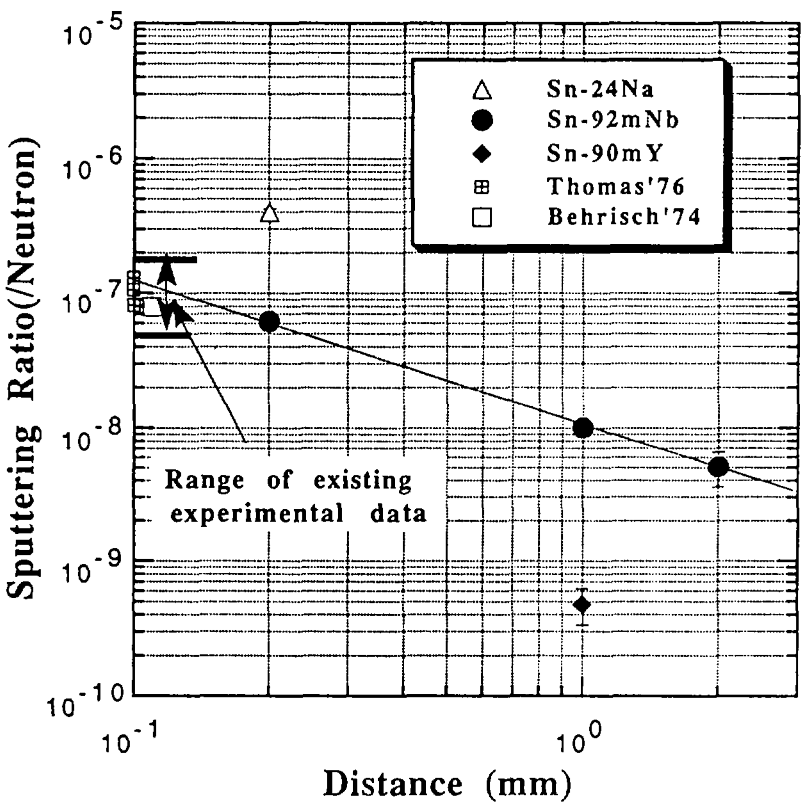

Fig. 2 Measured neutron sputtering ratios for recoil radioactivities in the air.

II-A-3

Measurement of $^{93}Nb(n,n')^{93m}Nb$ Cross Section at 14.4 and 14.9 MeV

Y. Ikeda, C. Konno, K. Kosako*1, K. Kawade*2 and H. Maekawa

The dosimetry reaction of $^{93}Nb(n,n')^{93m}Nb$ is characterized by the low threshold energy less than 0.1 MeV and the long half-life of 13.6 y. A lot of studies have been carried out to apply this reaction to the determination of fast neutron fluence. Not only for the conventional reactor dosimetry, the reaction has been recognized to be attractive for the DT fusion reactor dosimetry. In view of the suitable characters, extensive efforts have been devoted in the cross section evaluations. The IRDF-82[1)] was the first dosimetry file contained this reaction explicitly. Recently, the evaluation was updated by Wagner and implemented in IRDF-90[2)]. In the meantime, the JENDL Dosimetry File[3)] contained this reaction cross section, which was newly evaluated by Sakurai. Both new evaluations took the data of cross section at 14 MeV measured by Ryves[4)] as a reference, so that cross section values around 14 MeV are almost identical. Odano[5)] has recently reported the evaluation of the cross section without using the data of Ryves as the reference. His value gave a slightly higher value in the 14 MeV region than both evaluations in IRDF-90 and JENDL Dosimetry File. A number of experimental data have been reported in the energy range from 0.5 to 5 MeV, but only one data is available in the 14 MeV energy region.[4)] When the D-T fusion neutron spectrum are concerned, 14 MeV neutron flux strongly influences on the result. Hence, it has been desired to measure more data to arrive at more a comfortable situation of evaluation.

The present measurement was carried out to provide experimental data at 14 MeV region in the course of the on-going program for the activation cross section measurement at FNS. The D-T neutrons were generated by bombarding Ti-^{3}T mounted in a rotating target with d^+ beam of 20 mA and 350 keV. Two thin Nb foils with thickness of 12.5 μm were placed at a distance of 50 mm from the D-T neutron source at angles of 5° and 60° with respect to incident d^+ beam. Total fluence of about 4 x 10^{14}/cm^2 at the sample was obtained from irradiation for 32 h. After cooling time for 1.85 years, the activities of ^{93m}Nb were measured with a low energy photon spectrometer by counting Kα X-rays of 16.521 and 16.615 keV associated with deexciting γ-ray of the first level at 30.4 keV of ^{93}Nb. The data used in the reaction rate determination is summarized in Table 1. The neutron flux was determined by the reaction rates of $^{93}Nb(n,2n)^{92m}Nb$ and $^{63}Cu(n,\alpha)^{60}Co$ monitor reactions. Cross sections at energies of 14.5 and 14.9 MeV were obtained from the reaction rate ratios of $^{93}Nb(n,n')^{93m}Nb$ to the monitor reactions. The threshold energy is lower than 50 keV and the cross sections around 1 to 3 MeV energy region are about one order of magnitude larger than that in 14 MeV region as shown in Fig. 1. This results in large fraction of reaction rate below 10 MeV contributing to the total reaction rate even though 14 MeV neutrons dominate the neutron flux spectrum at the close vicinity of the neutron source. Thus, in the determination of reaction rate of $^{93}Nb(n,n')^{93m}Nb$ for 14 MeV neutrons, correction for low energy neutron component in the incident neutron spectrum is most important. The neutron spectrum at each sample position was calculated by a Monte Carlo code, MORSE-DD, with use of a precise model of target structure. The spectrum was used for the correction of low energy neutron contribution along with several evaluated cross sections available. Table 2 gives the cross sections obtained using correction factors derived from IRDF-90 and Odano's evaluation[5)]. The present data are given in Fig. 2 along with the data of Ryves[4)] and available evaluated cross sections in the energy range above 12

*1 Present address: Nuclear Energy Data Center (NEDAC), *2 Nagoya University

Table 1 Summary of data used in data processing

Item	Sample#1	Sample#2
Foil weight (g)	0.01244	0.01248
Number of Atoms	8.063×10^{19}	8.089×10^{19}
Irradiation angle (deg.)	5	60
Neutron flux (/cm2/s)	5.278×10^{9}	5.609×10^{9}
Cooling time (sec)	5.822828×10^{7}	5.830415×10^{7}
Collection time (sec)	89286	86400
Counts	1311 ± 136	1364 ± 133
Data commonly used		
Foil thickness	0.0125 mm	
Half-life	13.6 ± 0.3 year	
Avogadro's number	6.0221358×10^{23}	
Atomic weight	92.9064 g	
Irradiation time	284460 s	
Ka-X-ray intensity	8.98 ± 0.34 %	
Efficiency	0.018 ± 0.002	
Self-absorption	0.907 ± 0.007	

MeV. Though the errors of the present data are large, there is a good agreement within experimental error with Ryves's data at 14.3 MeV. However, present data gives systematically higher values than those of evaluations in IRDF-90, -82 and JENDL Dosimetry File. The data are rather close to Odano's evaluation which doesn't take the Ryves's data as the normalization in this energy region.

The present measurement provides new experimental data for ^{93}Nb(n,n')^{93m}Nb cross sections at 14.4 and 14.9 MeV. It is highly recommended to re-evaluate the cross section in particular for the 14 MeV region by taking the present data into account.

References

1) Cullen D. E., Kocherov N., and McLaughlin P. M.:"The International Reactor Dosimetry File (IRDF-82)," IAEA-NDS-41/R, rev.0 (1982).
2) Kocherov N. :"The International Reactor Dosimetry File (IRDF-90)," (1990).
3) Nakazawa M., et al.:"JENDL Dosimetry File," JAERI-1325 (1992).
4) Ryves T. B. and Kolkowski P.:J. Phys. G: Nucl. Phys. 7 529 (1981).
5) Odano N., Iwasaki S. and Sugiyama K.: Proc. Int. Conf on Nucl. Data on Sci. & Technol., Jülich, Germany, 1991.

Table 2 Results for cross sections

Energy(MeV)	Cross section (mb)		
	A	B	Averaged
14.5 ± 0.3	42 ± 7	45 ± 7	43.5 ± 7.0
14.9 ± 0.3	43 ± 7	46 ± 8	44.5 ± 7.5

A: IRDF-90 evaluation was used.
B: Odano's evaluation was used.

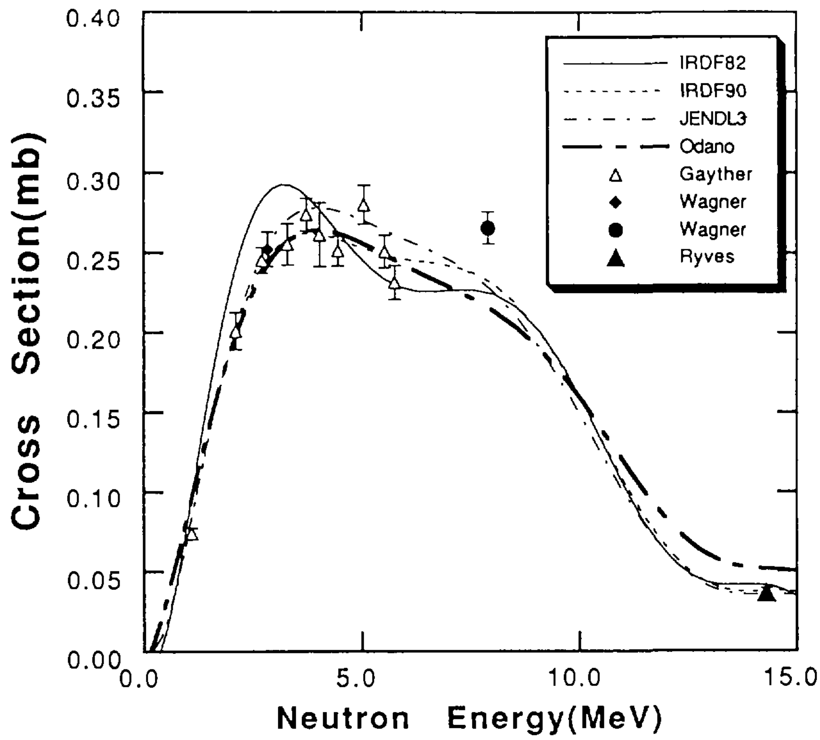

Fig. 1 Cross section curves of $^{93}Nb(n,n')^{93m}Nb$ for all energy region.

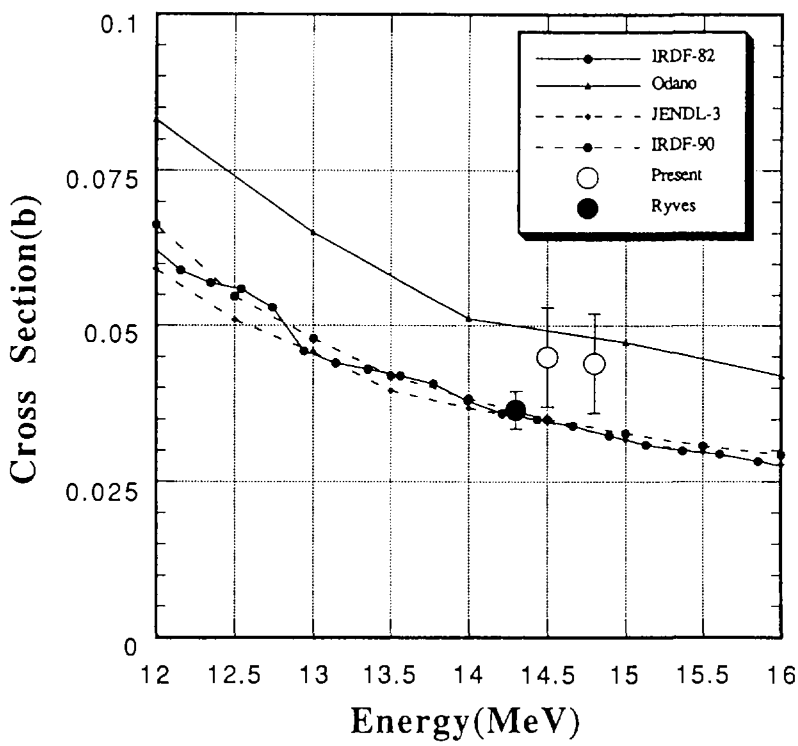

Fig. 2. Cross section of $^{93}Nb(n,n')^{93m}Nb$ at high energy region.

II-A-4

Cross Sections of Transmutation for ^{99}Tc by 14 MeV Neutrons

Y. Ikeda, E. T. Cheng*, C. Konno and H. Maekawa

An idea to utilize intense neutron source for material irradiation test, e. g., FMIF[1], IFMIF, ESNIT and Fusion Reactor[2], has been investigated to produce the high specific ^{99}Mo for medical diagnostics of liver and brain cancer. The ^{99}Tc(n,p)^{99}Mo reaction produces ^{99}Mo radioisotope with very high specific activity ratio, which is more preferable to activities obtained from fission products or ^{98}Mo(n,γ)^{99}Mo reaction in fission reactors. A preliminary study based on a cross section of 40 mb for ^{99}Tc(n,p)^{99}Mo taken from REAC-2[3] gave a result that an annual revenue of about $12M could be generated to finance the operation cost of FMIF.[1] The objectives of the present study are to measure the activation cross section for ^{99}Tc(n,p)^{99}Mo around 14 MeV energy region in order to give accurate estimation of ^{99}Mo radioactivity production utilizing FMIF (Fusion Material Irradiation Facility), and to provide basic data for better understanding transmutation reactions with radioactive target of ^{99}Tc; ^{99}Tc(n,α)^{96}Nb, ^{99}Tc(n,n'α)^{95}Nb and ^{99}Tc(n,n')^{99m}Tc.

Samples of ^{99}Tc were prepared from solution of 185 MBq ^{99}Tc (21.46 MBq/ml). [LOT#57 of TCS1 (delivered by Amersham, U.K.)] Amount of 17.3 μl corresponding to 10.03 μCi was pipetted from the original liquid solution and was deposited on a thin plastic plate. After drying the solution, the sample was sealed with another thin plastic plate. The size of the sample deposition was 3 mm in diameter. Each sample contained 3.5963 x 10^{18} of ^{99}Tc nuclei. Irradiation experiment was performed at the Fusion Neutronics Source (FNS) facility at JAERI. The 14 MeV neutrons were produced via ^{3}T(d,n)^{4}He reaction. Incident deuterium energy and current were 350 keV and 2 mA, respectively. The source neutron strength was about 3 x 10^{11}/s. Two identical samples were positioned at 10 mm distance from the source at 0^{o} and 135^{o} angles with respect to incident d^{+} beam direction. These angles corresponded to 14.9 and 13.5 MeV neutron energies. Irradiation time was about 6 hours. Two thin Nb foils were attached on the front and rear surface of the ^{99}Tc samples. The reaction of ^{93}Nb(n,2n)^{92m}Nb was used for the D-T neutron flux determination at the samples assuming a cross section of 455 $\pm$ 7 mb around 14 MeV for this reaction. Source neutron spectra were calculated by the MORSE-DD code with JENDL-3 nuclear data. In the calculation, fine structure of the neutron target system was modeled accurately. Low energy neutron flux contributions to the reaction rates were calculated by using the neutron spectra.

After irradiation, gamma-ray spectrum of radioactive sample was measured with a 117 % Ge detector (EG&G ORTEC). Activation rates for the reactions of interest were deduced from γ-ray counts by performing necessary corrections.

^{99}Tc(n,α)^{96}Nb:

The present results gave generally good agreements with data measured by Qaim.[4] Also, the systematics of REAC-ECN-3[7] gave reasonable agreement with the present data.

^{99}Tc(n,n'α)^{95}Nb:

The activity of ^{95}Nb with hale-life of 35 d was detected. However, the γ-ray counting statistics were so poor that the uncertainties of data were larger than those of the other reaction cross sections. This poor statistics was mainly due to the small number of the target nuclei of ^{99}Tc. Even though, the present data gave a general agreement with data of Qaim.[5]

Cross sections were obtained from measured reaction rates and determined neutron

---

* TSI Research, U.S.A.

fluxes. The results are tabulated in Table 1 along with data in the literature.

$^{99}Tc(n,p)^{99}Mo$:

The cross section of 14.0 ± 0.9 mb is in good agreement with data of 15.1 ± 2.3 by Qaim.[4] The value is supported by a comprehensive systematics for the (n,p) reaction cross section based on data measured at FNS, which give a range of this cross section at 14.9 MeV from 13 to 25 mb. From this result, the cross section of REAC-2, 52.7 mb, seems overestimated by a factor of 4. This may lead to reduce the estimation for amount of ^{99}Mo production.

$^{99}Tc(n,n')^{99m}Tc$:

The ^{99m}Tc is the daughter of ^{99}Mo deexciting with half-life of 6 h to the ground state of ^{99}Tc. Since the ^{99}Mo is simultaneously produced, the correction for the contribution from the decay of ^{99}Mo to ^{99m}Tc was essential in this case. The present data were comparable to the data previously reported. [5,6]

An overestimation by a factor of 4 in the amount of ^{99}Mo production by FMIF is suggested as long as the present cross section is valid. However, the idea of ^{99}Mo production using $^{99}Tc(n,p)^{99}Mo$ is still very attractive in terms high specific activity ratio of ^{99}Mo in comparison with the other methods; chemical separation from the fission products and $^{98}Mo(n,\gamma)^{99}Mo$ reaction. Thus, the feasibility study of the idea should be forwarded based on the more precise nuclear data.

Reference

1) Cheng E.T., Schenter R.E., Ikeda Y., Nuclear Data for the Production of Radioisotope in Fusion Material Irradiation Facility, ANS Transaction, 63 (1991) 169.
2) Engholm B. A., Cheng E. T., Schultz K. R., "Radioisotope Production in Fusion Reactors, " Fusion Technology, 10 (1986) 1290.
3) Mann F. M., "REAC2: Status of Codes and Libraries," Fusion Thechnol., 15 (1989) 449.
4) Qaim S. M., J.Inorg. Nucl. Chem., 35 (1973) 3699.
5) Golchert N. W.,Gardrer D. G. and Sedlet J., Nucl. Phys. 73 (1965) 349.
6) Goldstein G., J. Inorg. Nucl. Chem., 28 (1966) 676.
7) Gruppelaar H., Van Der Kamp H. A. J., Kopecky J. and Nierop D., "The REAC-ECN-3 Data Library with Neutron Activation and Transmutation Cross-Sections for Use in Fusion Reactor Technology," ECN-207 (1988).

Table 1 Measured cross sections and reference data in the literature

Reaction	Cross Section (mb) 13.5 MeV	Cross Section (mb) 14.9 MeV	References	
$^{99}Tc(n, p)^{99}Mo$	10.7 ± 1.0	14.0 ± 0.9	15.1 ± 2.28	-a)
			6.97 ± 1.11	-b)
			~ 5.	-c)
$^{99}Tc(n,\alpha)^{96}Nb$	4.5 ± 0.3	5.6 ± 0.4	7.12 ± 1.0	-a)
			2.02 ± 0.22	-b)
			7.5 ± 0.2	-c)
$^{99}Tc(n, n'\alpha)^{95}Nb$	-----	2.0 ± 1.6	1.28 ± 0.2	-a)
			< 1.0	-b)
$^{99}Tc(n, n')^{99m}Tc$	104 ± 6	76 ± 4	107 ± 13	-a)
			41.3 ± 6.6	-b)
			77 ± 4	-c)

a) Reference [4], b) Reference [5], c) Reference [6]

II-A-5

Experiment and Analysis of D-T Neutron Induced Long-Lived Radioactivities for Fusion Reactor Structural Materials

Y. Ikeda, A. Kumar*, C. Konno, Y. Oyama, K. Kosako, M. Z. Youssef*,
M. A. Abdou* and H. Maekawa

Production of long-lived radioactivity concerns scenario of waste disposal in a D-T fusion power reactor. In the framework of JAERI/USDOE collaborative program on fusion neutronics, an experimental effort has been conducted at FNS in order to verify the adequacy of nuclear data relevant to the long-lived activations along with accuracy of the calculation code systems. The present report describes the experimental analysis of decay radioactivities in molybdenum, silver, hafnium, tungsten and rhenium at cooling time of about two years after irradiation with 14.9 MeV neutrons. The tested calculation code systems are THIDA-2[1), REAC-2[2), DKR-ICF[3) and RACC[4). Here, the present status of the prediction accuracies are given as follows:

Mo: There are general agreements of the γ-lines between THIDA calculation and experiment. However, the assignment of γ-ray at 935 keV is open to be investigated. The THIDA calculation of ^{91m}Nb (62 d) [104.5 and 1205.0 keV] overestimates experiment slightly. There is no γ-ray at 235.7 keV due to ^{95m}Nb (3.6 d) in the measured spectrum, which is clearly given in the calculation. The calculation of activity of ^{88}Zr (83.4 d) agrees well with experiment.[γ-ray at 392.9 keV] Though ^{94}Nb has the long-half-life of 2 x 10^4 y, clear lines at 702.6 and 871.1 keV are observed. The C/E is 0.6 for THIDA, while 2.62 and 1.56 for REAC-2 and DKR-ICF, respectively. The THIDA calculation for ^{88}Y(106.6 d) seems reasonable. Underestimation (C/E=0.6) is found in calculations for ^{95}Nb(35 d) and ^{95}Zr(64.0 d) which dominate the γ-ray spectrum at 765.8 keV, and at 724.2 and 756.7 keV, respectively. The underestimation resultes in C/E=0.64 for total γ-ray intensity. In conclusion, the cross section of ^{94}Mo(n,p), ^{95}Mo(n,p) ^{96}Mo(n,np) and ^{98}Mo(n,α) should be checked.

Ag: The calculations of THIDA, REAC-2 and DKR-ICF largely overestimate the γ-ray intensity measured, resulting in C/E=3.39, 2.19 and 2.19, respectively. Higher energy region, mostly γ-rays due to ^{110m}Ag (249.8 d) dominate the spectrum at 744.3,763.9, 818.0, 884.7, 937.5, 884.3, 1384.3, 1475.8, and 1505.0 keV. There are systematically underestimation of experiment in all calculations: C/E= 0.02 for THIDA, 0.39 for REAC-2, 0.35 for DKR-ICF. In contrast, in the low energy part, ^{108m}Ag (127 y) governs the spectrum at energies of 433.9, 614.3 and 722.9 keV, where the calculations overestimated by a factor of 2 to 4. As shown in Fig. 1, overall γ-ray spectrum is dominated by ^{108m}Ag, C/E falls in 2.19 to 3.39.

The reason of the overestimation is as follows; The cross section of ^{109}Ag(n,2n)^{108m}Ag in the THIDA library is about 700 mb and half-life of ^{108m}Ag is 127 y. Recent experiment gives $T_{1/2}$ of ^{108m}Ag as 450 y[5), a factor of 3 longer than that used. When $T_{1/2}$ of 127 y is used, cross section value should be around 200 mb.[6) If the half-life is revised to be appropriate value, C/E will be improved excellently.

Hf: The THIDA calculation give a considerably large contribution of ^{172}Lu (6.7 d) in all energy region. Especially in high energy region above 800 keV, only γ-lines of ^{172}Lu occupy the spectrum. It seems, however, unreasonable because; a possible reaction and decay chain for the production of ^{172}Lu is {^{174}Hf[0.16%] (n,3n)^{172}Hf (5 y) ---> ^{172m}Lu ---> ^{172}Lu (6.7 d)}, while the cross section of (n,3n) is generally very small and abundance of ^{174}Hf is very small. Considering those, too much overestimation in the calculation is expected. The THIDA library

* University of California, Los Angeles

gives cross section 1.9 barn. The value, even if the reaction is possible from Q value, there must be some incorrect treatments in the evaluation. There is no γ-lines corresponding to the measured spectrum. The other activities observed are ^{173}Lu (1.37 y) and ^{178m2}Hf (31 y). The ^{173}Lu and ^{178m2}Hf are produced via ^{174}Hf(n,2n)^{173}Hf (24 h) -->^{173}Lu and ^{179}Hf(n,2n)-^{178m2}Hf, respectively. While there are clear γ-lines of ^{178m2}Hf at several energies, no correspondence is in the THIDA calculation because of lack of production cross section for the ^{178m2}Hf. In contrast, REAC-2 overestimates measurement by a factor of 377. This is simply because of unreasonably large cross section of 2.07 b, for which recent measurement give 6.3 mb.[6] For γ-lines of ^{173}Lu, there are in general agreements. The γ-ray at 342 keV of ^{175}Hf (70 d) is overestimated in calculations by a factor of 10 for THIDA, 1.94 for REAC-2. Since the γ-ray intensity of ^{175}Hf dominates the spectrum in the calculations, it results in a C/E = 9.42.
W: The THIDA calculation for tungsten presentes activities of ^{182}Ta (115 d), ^{181}Hf (42.4 d) and ^{185}W (75.1 d) as the contributors to the γ-ray spectrum. They are produced via ^{182}W(n,p) + ^{183}W(n,np), ^{184}W(n,α) and ^{184}W(n,γ)+^{186}W(n,2n), respectively. In the measured spectrum, however, there is no γ-rays associated with decays of ^{181}Hf and ^{185}W. It is found that THIDA has a problem in the γ-ray branching data of ^{182}Ta; the library gives orders of three less branching ratios for low energy γ-rays at 100.1, 113.7, 152.4, 156.4, 179.4, 198.3, 222.1, 229.3 and 264.1 keV. There are corresponding lines in the measured spectrum. These missing γ-ray branches lead to the underestimation in the calculation.
Re: There are clear one to one correspondence of the γ-lines between measured and calculated spectra as shown in Fig. 2. The activities contributing to the measured spectrum are ^{182}Ta (115 d), ^{184m}Re (165 d), ^{184}Re (38 d) and ^{185}W (75.1 d), produced via ^{185}Re(n,α)^{182}Ta, ^{185}Re-(n,2n)$^{184m\&g}$Re and ^{185}Re(n,p), respectively. In addition to these activities, THIDA gives the productions of ^{183}Ta (5.1 d), ^{183}Re (70 d) and ^{186m}Re (2 x10^5 y). Gamma-lines due to those activities are not detected in the measurement because; (1)^{183}Ta is the products of ^{187}Re(n,n'α) cross section of which is too small, (2) ^{183}Re the product of ^{185}Re(n,3n) cross section of which should be also very small, (3) ^{186m}Re the product of ^{187}Re(n,2n) has a very long half-life of 2 x 10^5 y, resulting in very low disintegration rate. The C/E of 2.06 is obtained. The calculation underestimates ^{182}Ta in the same reason as mentioned in tungsten case. Overall overestimation is governed by $^{184m+g}$Re production (C/E=2). One possible explanation for the overestimation is the too large isomer ratio of ^{185}Re(n,2n) in the library. The cross section of ^{185}Re(n,2n)^{184m}Re should be reduced to be a half of the present cross section as long as the present C/E is concerned.

From the present experimental analysis, largely scattered C/E values are observed in almost all radioactivities with half-lives ranging from several tens days to more than 10^4 years. This status of inaccuracy in the calculation forces us very crucial reevaluation of long-lived radioactivity wastes. The results also promote the importance for measurements of the basic activation cross section data along with the half-lives of particularly long-lived radioactivities.

References

1) Seki Y., et al., "THIDA-2: An Advanced Code System for Calculation of Transmutation, Activation, Decay Heat and Dose Rate," RSIC computer code collection, CCC-410 (1987).
2) Mann F. M., "REAC*2: Users Manual and COde Description," WHC-EP-0282, Westinghouse Hanford Company (1989).
3) Henderson D. L. and Yasar O., "A Radioactivity and Dose Rate Calculation Code Package," Vol. 1 and 2, RSIC computer code collection, CCC-323 (1987).
4) Jung J., "Theory and Use of the Radioactivity Code RACC," ANL/FPP/TM-122, Argonne National Laboratory (1979).
5) Schotzig U., Schrader H. and Debertin K., "Precision Measurements of Radioactive Decay Data," Proc. Int. Conf. on Nucl. Data for Sci. and Technol., May 1991, Jülich, Germany.
6) Ikeda Y., Kumar A. and Konno C., "Measurements of Long-lived Activation Cross Sections by 14 MeV Neutrons as FNS," ibid.

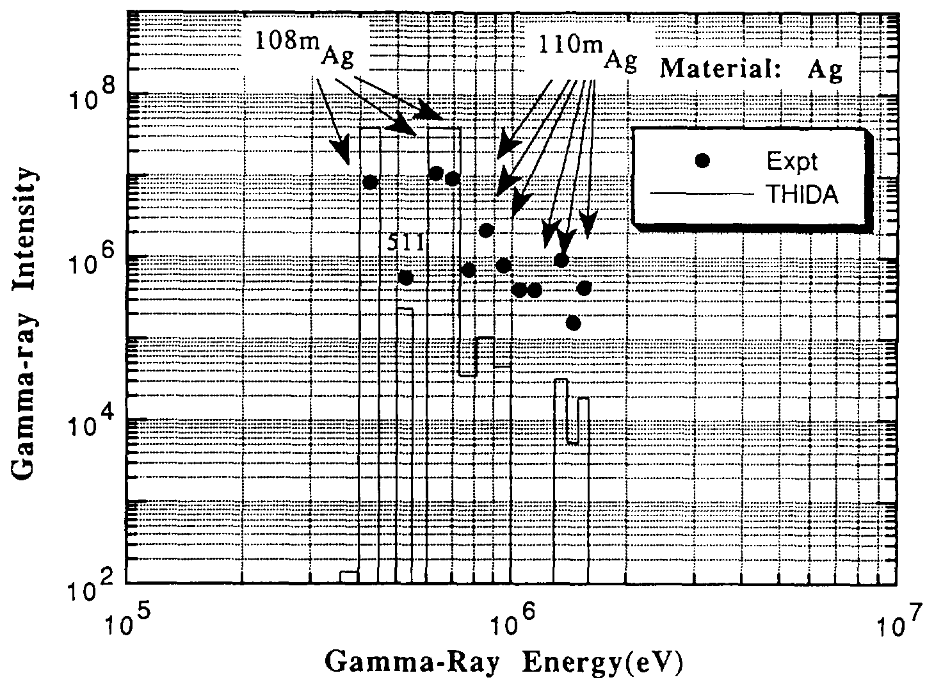

Fig. 1 Comparison of THIDA calculation with measurement for γ-ray spectrum of Ag.

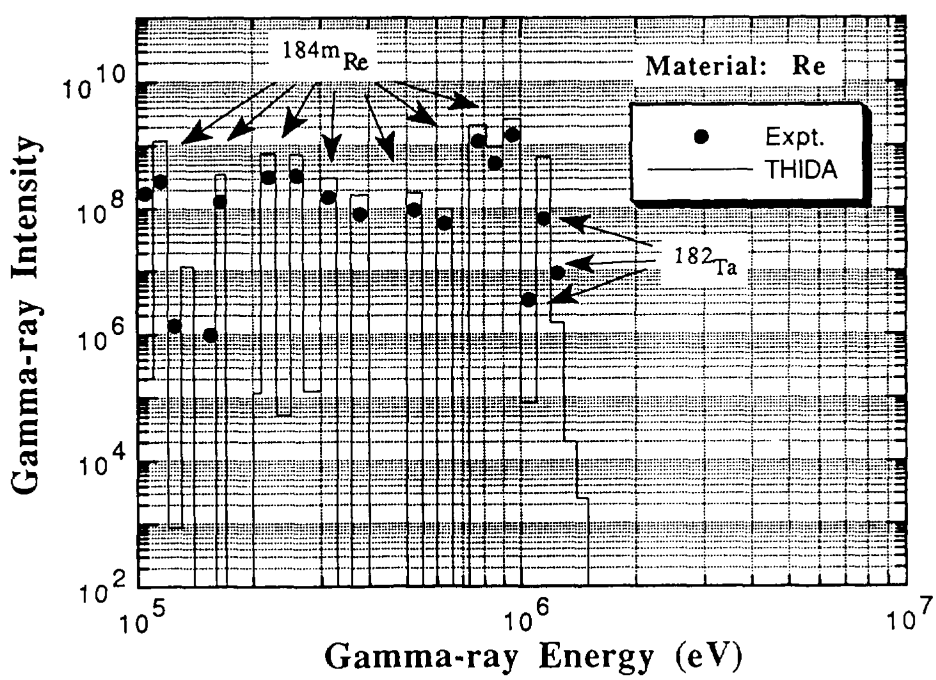

Fig. 2 Comparison of THIDA calculation with measurement for γ-ray spectrum of Re.

II-A-6

Neutron Activation Cross Section Measurements at 9.1 and 11.1 MeV Using $^{1}H(^{11}B,n)^{11}C$ Neutron Source at TANDEM Facility at JAERI

Y. Ikeda, S. Chiba, T. Fukahori, K. Hasegawa, M. Mizumoto
and C. Konno

Continuous program on activation cross section measurements for important dosimetry reactions at an energy range from 9 to 13 MeV has been underway by using a neutron source incorporated with $^{1}H(^{11}B,n)^{11}C$ reaction.[1] The present report gives the most recent results of the cross section measurements for the reactions listed in Table 1. The neutron energies applied were 9.1 and 11.1 MeV which were realized with 55 and 60 MeV ^{11}B beams incident into $^{1}H_2$ gas target, respectively. In addition to the irradiation with gas in, separate irradiation with gas out was performed for each energy in order to subtract the parasitic neutrons due to interaction of ^{11}B beam with the target structure. The neutron spectra in the forward direction with respect to the ^{11}B beam direction were measured with the TOF technique incorporated with two NE213 scintillation spectrometers. They are shown in Fig. 1 for both runs corresponding to gas in and out. Obviously, they look broadened in the peaks. This was attributable to the poor time resolution in the TOF measurement. One should notice that there is appreciable difference in the neutron flux below 5 MeV between spectra of gas in and gas out runs for 11 MeV (60 MeV ^{11}B) operation.

Stacked foils of Ti, V, Fe, Co, Zn, Zr and Nb sandwiched with both Al and Au monitor foils were irradiated at a distance of 100 mm from the center of target cell for 11 hours for gas in and for 3 to 4 hours for gas out. After irradiation for each run, activities were measured with Ge detectors and reaction rates were deduced by performing necessary corrections in terms of decay times, natural abundance, detector efficiency, γ-ray self absorption, and so forth. The neutron flux was determined from the reaction rate of monitor reaction of $^{27}Al(n,\alpha)^{24}Na$ and its cross section value taken from IRDF-90. The neutron flux at each foil was derives by interpolating reaction rates of $^{27}Al(n,\alpha)^{24}Na$ on both front and rear sides.

The spectra were used not only in the determination of mean reaction energy, but also in the correction for the low energy neutron component to the net reaction rate of interest. The mean neutron energies determined were 9.1 and 11.1 MeV. Fortunately, the correction for the low energy neutron contribution was not serious because of rather high threshold energy of almost all reactions, except for $^{64}Zn(n,p)^{64}Cu$, threshold energy of which is around 1 MeV. Most dominant experimental error arose in the reaction rate due to poor statistics of γ-ray counts. This was simply because of low neutron yields in the present operation of ^{11}B beam.

The present results are summarized in Table 2. It should be noted that the data are very preliminary. Further fine treatment of the data correction is needed, in particular, for the terms correlated with the neutron energy spectrum.

Reference

1) Y. Ikeda, et al., Proc. Intl. Conf. on Nucl. Data for Sci. & Technol., Jülich, Germany, 13-17 May 1991 (issued in 1992: Editor S. M. Qaim) pp. 294-296.

Table 1 Reactions Investigated and Associated Decay Data

Reaction	Half-life	Abundance	γ-Energy	γ-ray branching	Atomic mass
1. $^{48}Ti(n,p)^{48}Sc$	1.821 d	0.737	983.5	1.0	47.88
2. $^{51}V(n,\alpha)^{48}Sc$	1.821 d	0.9975	983.5	1.0	50.9415
3. $^{56}Fe(n,p)^{56}Mn$	2.5785 h	0.9172	846.81	0.989	55.847
4. $^{59}Co(n,\alpha)^{56}Mn$	2.5785 h	1.0	846.81	0.989	58.9332
5. $^{64}Zn(n,p)^{64}Cu$	12.701 h	0.486	511	0.358	65.39
6. $^{90}Zr(n,p)^{90m}Y$	3.19 h	0.5145	202.5	0.966	91.224
7. $^{93}Nb(n,2n)^{92m}Nb$	10.15 d	1.0	934.53	0.990	92.9064
8. $^{93}Nb(n,\alpha)^{90m}Y$	3.19 h	1.0	202.5	0.966	92.9064
9. $^{197}Au(n,2n)^{196}Au$	6.183 d	1.0	355.58	0.87	196.9665
10. $^{27}Al(n,\alpha)^{24}Na$ *	15.02 h	1.0	1368.6	1.0	26.98154

* Monitor Reactions

* Data are taken from Table of Radioactive Isotopes.

Table 2 Results of Cross Section Measurements

Reaction	Cross Section (mb) 9.1 MeV	11.1 MeV
1. $^{48}Ti(n,p)^{48}Sc$	26.0 ± 2.1	--------
2. $^{51}V(n,\alpha)^{48}Sc$	4.9 ± 2.0	9.1 ± 1.2
3. $^{56}Fe(n,p)^{56}Mn$	58.0 ± 5.0	93.9 ± 4.8
4. $^{59}Co(n,\alpha)^{56}Mn$	12.8 ± 1.8	20.0 ± 1.5
5. $^{64}Zn(n,p)^{64}Cu$	287 ± 30	232 ± 18 a)
6. $^{90}Zr(n,p)^{90m}Y$	2.1 ± 2.9b)	6.8 ± 2.0
7. $^{93}Nb(n,2n)^{92m}Nb$	---------	243. ± 26
8. $^{93}Nb(n,\alpha)^{90m}Y$	2.3 ± 1.1	3.0 ± 0.7
9. $^{197}Au(n,2n)^{196}Au$	379 ± 40	1680 ± 100
10. $^{27}Al(n,\alpha)^{24}Na$ *	73.83	109.06

*; Monitor Reaction: Cross section data are refered from IRDF-90

a); Treatment of background subtraction is insufficent. Further investigation is needed by taking neutron spectum into accounts.

b); Poor statistics gives only an upper limit of this cross section.

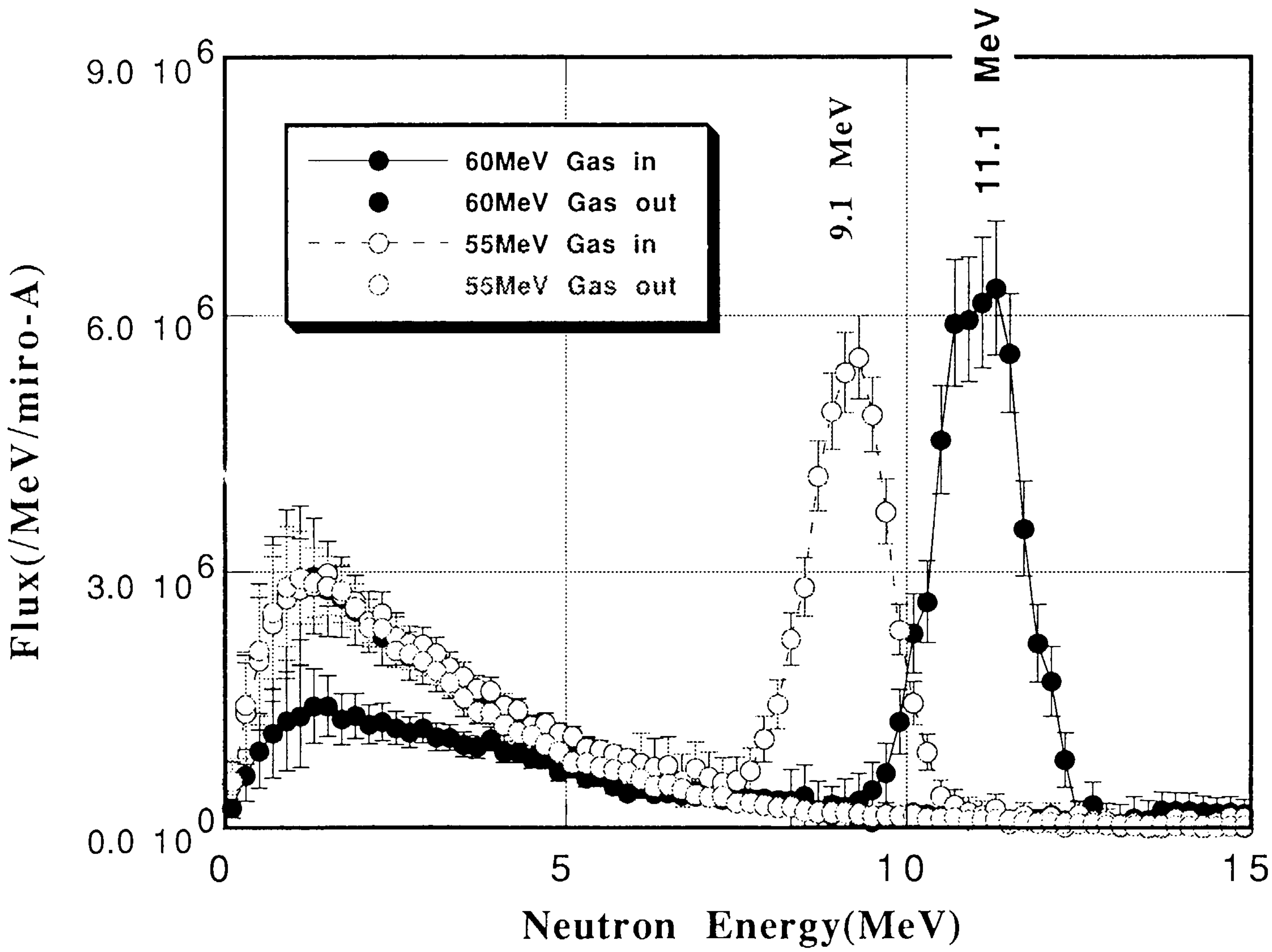

Fig. 1 Energy Spectra of $^{1}H(^{11}B,n)^{11}C$ Neutron Source at 0° Direction Measured by TOF

B. Nuclear Data Center and Working Groups of Japanese Nuclear Data Committee

II-B-1 Integrated Nuclear Data Evaluation System

T. Fukahori and T. Nakagawa

Nuclear data evaluation must be done by using experimental data and by means of many complicated theoretical calculations with various basic data such as optical potential parameters, level density parameters, and level scheme. Integrated Nuclear Data Evaluation System (INDES) is being developed to support the evaluation work. Roughly classified, the INDES functions are of three categories, which are to retrieve basic data described above, to set up input data of theoretical calculation codes automatically, and to select the most suitable set of theoretical calculation codes applying knowledge engineering technology.

Parameters to be used in theoretical calculations are stored in Evaluation Data Files (EVLDF). The parameters provided in EVLDF are optical potential parameters of nuclei, information of excited levels, level density parameters, basic information of nuclei, etc. Existing evaluated nuclear data are stored in magnetic disks of a large computer system in JAERI. Their MAT numbers, data-set names, etc. are stored in an index file of the evaluated data. Experimental data on the neutron induced reactions are stored in NESTOR-2 system by receiving them from the NEA Data Bank and by converting their format from EXFOR. On the nuclear structure data, one can access Evaluated Nuclear Structure Data File (ENSDF).

INDES consists of several FORTRAN programs called as segments interactively executed by calling them with TSS command procedures from the root segment. A group of segments supplies evaluators with useful information for nuclear data evaluation from the databases mentioned above. One segment was prepared for retrieval of parameters stored in EVLDF. Since theoretical calculations take a long CPU time, we have to submit batch jobs for the calculations. The input data and JCL for the theoretical calculation codes are semi-automatically produced in the JCL set-up segments. INDES requires only limited number of input such as atomic and mass number, name of a parameter set, energy points.

In order to use INDES effectively, a prototype of nuclear data evaluation guidance system (ET; Evaluation Tutor)[1] was produced by applying knowledge engineering technology. ET supports users in selecting a set of suitable theoretical calculation codes. The codes considered in ET are DWUCKY[2], ECIS[3], JUPITOR[4], CASECIS[5], EGNASH[2], TNG[6], PEGASUS[7], ALICE-F[8], CASTHY[9], ELIESE-3[10], RESCAL[11] and HIKARI[12]. ET consists of an inference engine, frames, a rule-base, two example-bases and calculating modules for certainty factors. The frames store functions of the theoretical calculation codes. The rules stored in the rule-base are used to select the theoretical calculation codes in the inference engine. The two example-bases are used to obtain basic certainty factors of theoretical calculation codes from their frequencies of use. One example-base is created from the experiences of JENDL-3 evaluation work, and another one is a supplementary example-base which stores results of code selection performed by ET.

A flow of ET to select a set of the recommended codes is described below. Firstly, the user inputs the basic data such as a target nucleus, a projectile and the incident energy region. The rules in the rule-base are executed to make a preliminary decision of code selection. All the codes in the frames are classified into four reaction processes. If a process is judged not to need to be considered, the codes corresponding to the process are omitted from the selection. The certainty factors for the codes in each process are calculated on the basis of information in the frames and the example-base. Then, the code having the largest certainty factor is selected as the recommended theoretical calculation code for each reaction process. For the codes requiring other auxiliary codes, the related codes are added to the set of recommended codes. The result of the code selection is stored in the supplementary example-base and is used at the next basic certainty factor calculation.

INDES helps not only beginners of the nuclear data evaluation being unfamiliar with using the theoretical calculation codes but also experienced evaluators to make input data for preliminary calculations. Some segments are planed to be enlarged and several new segments will be produced to make INDES more powerful. The rule-base and codes treated in ET should be expanded to more detailed procedures.

References

1) Fukahori T. and Nakagawa T., JAERI-M 92-027, p.214 (1992).
2) Yamamuro N., JAERI-M 90-006 (1990).
3) Raynal J., IAEA SMR-9/8 (1970).
4) Tamura T., Rev. Mod. Phys., 37, 679 (1965).
5) Computer Program CASECIS for CASTHY-ECIS combined calculations.
6) Fu C.Y., ORNL/TM-7042 (1980).
7) Iijima S., Sugi T., Nakagawa T. and Nishigori T., JAERI-M 87-025, 337 (1987).
8) Fukahori T., Computer Program ALICE-F for medium energy preequiliblium process calculation (1990) unpublished.
9) Igarasi S. and Fukahori T., JAERI-1321 (1991).
10) Igarasi S., JAERI-1224 (1972).
11) Shibata K. and Chiba S., Computer Program RESCAL for R-matrix theory calculations (1987) unpublished.
12) Kitazawa H., Computer Program HIKARI for direct-semidirect capture calculations (1980) unpublished.

II-B-2 Prototype of Evaluation Guidance System in Integrated Nuclear Data Evaluation System

T. Fukahori and T. Nakagawa

A paper on this subject was published in JAERI-M 92-027 (1992) p.214-224 with the following abstract:

Integrated Nuclear Data Evaluation System (INDES) is being developed to keep experiences of nuclear data evaluation for JENDL-3 and to support new evaluations. One of the INDES functions is to set up input data of theoretical calculation codes automatically. In order to use INDES effectively, a prototype of nuclear data evaluation guidance system (E.T.; Evaluation Tutor) was made to help users in selecting a set of suitable theoretical calculation codes by applying knowledge engineering technology. E.T. consists of an inference engine, frames, a rule-base, two example-bases and calculating modules of certainty factors. The inference engine and the calculating modules are written in FORTRAN77.

II-B-3 Evaluation of Nuclear Data in the Medium Energy Region for ^{27}Al

T. Fukahori

Nuclear data in the medium energy region are necessary to many applications, for example, design of spallation neutron sources. However, the evaluation work has never been made, except for those of iron[1], lead and bismuth. The code ALICE-F has been developed to calculate the data of lead and bismuth in the energy range of 1-1000 MeV by modifying the code ALICE-P[1], which has been made by Pearlstein with modification of the code ALICE[2]. In order to check applicability of ALICE-F to calculation for nuclide in light mass region, the calculation of nuclear data for ^{27}Al has been performed. The calculated results of the ^{27}Al(p,x)^{24}Na reaction were almost in good agreement with their experimental data. However more modification might be needed to reproduce all the experimental data better.

References

1) Pearlstein S., J. Astrophys., 346 (1989) 1049
2) Blann M., CODE ALICE/85/300, UCID-20169 (1985)

II-B-4

Reich-Moore R-matrix analysis of neutron transmission and fission cross section of ^{239}Pu in the resonance energy range

Herve Derrien

The resonance parameters of ^{239}Pu were obtained in the energy range from 1 keV to 2.5 keV with the Bayesian code SAMMY[1] by analysing the high resolution transmission measurements of Harvey et al.[2] and the high resolution fission measurements of Weston et al.[3] The resonance parameters obtained at ORNL by a previous analysis[4] in the energy range from thermal to 1 keV, using the 1984 data of Weston et al.[5] as basis for the fission cross section, were up-dated following the renormalization of the fission cross section by Weston et al.[6]

1) The energy range from 1 keV to 2 keV

Preliminary resonance parameters were obtained at ORNL[4] from the analysis of the Harvey thick sample transmission data and of the preliminary results of the 1988 fission measurements of Weston et al. The analysis was restarted at JAERI with a version of SAMMY adapted by T.Nakagawa to the FACOM-M780. The preliminary set of parameters obtained at Oak Ridge was used as prior informations to start the SAMMY calculations. The analysis was performed on the thick and medium sample transmissions of Harvey data and on the 1988 fission data released by Weston at the beginning of 1991. The definitive SAMMY fits were performed after renormalization of the 1988 data of Weston on the ENDF/B-VI standard values[7] between 1 keV and 2 keV, in agreement with the 1991 new measurements of Weston et al.[6]

The average cross-sections calculated from the resonance parameters are compared to the experimental values in Table 1. The calculated fission cross-sections are in very good agreement with the experimental data. There are large differences between the calculated capture cross sections and the experimental data of Gwin et al.[8, 9] averaged over 0.1 keV intervals; but on the interval from 1.0 keV to 2.0 keV the average values are consistent within 1.0%.

2) The energy range from 2.0 keV to 2.5 keV

Compared to the low energy range, more than 90% of the resonances could still be identified in the transmission data between 2 keV and 2.5 keV. Therefore the correlated SAMMY analysis of Harvey transmissions and Weston fission was still feasible in this energy range. The resonance parameters obtained are consistent and have nearly the same statistical properties as those of the resonances in the energy range from 0 to 2 keV. A quite good fit of the transmission and fission data was obtained. However, the calculated fission cross sections were, on average, 1.4% lower than the experimental values. This difference, which is not larger than the systematic errors on the experimental data,could be due to the difficulties of identifying the wide J=0+ resonances in the experimental data, owing to the effects of the increasing resolution and Doppler widths.

The cross sections, calculated from the resonance parameters and averaged over 0.1 keV intervals, are given in Table 2.

3) Renormalization of the data in the energy range from thermal to 1 keV.

A new fission measurement was performed by Weston et al. in 1991 in order to check their 1984 data. A careful normalization of the data in the thermal energy range showed that the 1984 data should be renormalized by about +3%[6]. To take into account this renormalization, the resonance parameters obtained at ORNL in the energy range from thermal to 1 keV[4] were modified in the following way:

a) increase of the fission width by 3% and decrease of the capture width by a quantity equal to the variation of the fission width in the narrow resonances(mainly 1+ resonances); this correction did not change the total cross-section in the corresponding resonances;

b) adjustment of the neutron width of the 0+ resonances by a new fit of the transmission data and of the renormalized Weston et al. 1984 data in energy ranges where the contribution of the 0+ resonances is dominant, and increase of the other(small) 0+ neutron widths by 3%. No severe inconsistency was observed between the transmission data and the new fission data over the dominant 0+ resonances; the differences between the previous fits of the transmission and the new fits were consistent within the experimental error bars.

The fission cross-sections calculated from the new set of resonance parameters are compared in Table 3 with the new results of Weston, the renormalized 1984 data of Weston and the ENDF/B-VI standard values.

REFERENCES

1) N.M.LARSON et al., ORNL/TM-7485, ORNL/TM-9179, ORNL/TM-9719/R1
2) J.A.HARVEY, Nuclear Data for Science and Technology, Mito 1988, page 115
3) L.W.WESTON et al., to be published
4) H.DERRIEN and G. DE SAUSSURE, ORNL-TM-10986(1988)
5) L.W.WESTON et al., Nucl. Sci. Eng., 88, 567(1984)
6) L.W.WESTON, Private communication(1992)
7) A.CARLSON et al., preliminary results(sept. 8 1987)
8) R.GWIN et al., Nucl. Sci. Eng., 45, 25(1971)
9) R.GWIN et al., Nucl. Sci. Eng., 61, 116(1976)

Table 1 Ave:age Cross Section (barn)

Energy keV	Total Calc(a)	Total Exp(b)	Fission Calc(a)	Fission Exp(c)	Capture Calc(a)	Capture Exp(d)
1.0–1.1	24.47	24.95	5.549	5.581	4.728	5.04
1.1–1.2	22.82	23.10	5.985	6.017	3.757	2.95
1.2–1.3	22.29	22.90	4.601	4.501	4.287	4.00
1.3–1.4	22.63	22.85	6.997	6.997	3.012	2.52
1.4–1.5	20.42	20.95	4.041	4.059	3.450	3.57
1.5–1.6	18.30	18.95	2.564	2.613	3.521	3.89
1.6–1.7	21.82	21.90	3.952	3.955	3.833	4.36
1.7–1.8	21.26	21.35	3.400	3.425	4.091	4.37
1.8–1.9	23.76	23.30	5.178	5.187	3.639	3.14
1.9–2.0	18.48	18.90	2.152	2.180	3.205	4.06
1.0–2.0	21.63	21.92	4.442	4.446	3.752	3.79

(a) total, fission and capture cross–sections calculated from the resonance parameters.
(b) experimental total cross–sections obtained from average experimental effective cross–sections.
(c) Weston 1988 high resolution fission cross–sections normalized to ENDF/B–VI standard.
(d) Gwin 1971 data normalized to Gwin 1976 data.

Table 2 Average Cross Sections (barn)

Energy keV	Total Calc(a)	Total Exp(b)	Fission Calc(a)	Fission Exp(c)	Capture Calc(a)
2.0–2.1	17.34	17.30	2.034	2.062	3.223
2.1–2.2	20.27	19.80	2.949	2.999	4.051
2.2–2.3	19.34	19.10	2.357	2.393	3.324
2.3–2.4	21.28	21.20	3.646	3.679	3.640
2.4–2.5	20.03	20.60	3.956	4.024	3.128
2.0–2.5	19.65	19.60	2.989	3.031	3.473

(a) total, fission and capture cross–sections calculated from the resonance parameters.
(b) average total cross–sections obtained from the average experimental effective cross–sections.
(c) 1988 high resolution data of Weston normalized to ENDF/B–VI standard.

Table 3 Average Cross Sections (barn)

Energy (eV)	Calcul	Weston 1991	Weston 1984	Standard
0.010–10.	80.12	79.98		
9–20	94.74	94.91		
20–40	17.52	17.76	17.97	
40–60	50.64	50.90	50.87	
60–100	54.42	54.38	54.33	
100–200	18.63	18.59	18.56	18.66
200–300	17.85		17.89	17.88
300–400	8.31		8.34	8.43
400–500	9.59		9.58	9.57
200–500	11.92	11.93	11.93	11.96
500–600	15.39		15.57	15.86
600–700	4.37		4.30	4.46
700–800	5.51		5.53	5.63
800–900	4.84		4.89	4.98
900–1000	8.33		8.38	8.30
500–1000	7.69	7.73	7.73	7.79
20–1000	13.09	13.11	13.11	

II-B-5

Average neutron total cross section of ^{239}Pu in the energy range from 1 keV to 500 keV

Herve Derrien

The average neutron total cross section of ^{239}Pu were obtained in the energy range from 1 keV to 500 keV from the high resolution transmission measurements performed by Harvey et al. at the Oak Ridge Electron Linear Accelerator(1). In the energy range from 1 keV to 10 keV, the average effective cross sections of three samples were extrapolated to the true total cross section(zero sample thickness). Above 10 keV the self-screening corrections to the effective cross sections of the thick sample were calculated by simulation of the cross sections from the resonance parameters.The results are given with 2% to 4% accuracy in the energy range from 1 keV to 10 keV and with better than 2% accuracy in the energy range above 10 keV. They are particularly useful to meet the needs of accurate experimental data in the energy range from 1 keV to 50 keV.

The results are compared with some other experimental data and with the JENDL-3 and ENDF/B-VI evaluations in Figs. 1, 2 and 3.

This work was published in Journal of Nuclear Science and Technology, 29, August 1992.

References

1) Harvey J.A. et al., Nuclear Data For Science and Technology, 1988, Mito,page 115.
2) Uttley C.A., Internal Report, Harwell (1964).
3) Cabe J. et al., CEA-R-4524 (1973).
4) Poenitz W.P. et al., Nucl. Sci. Eng., 78, 333 (1981).

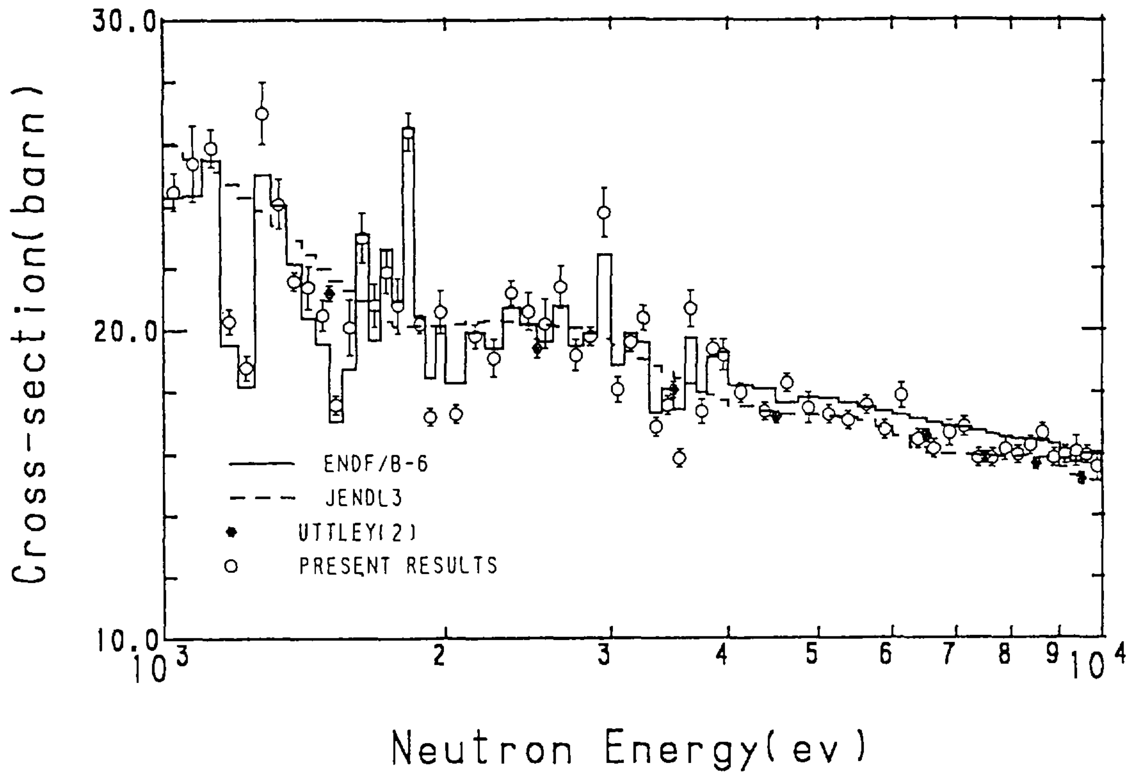

Fig.1 ^{239}Pu total cross section in the energy range from 1 to 10 keV

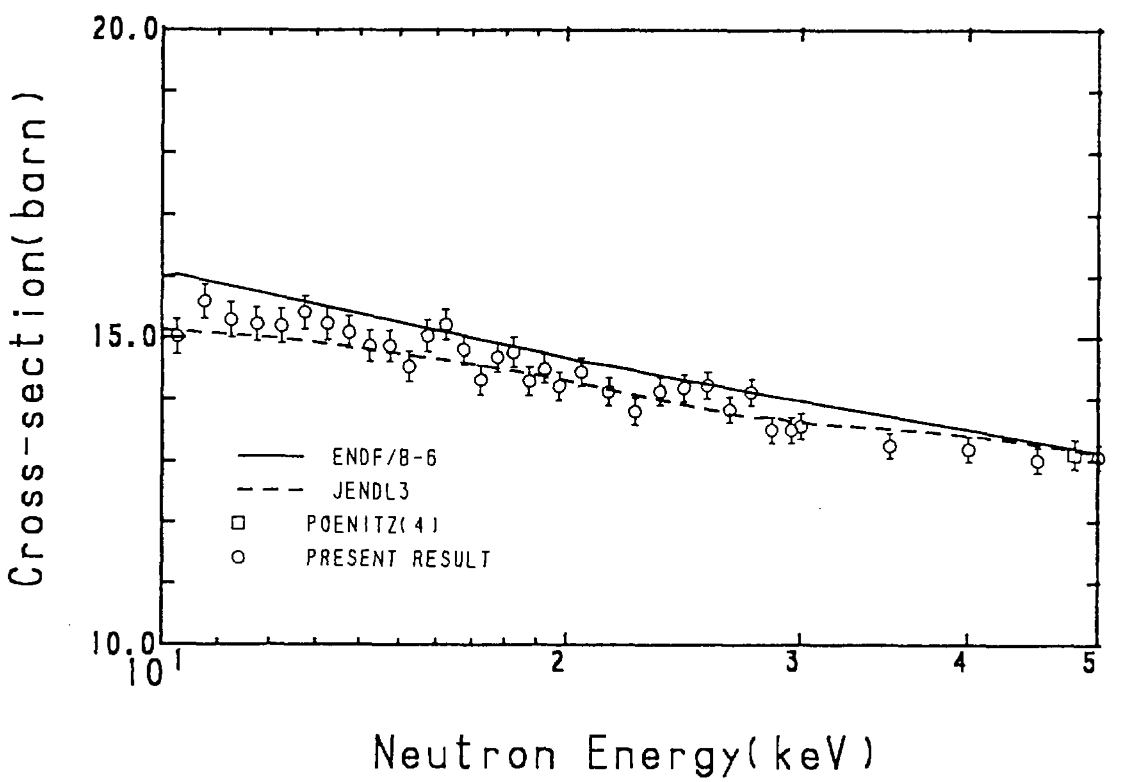

Fig.2 ^{239}Pu total cross section in the energy range from 10 to 50 keV

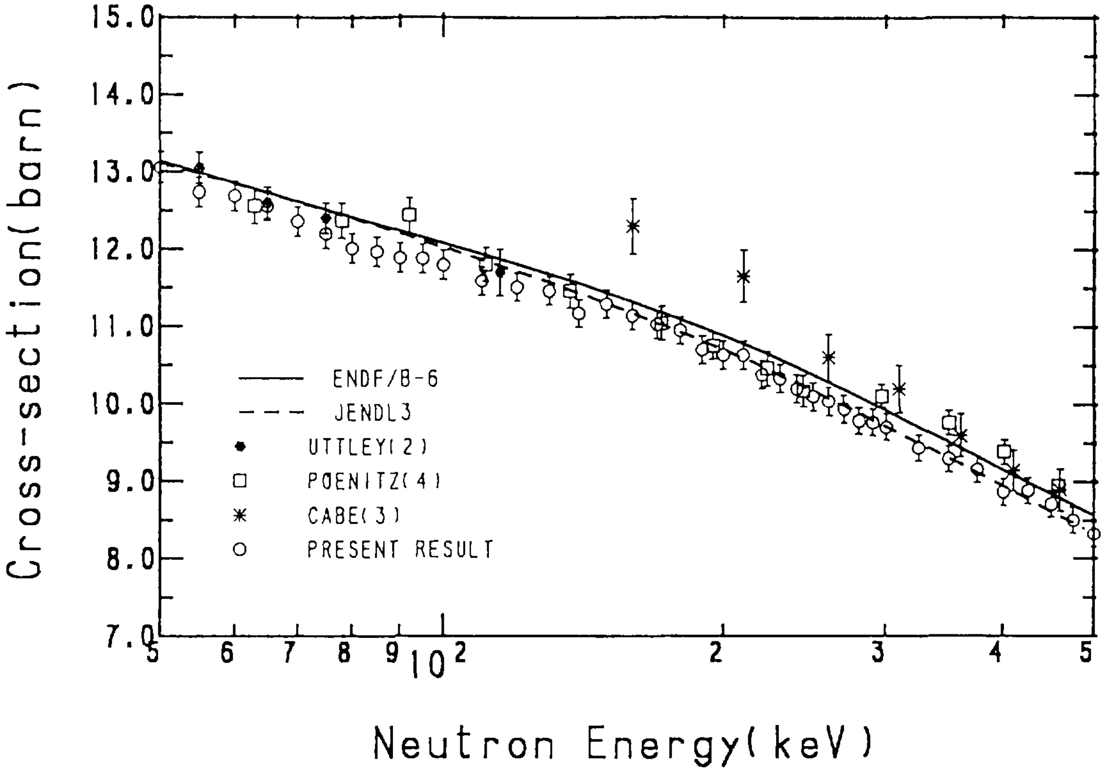

Fig.3 ^{239}Pu total cross section in the energy range from 50 to 500 keV

II-B-6 ALICE-F Calculation of Nuclear Data up to 1 GeV

T. Fukahori

A paper on this subject was published in JAERI-M 92-039 (1992) p.114-122 with the following abstract:

In design of a spallation neutron source and accelerator shielding, medical and space applications etc., medium energy nuclear data are required in the 1-1000 MeV range. Evaluated nuclear data for proton induced reactions in this energy region, however, have not been prepared enough. In this paper, calculations of neutron and proton induced nuclear data for ^{208}Pb and ^{209}Bi have been performed in the energy range from 20 MeV to 1 GeV by using ALICE-F code. A search of the best ALICE-F parameters and options has been carried out. The Pearlstein's systematics for the energy-angular distributions of emitted neutrons was employed. The calculated results are in good agreement with the experimental data.

II-B-7 Comparison of Double-Differential Neutron Emission Cross Sections Calculated from Evaluated Nuclear Data Libraries with Experimental Data

T. Fukahori, S. Chiba and T. Asami*

A paper on this subject was published in JAERI-M 92-053 (1992) with the following abstract:

The energy-angle double differential cross sections of emitted neutrons (DDXs) from neutron induced reactions are fundamental data for fusion neutronics calculation. The third version of Japanese Evaluated Nuclear Data Library (JENDL-3) was produced aiming at the applications related to the fission neutronics as well as fusion reactors. In order to check the reliability of the evaluated data, the DDX data for 32 elements from lithium to uranium calculated from JENDL-3 were compared with experimental data and values calculated from other two major evaluated nuclear data libraries, ENDF/B-VI and JEF-2. The comparison was made at the neutron incident energies of 4.2, 5.4, 6.0, 14.1 and 18.0 MeV, and at the angles of 30°, 60°, 90°, 120° and 150°. It was found that the DDX data calculated from JENDL-3 could reproduce overall trend of experimentally observed values. However, some discrepancies were also recognized.

---

* Nuclear Energy Data Center
Tokai-mura, Naka-gun, Ibaraki, 319-11 Japan

II-B-8 Examination of Various Kinds of Systematics of Double-Differential Particle Emission Cross Sections for Medium-Heavy Nuclei Important to Fusion Neutronics

Baosheng Yu*, Satoshi Chiba and Tokio Fukahori

A paper on this subject was published in Journal of Nuclear Science and Technology 29, pp. 677~689 (1992) with the following abstract:

Various kinds of systematics used to calculate the double-differential light particle emission cross sections from nuclear reactions induced by light particles are examined for medium-heavy nuclei important in fusion neutronics applications. Fixing the incident and outgoing particles to neutrons, and the incident energy at 14 MeV, results calculated by the systematics, supplemented by the statistical model calculations, are compared with experimental data measured by two japanese groups. It is concluded that systematics derived by Kumabe et al. and Kalbach has good accuracy in reproducing these data. Discrepancies in the experimental data are pointed out, and suggestions to future compilations of a special purpose file of JENDL for fusion neutronics are made.

* : Chinese Nuclear Data Center, China Institute of Atomic Energy

II-B-9 Evaluation of the Double-Differential Cross Sections for JENDL Fusion File

Satoshi Chiba, Baosheng Yu* and Tokio Fukahori

A paper on this subject was submitted to the IAEA Research Co-Ordination Meeting on Measurement and Analysis of 14 MeV Neutron-Induced Double-Differential Neutron Emission Cross Sections Needed for Fission and Fusion Reactor Technology (31 March – 2 April, 1992 at Chiang Mai University, Chiang Mai, Thailand), with the following abstract:

In order to improve accuracy of the neutron DDX (double differential cross section) data stored in JENDL-3, preparation of JENDL Fusion File is in progress as a part of post JENDL-3 special purpose file activities. The main effort is placed to adopt the energy-angle correlation of neutrons seen in observed data into the evaluated data library. JENDL Fusion File is also intended to contain the DDX of secondary charged particles, which is required in material damage study as basic data for primary knock-on atom spectra (PKAS) and kinetic energy release in materials (KERMA) calculations. The DDXs are calculated by known systematics, and expressed by a compact form in ENDF-6 format. The multistep statistical model was used to calculate various quantities required in the evaluation.

* : Chinese Nuclear Data Center, China Institute of Atomic Energy

II-B-10

JENDL-3 Fission Product Nuclear Data Library

M. Kawai[1)], S. Iijima[1,a)], T. Nakagawa, Y. Nakajima, T. Sugi, T. Watanabe[2)], H. Matsunobu[3)], M. Sasaki[4)], A. Zukeran[5)]

A paper on this subject was published in J. Nucl. Sci. Technol., 29, 195 (1992) with the following abstract:

Neutron nuclear data in the energy range between 10^{-5} eV and 20 MeV have been evaluated for 172 nuclides from ^{75}As to ^{159}Tb in the fission product mass region to provide data for the JENDL-3 fission product nuclear data library. Evaluation was made on the basis of recent experimental data reported up to 1988 and the nuclear model calculations. Resonance parameters have been evaluated on the basis of measured data set and a REPSTOR system developed in JAERI. The spherical optical model and statistical theory were applied to calculation of the total, capture, elastic and inelastic scattering cross sections, and the multistep evaporation model and pre-equilibrium theory were used for threshold reaction cross section calculations. For the even-even nuclides around fission yield peaks, direct inelastic scattering cross sections were calculated with the distorted wave Born approximation. Nuclear model parameters, such as optical model parameters, level-density parameters, gamma-ray strength functions and Kalbach constant of the pre-equilibrium model were determined so as to give a good agreement between the calculated and measured cross sections. The parameter systematics were obtained as a function of nuclear mass or atomic number. For thermal capture cross sections, a simple relation between measured and calculated cross sections was found as a function of level spacing. The evaluated results were compiled in the ENDF-5 format.

---

1) Toshiba Corp.
a) Deceased November 14, 1990
2) Kawasaki Heavy Industries, Ltd.
3) Sumitomo Atomic Energy Industries, Ltd.
4) Mitsubishi Atomic Power Industries, Inc.
5) Energy Research Laboratory, Hitachi Ltd.

II-B-11

JENDL Gas-production cross section file

T. Nakagawa and T. Narita

The JENDL gas-production cross section file was compiled by taking cross-section data from JENDL-3. The data were given for ^{6}Li, ^{7}Li, ^{9}Be, ^{10}B, ^{11}B, ^{12}C, N, ^{19}F, ^{27}Al, Si, Ti, ^{51}V, Cr, ^{25}Mn, Fe, ^{59}Co, Ni, Cu, ^{75}As, Se, Zr, ^{93}Nb and Mo. Graphs of the cross sections and brief description on the evaluation methods are given in Ref. 1.

Reference

1) (Eds.) T. Nakagawa and T. Narita: "JENDL Gas-production Cross Section File", JAERI-M 92-076 (1992).

II-B-12

Evaluation of JENDL Fusion File

Satoshi Chiba, Baosheng Yu* and Tokio Fukahori

A paper on this subject was published in JAERI-M 92-027 (1992) pp. 35~44 with the following abstract:

In order to improve accuracy of neutron DDX (double differential cross section) related data stored in JENDL-3, preparation of a special purpose file, "JENDL Fusion File", is in progress. ENDF-6 format is adopted for this file, and energy-angle correlation in measured data is taken into consideration. This file contains not only the neutron DDX but also those of charged particles. The latter is needed for material damage estimation. The DDXs are expressed by a compact form calculated from systematics. The multistep statistical model calculation is carried out to provide basic data needed in the systematics calculations.

---

* : Chinese Nuclear Data Center, China Institute of Atomic Energy

II-B-13

Study of Fast Neutron Cross Sections at JAERI Tandem Accelerator

S. Chiba, M. Sugimoto, Y. Ikeda and Y. Yamanouti

A paper on this subject was published in the Proceedings of Beijing International Symposium on FAST NEUTRON PHYSICS (9–13 September 1991 at Beijing, China), Edited by Sun Zuxun et al., World Scientific (1992), with the following abstract:

Using the JAERI Tandem Accelerator, fast neutron cross sections have been measured. In this paper, activities on these neutron cross section measurements are briefly introduced. Firstly, the neutron sources used in the Tandem facility are explained. Then, methods of the experiments and examples of their results are described, placing emphasis on the results in the energy region between 7 and 13 MeV where the $^{1}H(^{11}B,n)^{11}C$ reaction was used as a neutron source.

II-B-14

Neutron Scattering: Technological Achievements and Illustrative Results

S. Chiba, A. Takahashi[a], H. Klein[b] and A. Smith[c]

A paper on this subject was submitted to the International Conference on Nuclear Data for Science and Technology (13–17, May, 1991 at Jülich, Germany), with the following abstract.

Contemporary neutron scattering endeavors (energies ≤ 25 MeV), using monoenergetic sources and the time-of-flight technique, are reviewed. Facilities and techniques are described, with attention to the optimization of measurement systems. Discrete scattering results are illustrated in fundamental and applied contexts. Techniques for and results from continuum neutron emission studies are discussed, with the implications on physical models and on neutron applications in energy systems.

---

a : Osaka University
b : Physikalisch–Technische Bundesanstalt Braunschweig
c : Arognne National Laboratory

II-B-15

Neutron Scattering and Optical Model Potentials of Several Fission Product Nuclei

Satoshi Chiba and Alan B. Smith*

A paper on this subject was submitted to NEANSC Specialists' Meeting on Fission Product Nuclear Data (May 25-27, 1992 at JAERI, Japan), with the following abstract:

Some remarks on the neutron scattering experiments and optical model potentials in the fission product mass region are described. Status on the recent measurements is briefly summarized, and some systematic trends of the empirically determined optical model potential and deformation parameters are addressed. In this mass region, effects of the Z = 50 and N = 50 and 82 magic numbers play an important role in neutron scattering, and those effects are embedded in the phenomenological model parameters. It is shown that blind use of the global parameters will in some cases introduce differences in the calculated total, elastic and reaction cross sections as much as 20%, while for inelastic scattering the differences can be much larger. An example of the application of the dispersion relationship which relates the bound-state shell model potential and the positive energy optical model potential is also presented. Emphasis is placed on neutron scattering from Zr for which the most recent data are available.

* : Engineering Physics Division, Argonne National Laboratory

II-B-16

Data Book for Calculating Neutron Yields from (α,n) Reaction and Spontaneous Fission

H. Matsunobu*, T. Oku*, S. Iijima**
Y. Naito, F. Masukawa, and R. Nakasima***

A data book on this subject was published in JAERI Report 1324 January (1992), (in Japanese) with the following abstract:

Neutron yields from (α,n) reaction and spontaneous fission, which are very important in analyzing radiation shielding of spent fuel storage, transport, and safe handling, were collected and evaluated to determine the recommendable values. For thick target neutron yields from (α,n) reactions, the most accurate data of West and Sherwood, the newest evaluated data of Heaton et al., and the data of high atomic number nuclides evaluated by Nakasima were adopted. And the experimental data at a high energy region of Stelson and McGowan were also used as references. The data for estimating neutron yields of unmeasured elements are also prepared in this Data Book by using theoretical values of (α,n) excitation function and the evaluation formulas on stopping power by Ziegler. For neutron yields from spontaneous fission, the values recommended by S. Raman were mainly adopted. Neutron energy spectra of (α,n) reaction and spontaneous fission were also included in this Data Book. Neutron production data of compounds can be obtained by using the neutron yield and stopping power of each single element.

The present work was performed as a part of activities of the Working Group on Evaluation of Nuclides Generation and Depletion in Japanese Nuclear Data Committee.

Japan Atomic Energy Research Institute
* Sumitomo Atomic Energy Industries, Ltd.
** Toshiba, Ltd.
*** Hosei University

III. Kinki University

A. Atomic Energy Research Institute

III-A-1

Methods and Results of Evaluation of Nuclear Data for Thorium Cycle Development

Takaaki Ohsawa and Toshikazu Shibata

A paper on this subject was published in the *Proceedings of the Indo-Japan Seminar on Thorium Utilization* (Dec. 1991), pp.197-203, Indian Nuclear Society and Atomic Energy Society of Japan, with the following abstract:

The nuclear data for nuclides required for thorium fuel cycle development were evaluated. New method of calculation was developed to analyze the neutron inelastic scattering cross sections and angular distributions. This method combined the coupled-channel theory and the Hauser-Feshbach formalism to treat the direct and compound inelastic scattering in a unified way. The asymmetric distorted-wave approximation was used to estimate the direct component for the moderately coupled states. Present status and problems to be solved of the nuclear data relevant to thorium cycle are also briefly reviewed.

III-A-2 Theoretical Models for Calculation of Fission Neutron Spectra

Takaaki Ohsawa

A paper on this subject was published in the *Proceedings of the 1991 Symposium on Nuclear Data*, JAERI-M 92-027 (March, 1992), pp.82-97, with the following abstract:

Progress in the theoretical calculation of the fission neutron spectra is reviewed with emphasis on recent developments.

New developments in the study of theoretical models to describe the neutron emission from fission fragments have been made during the last ten years. The models are grouped into three categories: *(1)* Approximate statistical models, such as Madland-Nix model; *(2)* Cascade evaporation models, as proposed by Märten and Seeliger, and also by Hu and Wang; *(3)* Hauser-Feshbach-type models, as proposed by Browne and Dietrich and refined by Gerasimenko *et al.*

In this review, the essential features of these models are outlined, and relevant problems of each model are discussed. Some recent attempts of improvement of the Madland-Nix model, including that proposed by the present author, are also mentioned.

B. Department of Reactor Engineering

III-B-1

Measurements and Calculations for Correction Factors of Cascade Gamma Coincidence Summings of a 60 ml Ge Detector

O. Horibe and Y. Mizumoto

A paper on this subject was published in J. of Faculty of Sci. and Tech., Kinki Univ. No. 27, (1991) 27-38 with the following abstract:

The correction factors for cascade gamma sources at the source-detector distances specified are obtained from the measurements and probability calculations. These obtained two values are shown to be in good agreement with each other. Correction factors are also calculated for cascade gammas of several nuclides which are useful for our cross section measurements. In Appendix, counting losses of photo peak areas due to random coincidence summings of gammas incident on the detector are measured as a function of incident intensity of the gammas to distinguish the losses from those in the measurements. Total detection efficiencies of the detector are also measured, which are needed for the probability calculations.

IV. Kyoto University

A. Department of Nuclear Engineering

IV-A-1

Measurement of Fission Cross Section of ^{237}Np in Resonance Region with Lead Spectrometer

I. Kimura, A. Yamanaka*, S. Kanazawa, K. Kobayashi**,
S. Yamamoto**, Y. Nakagome**, Y. Fujita**, T. Tamai**

A paper on this subject was presented at the International Seminar on Interaction of Neutrons with Nuclei held at Dubna, Russia in April 1992 and will be submitted to J. Nucl. Sci. Technol soon.

Among several transuranium actinides produced by power reactors, ^{237}Np is thought to be one of the most burdensome ones, because of its large production rate in a reactor, very long half life and alpha activities in its decay chain. In order to transmute ^{237}Np to nuclides with much shorter half lives, it is proposed to use its fission reaction ^{237}Np(n, f).

The cross section for the ^{237}(n, f) reaction above its threshold energy is practically sufficient enough to evaluate a transmutation system of ^{237}Np. However there exists large discrepancy in the cross section data for this reaction below its threshold energy. Jiacoletti et al. and Hoffman et al. measured it by the neutrons from Physics 8[1) 2)] and Plattard et al. did with an electron linear accelerator[3)]. However the data by the former two are about 3 times larger than those by the latter. In two newly evaluated data files, JENDL-3[4)] and ENDF/B-VI[5)], the data are close to those of the latter.

Making use of a lead neutron slowing-down spectrometer combined with an electron linear accelerator and back-to-back type double fission chambers, we measured the cross section of the ^{237}Np(n, f) reaction normalized by that of the ^{235}U(n, f) reaction from a few eV to about 7 keV with energy resolution of about 40%. The experimentally obtained result is compared with JENDL-3 and ENDF/B-VI and with the previously measured data by Hoffman et al. and by Plattard et al., as shown in Figs. 1 and 2. Although the shape of the cross section curves of JENDL-3 (below 130 eV), of ENDF/B-VI and of the Plattard et al.'s data satisfactorily agree with that of present measured one, the absolute value of all of these three data is about one third of the present result. On the contrary, the data by Hoffman et al. is close to the present result absolutely.

Present result is still preliminary and will be finally reexamined very soon.

---

* Present Address: Hitachi Ltd.
** Research Reactor Institute, Kyoto University

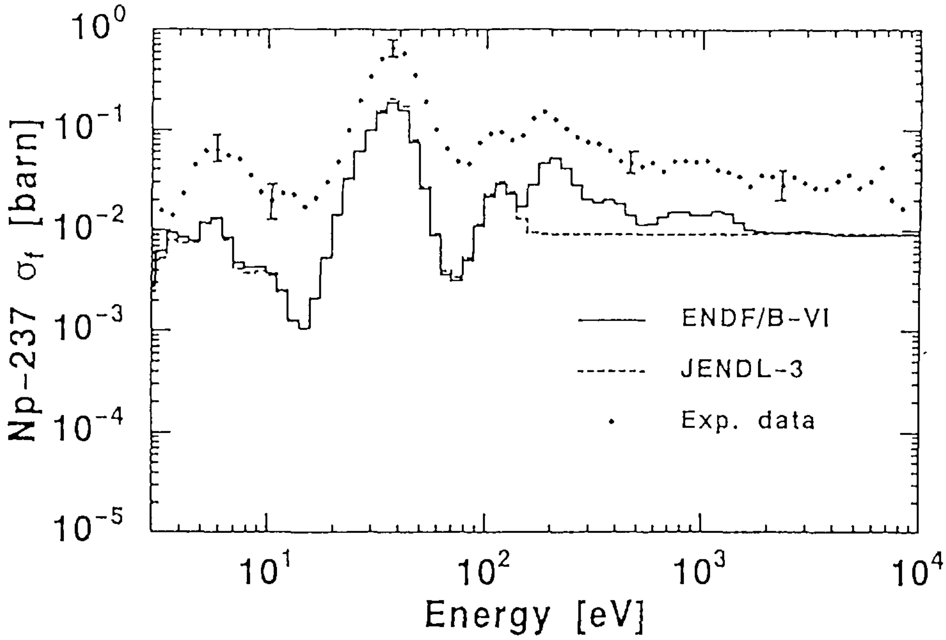

Fig. 1 Fission cross section of Np-237 (1)
(Present result compared with JENDL-3 and ENDF/B-VI).

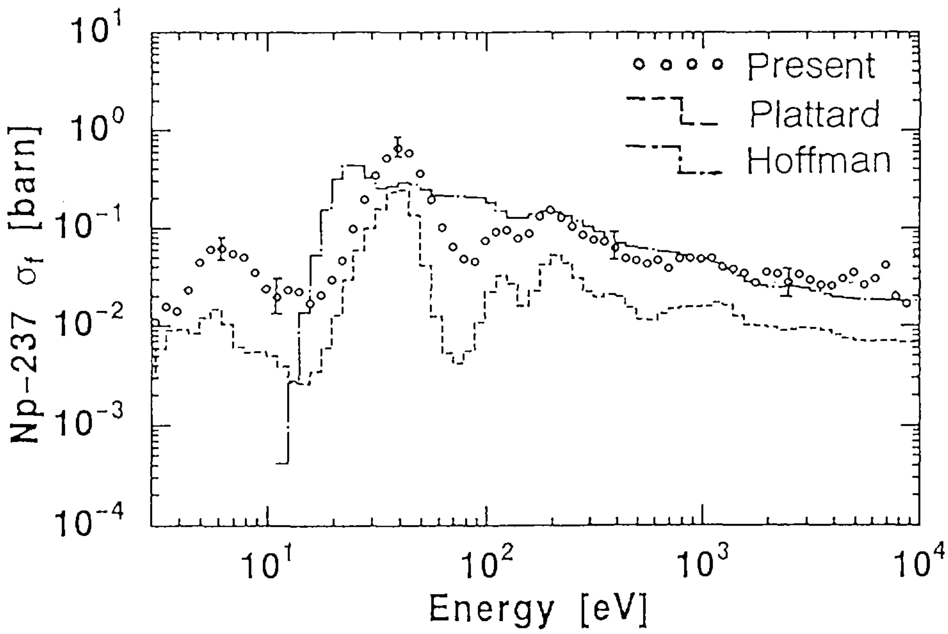

Fig. 2 Fission cross section of Np-237 (2)
(Present result compared with earlier experimental data).

References:

1)R. J. Jiacoletti and W. K. Brown, Nucl. Sci. Eng., 48 (1972) 412.

2)M. Hoffman, et al., Bull. American Phys. Soc., 21 (1976) 655 (Their data are recorded in EXFOR tape).

3)S. Plattard, et al., Nucl. Sci. Eng., 61 (1976) 477.

4)K. Shibata, et al., JAERI 1319 (1990).

5)R. F. Rose (ed.), BNL-NCS-17541 (4th ed.) (1991).

IV-A-2

Measurement of (n,Xγ) Cross Sections of Iron for Neutrons up to 33 MeV

E.Tanabe, K.Shin and T.Nakamura*

1 Introduction

There are increasing number of applications of accelerators to variety of fields such as medical therapy, radioactive waste incinerations, spallation radiation sources, and so on. In these facilities, energies of induced and applied radiations are rather higher than those in fission and fusion reactors. Among these radiations, neutrons play important roles. However, measured data of neutron cross sections are rare at the energies above fusion energy.

In this report, measurement of gamma-ray production cross sections of iron was made for neutrons up to 33 MeV.

2 Experimental Method

The experimental layout is shown in Fig.1. An AVF cyclotron at CYRIC, Tohoku university was used in the experiment. White neutrons were produced by (p,n) reactions with a 20-mm thick Be target, which was bombarded by 35-MeV proton beam from the cyclotron. And an iron sample of 2-cm thickness and 20-cm$\times$20-cm cross section area was in the neutron beam. Neutron spectrum at the sample position was obtained by the time of flight method using a 3-inch diameter by 3-inch length NE-213 scintillator at the place of iron sample. Gamma rays produced in the iron sample by neutrons were observed by a 2-inch diameter by 1-inch length BGO scintillator.

3 Data Analysis

3.1 Response Function of the BGO Scintillator

Response functions of the BGO scintillator were calculated by the Monte Carlo method by the EGS4 code. Calculations were made at intervals of 0.25 MeV at energies below 2 MeV, 0.5 MeV at 2 MeV to 10 MeV, 1.0 MeV at 10 MeV to 30 MeV, and 2.0 MeV at 30 MeV to 50 MeV. These intervals are determined by considering the resolution of the scintillator and electronics system. Calculated result was arranged into a 54$\times$54 square matrix.

3.2 Analysis of Neutron Spectrum

Neutron data of the NE-213 were obtained by discriminating against gamma-ray data based on the difference in the rise time, using contour plots of pulse height vs. rise time like one in Fig.2. Right part to the solid line in the figure, corresponds to neutrons which have slower rise time than gamma-rays. Neutron flight-time signals which were tagged by the rise-time discrimination were converted to neutron energy spectrum using the detector efficiency. Thus obtained spectrum is shown in Fig.3.

*Cyclotron Radio Isotope Center, Tohoku Univ.

3.3 Analysis of Gamma-ray Spectrum

Neutron time spectrum was bunched into bins, for each of which gamma-ray pulse height distributions were obtained by the BGO scintillator. The neutron energy bin width is 3 MeV which is enough to eliminate statistical errors. Using the response matrix previously described, the pulse height data were unfolded with the FERDO code to gamma-ray spectra, where the pulse height distribution was calibrated by gamma-rays from Am-Be and ^{137}Cs sources.

3.4 Gamma-ray Production Cross Sections

Using neutron spectrum $\Phi(E)$, and corresponding gamma-ray spectrum $\phi(E')$ obtained above, gamma-ray production cross section $\sigma(E, E')$ is described by Eq.(1),

$$\sigma(E, E') = \Phi(E)\eta_n\eta_\gamma NV/\phi(E'), \tag{1}$$

where N is the atomic density, V is the volume of iron sample, and η_n, η_γ are corrections for neutron and gamma-ray attenuation in the iron sample, respectively.

When a gamma ray is generated in the sample at depth x, attenuation of gamma ray is described as $e^{-\mu x}$ with linear attenuation coefficient μ. Then η_γ is given by Eq.(2),

$$\eta_\gamma = \frac{1}{l}\int_0^l e^{-\mu x}\mathrm{d}x, \tag{2}$$

where $l = l_0/\cos\theta$,l_0 is the thickness of the sample, and θ is the angle of the BGO scintillator with respect to the neutron beam axis.

Attenuation of neutron was assumed to be caused only by non-elastic scattering. When $\phi_n(x)$ is neutron flux in the sample at depth x, $\phi_n(x)$ is described as $\phi_n(x) = \phi_n(0)e^{-Nx\sigma_{non}}$, where σ_{non} is non-elastic scattering cross section. Then η_n is given by Eq.(3),

$$\eta_n = \frac{1}{l_0}\frac{1}{N\sigma_{non}}\left(1 - e^{Nl_0\sigma_{non}}\right). \tag{3}$$

4 Results

Typical examples of the measured differential gamma-ray production cross sections are shown in Figs.4 and 5, and integrated gamma-ray yield above $E_\gamma = 1.5$ MeV in Fig.6. At lower neutron energies, where other data exist, our results give good agreement within statistical errors to those of Dickens et al.[1] and Chapman et al.[2]. Also these data agreed fairly well with calculated data by Young[3] at energies up to 33 MeV.

References:

1)Dickens et al., *NSE 50*, 311-336(1973)

2)Chapman et al., *ORNL-TM-5416*, ORNL(1976)

3)P.Young, private communication

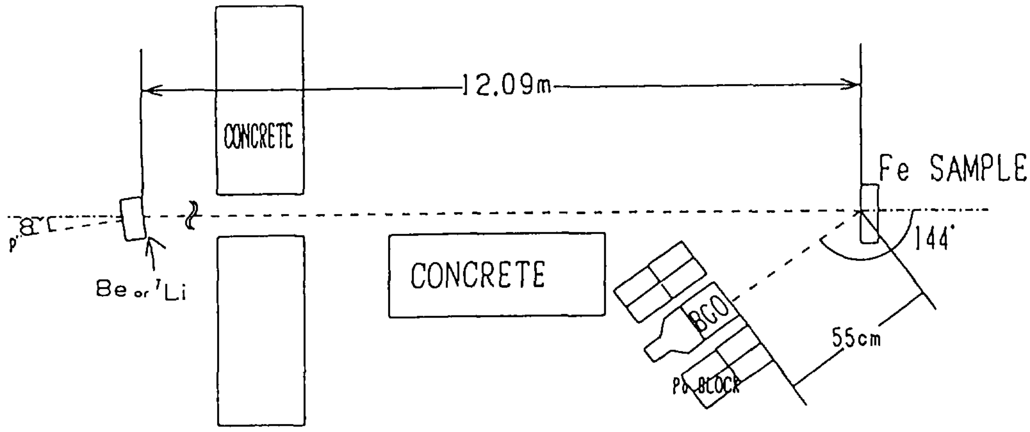

Fig.1 Experimental arrangement for measuring neutron induced gamma-ray from iron sample by BGO spectrometer.

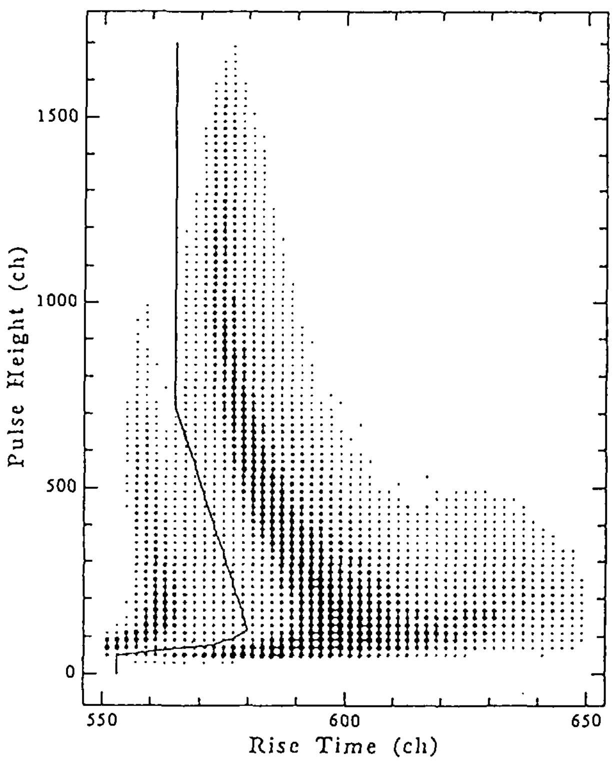

Fig.2 Two dimensional plot of pulse height vs. rise time in NE-213 bombarded by neutrons from 20mm thick Be target

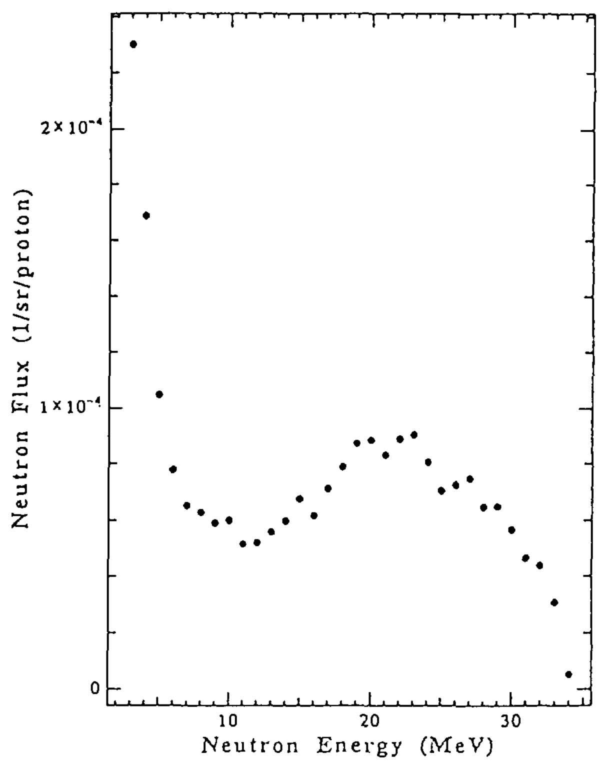

Fig.3 Emitted neutron spectrum from 20mm thick Be target bonbarded by 35MeV proton

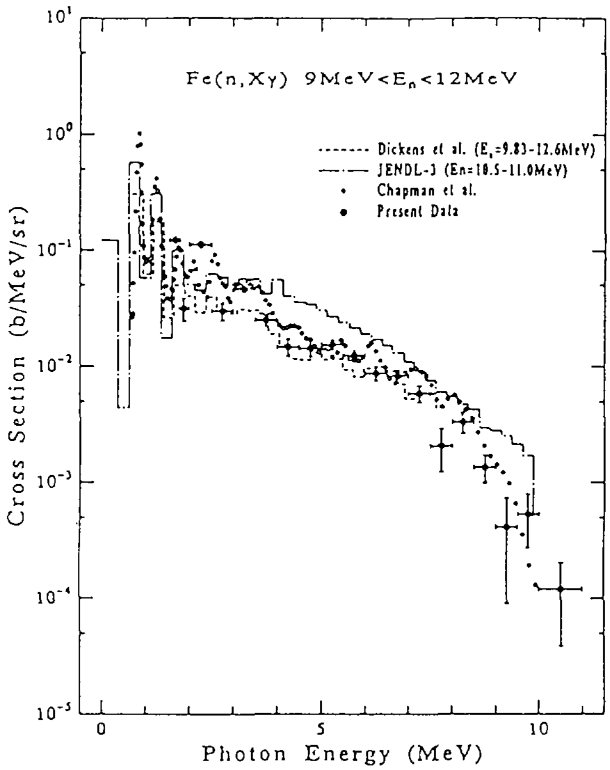

Fig.4 Differential cross section for neutron energy between 9 and 12MeV

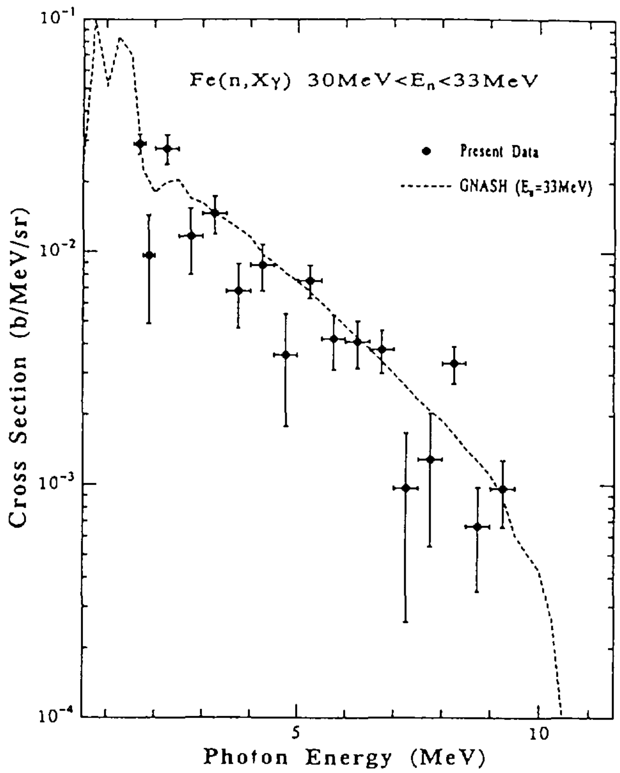

Fig.5 Differential cross section for neutron energy between 30 and 33MeV

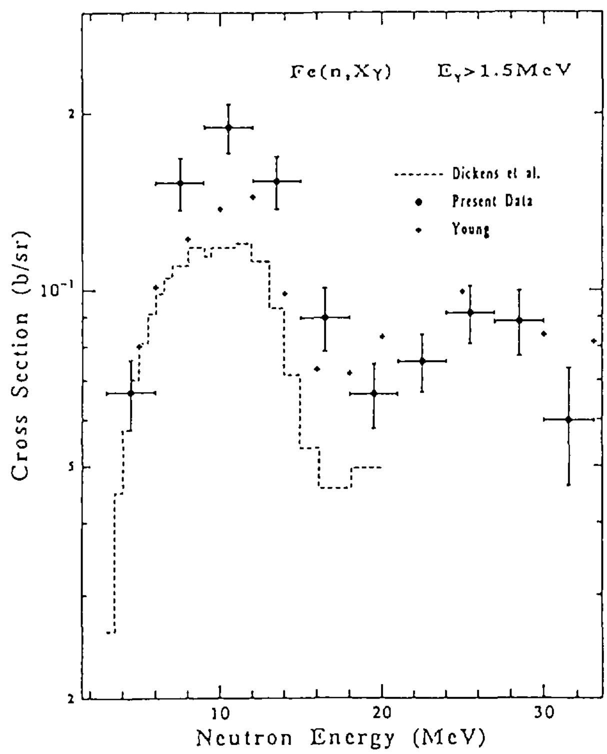

Fig.6 Total gamma-ray production cross section for gamma ray energy above 1.5MeV

B. Research Reactor Institute

IV-B-1 Gamma-Rays and Half-Life of ^{157}Pm

T. Sharshar, K. Okano, Y. Kawase and S. Yamada

The identification of the nuclide ^{157}Pm has previously been reported[1,2]. As the beam intensity of KUR-ISOL has increased recently, precise measurements of the half-life of ^{157}Pm and γ-rays following its decay have been carried out using a $4\pi\beta$-γ coincidence system[3] to suppress room backgrounds. In this system, an ORTEC $491mm^2$ planar LEPS and a $230cm^3$ CANBERRA HPGe detector were used for X- and low-energy γ-rays and for higher-energy γ-rays, respectively. In addition to the β-gated spectra, γ-singles spectra were also recorded simultaneously for intensity determination. The source-to-detector distance was 1.2 and 2.0cm for the LEPS and the HPGe detector, respectively. The energy calibration was performed using sources of ^{241}Am, ^{152}Eu, ^{137}Cs, ^{60}Co and ^{57}Co. The decay rates of β-gated X- and γ-rays were determined by analyzing 16 spectra taken at 0.5s time interval.

As an example, the β-gated γ-ray spectrum measured at mass 157 as obtained with LEPS is shown in Fig. 1. Altogether, thirty γ-rays associated with the decay of ^{157}Pm have been identified as listed in Table 1. As no definite decay scheme is not yet known, coincidence-summing correction for the relative intensity could not be applied. But this is possible in future when the decay scheme is clarified. By taking the average of the half-lives of Sm K X-rays and several strong γ-rays (see Table 1), the half-life of the ^{157}Pm was determined as 10.66(16)s.

In the present experiments, thirteen new γ-rays were observed in the decay of ^{157}Pm, as Greenwood et al. reported[1] that some seventeen γ-rays could be associated with its decay although energy values of only four γ-rays were given (see Table 1).

References:

1) R. C. Greenwood, R. A. Anderl, J. D. Cole and H. Willmes: Phys. Rev., C35, 1965,(1987).

2) R. C. Greenwood, R. A. Anderl, J. D. Cole, M. A. Lee and H. Willmes: AIP Conf. Proc. 164, ed. I. S. Towner, p782, Amer. Inst. Phys., New York (1988).

3) T. Sharshar and K. Okano, Annu. Rep. Res. Reactor Inst. Kyoto Univ., 25, (1992).

Table 1. Energies, relative intensities and half-lives of Sm K X-rays and γ-rays following the decay of ^{157}Pm.

Present results			Ref.1)	Refs.1,2)
Energy (keV)	Relative intensity [a]	$T_{1/2}$ (s)	Energy (keV)	$T_{1/2}$ (s)
Sm K_α	3229 (170) [b]	10.8 (4)		
Sm K_β	810 (50) [b]	12.0 (15)		
52.5 (1)	298 (15) [b]	12.0 (20)	52.6	
73.3 (1)	105.9(45) [c]			
108.2 (1)	244 (19) [d]	11.7 (17)	108.2	
132.1 (1)	135 (12) [d]			
160.5 (1)	4161 (150) [d]	10.69 (20)	160.5	
163.9 (1)	444 (15) [d]	9.6 (12)		
180.6 (2)	117 (18) [d]			
188.0 (1)	1000	10.15 (60)	187.9	
209.7 (1)	172 (15)			
222.8 (2)	139 (17)			
258.4 (1)	112 (14)			
265.5 (1)	285 (23)			
296.1 (1)	524 (33)	9.4 (12)		
300.4 (2)	41.7(24) [e]			
348.4 (2)	169 (13)			
418.4 (3)	50 (14)			
430.3 (2)	72 (22)			
495.5 (1)	228 (13)			
518.7 (1)	340 (17)	10.7 (10)		
568.8 (1)	262 (15)			
571.1 (1)	513 (23)	10.5 (8)		
641.8 (2)	160 (19)			
721.9 (2)	142 (19)			
783.6 (1)	154 (16)			
850.4 (1)	371 (21)	11.8 (12)		
856.5 (2)	55 (14)			
868.0 (2)	66.4(49) [e]			
1073.1 (1)	329 (31)			
1117.3 (3)	58.7(43) [e]			
1369.3 (2)	196 (21)			
		10.66 (16) [f]		10.90 (20) [g] 10.50 (12) [h]

a) Calculated from singles spectra taken with a 230 cm^3 HPGe detector, except the values noted as b)-e).
b) Calculated from singles spectra taken with a LEPS.
c) The weighted average of values calculated from β-gated spectra taken with the LEPS and the 230 cm^3 HPGe detector.
d) The weighted average of values calculated from singles spectra taken with the LEPS and the 230 cm^3 HPGe detector.
e) Calculated from β-gated spectrum taken with the 230 cm^3 HPGe detector.
f) The weighted average of listed half-lives of Sm K X-rays and γ-rays.
g) From ref.1.
h) From ref.2.

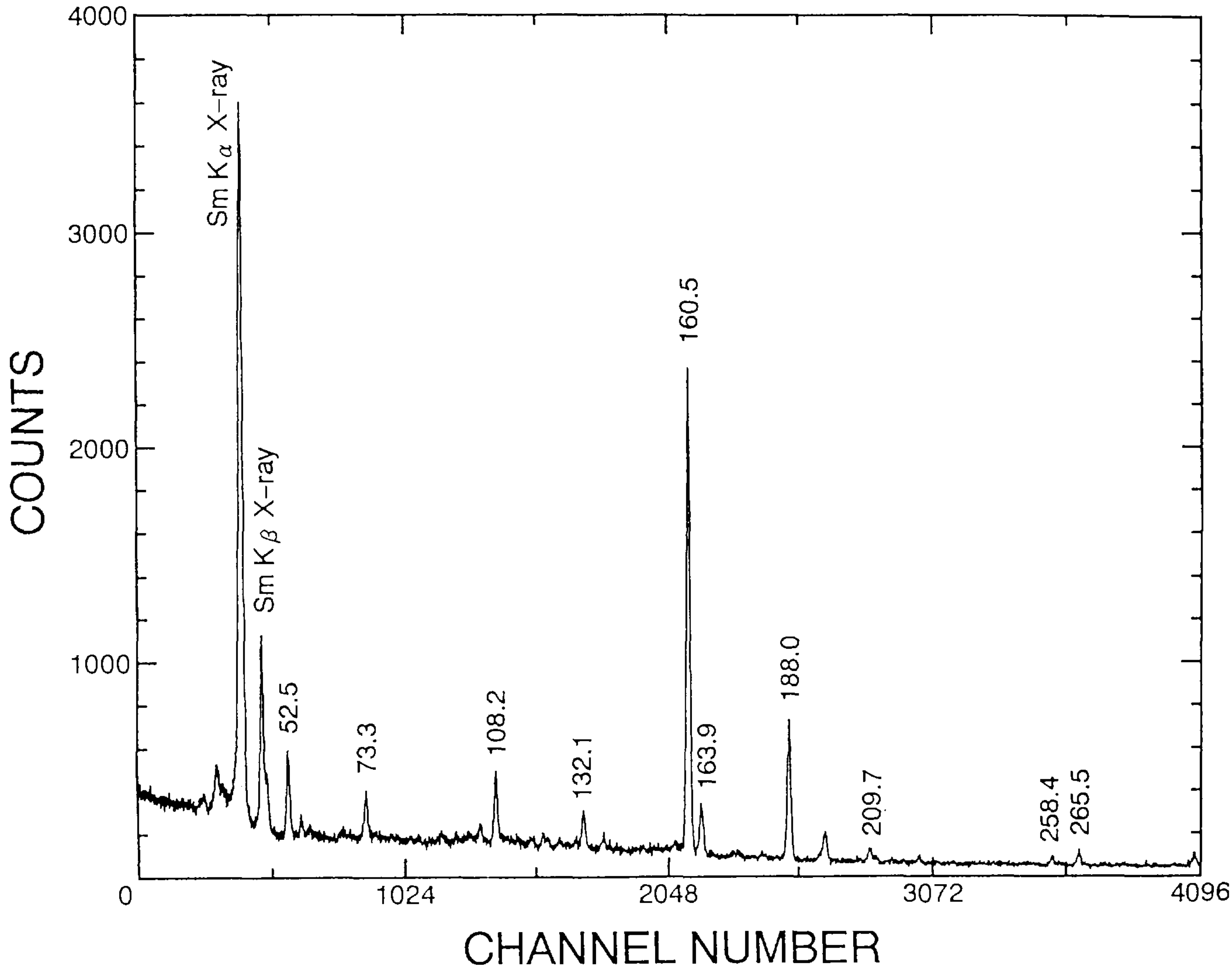

Fig. 1. Beta-gated γ-ray spectrum observed at mass 157. The lines assigned to originate from the decay of ^{157}Pm are indicated. All energies are in keV.

V. Kyushu University

A. Department of Physics

V-A-1

Band Structure of ^{81}Y

S.Mitarai, T.Kuroyanagi, A.Odahara, J.Mukai H.Tomura, S.Suematsu, D.Jerrestam[1], J.Nyberg[1], G.Sletten[1], A.Atac[1], S.E.Arnell[2], H.A.Roth[2] and O.Skeppstedt[2]

Improved Si Ball[1)] have been used in NORDBALL[2)] experiments. The NORDBALL spectrometer with 20 ACS Ge detectors in conjunction with Si Ball and Neutron Wall[3)] provided a new section far from beta- stabity line because of high quality for channel selection and high detection efficiency. Systematic trend of neutron deficient nuclei in the A=80 region where protons and neutrons occupy the same orbit, can provide important information about the p-n interaction and shape-driving forces of the g9/2 orbitals.

Experiments were carried out using ^{58}Ni targets and projecticles of ^{28}Si and ^{32}S at beam energies from 110 to 128 MeV. As a part of the studies in the A=80 region, ^{81}Y was populated by the reactions $^{58}Ni(^{28}Si,\alpha p)$ and $(^{32}S,2\alpha p)$ with the partial cross sections below 10 mb. Dynamic moment of inertia(fig.1) for ^{81}Y shows a peak around $h\omega$=0.68 MeV where alignment gain(fig.2) is about 4h. In the ^{80}Sr core, the first upbend appeares at a frequency of 0.55 MeV and has been interpreted as caused by the alignment of the g9/2 proton pair. However, as the odd proton blocks the proton alignment, the second upbend in ^{80}Sr at a frequency above $h\omega$=0.7 MeV corresponds to the alignment in ^{81}Y and is due to the alignment of g9/2 neutron pair. An N=42 isotone ^{79}Rb has a peak at $h\omega$=0.6 MeV and its core ^{78}Kr has the second upbend around $h\omega$=0.88 MeV.

This large shifts in frequencies for νg9/2 alignment in ^{79}Rb indicate shape changes and is differnt from one in ^{81}Y. The data analysis of ^{81}Y is stll in progress.

---

[1]Niels Bohr Institute, Kopenhagen University, Riso , DK-4000, Roskilde, Demmark
[2]Department of Physics, Chalmers University of Tec hnology, S-412 96 Gothenberg, Sweden

References
1)T. Kuroyanagi, S. Mitarai, S. Suematsu, B.J. Min, H. Tomura, J. Mukai, T. Maeda, R. Nakatani, G. Sletten, J. Nyberg and D. Jerrestam, Nucl. Instr. and Meth. A316(1992) 289
2)G. Sletten, J. Gascon and J. Nyberg, Proc. Int. Conf. on the spectroscopy of Heavy Nuclei, Crete, Greece, 1989, Inst. Phys. Ser. 105 (1989)
3)S.E. Arnell, H.A. Roth, O. Skeppstedt, J. Bialkowski, M. Moszynski, D. Wolski and J. Nyberg, Nucl. Instr. and Meth. A300 (1991) 303

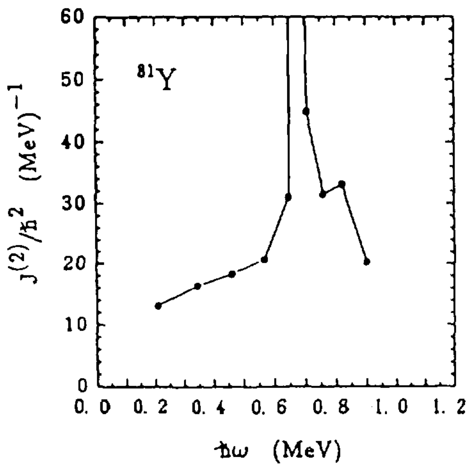

Fig.1 Dynamic momemt of inertia

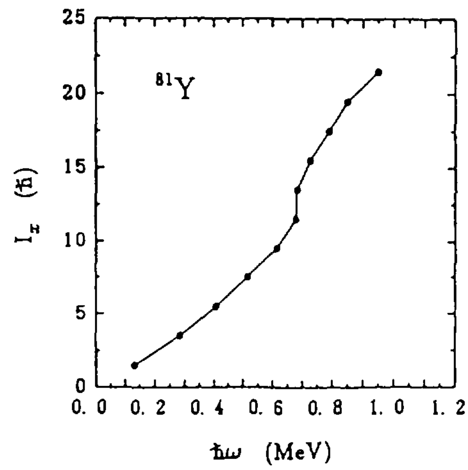

Fig.2 Aligned angular momentum

V-A-2

A Rotational Band in ^{82}Zr

S. Mitarai, T. Kuroyanagi, A. Odahara, J. Mukai, H. Tomura, S. Suematsu,
D. Jerrestam[1], J. Nyberg[1], G. Sletten[1], A. Atac[1], N. Gjørup[1], J. Jongmann[1], S. E. Arnell[2], H. A.Roth[2], and Ö. Skeppstedt[2].

A paper on this subject has been submitted to **Zeitschrift für Physik A**.

Abstract

The neutron deficient nucleus ^{82}Zr has been studied through the reaction ^{58}Ni(^{28}Si,2p2n)^{82}Zr with a calculated cross section of 0.3% of the total fusion cross section at E(^{28}Si) = 128MeV. Gamma rays from excited states of ^{82}Zr were measured and identified using the NORDBALL escape-suppression array at the Niels Bohr Institute. Reaction channel selection was performed by use of neutron and charged particle detector arrays in conjunction with the germanium detectors. A rotational band in ^{82}Zr has been identified with spins up to 20 h by analysis of reaction channel selected γ-γ coincidence matrices. Band crossings were identified at frequencies 0.57 and 0.69 MeV.

---

[1] *Niels Bohr Institute, DK-4000 Roskilde, Denmark.*
[2] *Department of Physics, Chalmers University of Technology, -412 96 Göthenburg, Sweden.*

V-A-3

Isomer of ^{88}Tc

A. Odahara, T. Shizuma, E. Ideguchi, J. Mukai*, H. Tomura, B. J. Min**, S. Suematsu, K. Heiguchi***, T. Komatsubara*, K. Furuno*, T. Kuroyanagi and S. Mitarai

The β-decay of ^{88}Tc was studied by means of $\beta\gamma$ and $\gamma\gamma$ coincidences. The nucleus ^{88}Tc was produced by the ^{58}Ni(^{32}S,pn) reaction at 96~105 MeV using Kyushu University and Tukuba University Tandem Accelerator. Since the cross section of this reaction channel is small(~0.5mb) and the β-decay half life is short(~5sec), the rotation disk[1] and the tape transport systems were used to reduce the background originating from long lived activities.

The projection of the $\gamma\gamma$ coincidence data is shown in fig.1. Three transitions of the 741 ($2^+ \rightarrow 0^+$), 915 ($4^+ \rightarrow 2^+$) and 972 ($6^+ \rightarrow 4^+$) keV following the β-decay of ^{88}Tc were observed. The decay curves are shown in fig.2. M.Weiszflog et.al.[2] reported that the 8^+ or 7^- levels in ^{88}Mo were populated by the β-decay of ^{88}Tc. However, in this work, the transitions of the 586 ($8^+ \rightarrow 6^+$), 992 ($5^- \rightarrow 4^+$) and 703 ($7^- \rightarrow 5^-$) keV were not observed with the γ-ray intensities reported previously. The life time and the beta maximum energy of ^{88}Tc were determined for the first time. They are summarized in Table 1. The half life of the 972 keV γ-ray is longer than those of the 741 and 915 keV γ-rays, though they overlap within the present experimental accuracy.

The 2^+,4^+ and 6^+ states in ^{88}Mo are populated by the β-decay of ^{88}Tc, as seen in Table 2. This means that there is an isomer in ^{88}Tc considering the β-decay selection rule. From these results, the decay scheme of ^{88}Tc is proposed in fig.3.

References :

1) K. Heiguchi et. al., Kushu Univ. Tandem Accelerator Lab. Report (1985-1987) p.33
2) M. Weiszflog et. al., Z. Phys. A - Hadrons and Nuclei **342**, 257(1992)

Addresses:
*Institute of Physics and Tandem Accelerator Center, University of Tukuba, Tukuba, Ibaraki 305, Japan
**Design Analysis Department, Korea Atomic Energy Research Institute, PO Box 7, Daeduk-Danji, Daejeon 305-606, Korea
***Graduate School of Science and Technology, Niigata University, Niigata 950-21, Japan

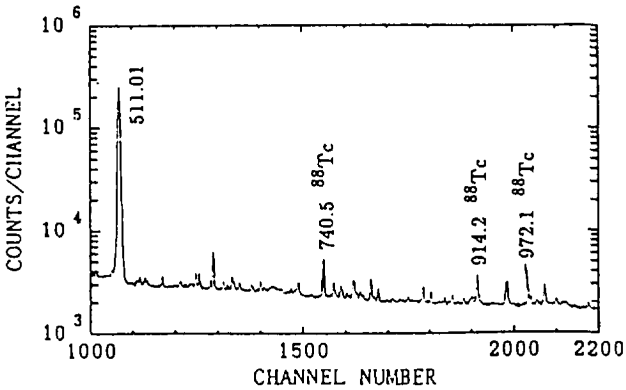

fig.1. The projection spectrum of the $\gamma\gamma$ coincidence data

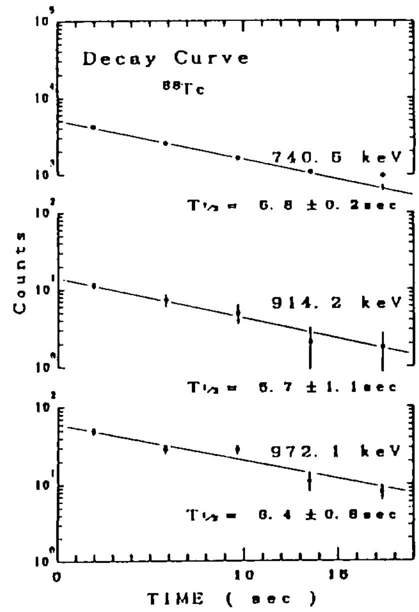

fig.2. The decay curves of the 741, 915 and 972 keV γ-rays following β-decay of ^{88}Tc

Table 1.
Decay characteristics of ^{88}Tc

γ-ray energy [keV]	life time [sec]	relative intensity	E_β^{max} [MeV]
740.53(5)	5.8(2)	100	6.8(13)
914.23(18)	5.7(11)	44.2(58)	5.9(13)
972.07(23)	6.4(8)	19.5(37)	4.9(13)

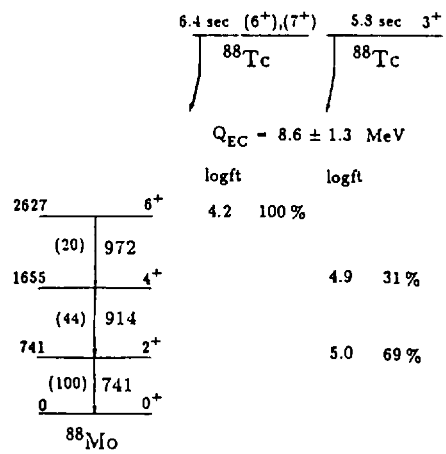

fig.3. The decay scheme of ^{88}Tc

V-A-4 The β-decay of the New Isotope ^{86}Mo

T. Shizuma, E. Ideguchi, A. Odahara, H. Tomura, T. Kuroyanagi,
S. Mitarai, K. Furuno*, T. Komatsubara*, J. Mukai* and K. Heiguchi**

The new neutron deficient isotope ^{86}Mo was firstly identified through its β-decay studies. The half life and maximum β^{+}-ray energy were determined.

The new isotope ^{86}Mo was produced by the ^{54}Fe(^{35}Cl,1p2n) reaction. The 103 MeV ^{35}Cl beam was supplied from the tandem accelerator at Kyushu University. The ^{54}Fe(97.08%, 0.80 mg/cm^2) target was made by electroplating on the Au foil of 2 mg/cm^2. The γ- and β-rays were detected by two pure Ge detectors with Be windows. The Rotation Disk Transport System[2] was used to reduce effects of the γ-rays emitted from the long lived activities.

The γ-rays of 47.2 and 49.8 keV were found as the unknown γ-rays in a projected γ-ray spectrum of $\beta\gamma$, $\gamma\gamma$-coincidence matrix [Fig.1]. The γ-ray of 49.8 keV and the K_α X-rays of Nb were observed in coincidence with the γ-ray of 47.2 keV [Fig.2a]. The similar coincidence relation was obtained in the spectrum gated by the γ-ray of 49.8 keV [Fig.2b]. The observation of the K_α X-rays of Nb is a enough evidence to prove that the two γ-rays follow the β-decay of ^{86}Mo, because other Mo isotope with significant cross section produced simultaneously in the reaction is only ^{87}Mo of which the β-decay has been studied in detail[3]. Furthermore it was confirmed that the two γ-rays of 49.8 and 187.0 keV were in coincidence as shown in the gated spectra [Fig.2b,2c]. Thus the γ-rays of 47.2, 49.8 and 187.0 keV are attributed to the β-decay of ^{86}Mo.

The half life of ^{86}Mo was determined to be 19.7$\pm$0.9 sec from the analysis of the decay curve of 49.8 keV γ-ray [Fig.3]. This value nearly agrees with the predicted value of 10 sec by the gross theory[4]. From the β-ray spectrum in coincidence with the 49.8 keV γ-ray, the endpoint of β-ray was determined to be 4.4$\pm$0.2

* Permanent Address: Institute of physics, University of Tsukuba, Tsukuba, Ibaraki 305, Japan
** Permanent Address: Department of Physics, Faculty of Science, Niigata University, Niigata 950-21, Japan

MeV (statistical error only) by means of $\sqrt{N}$ plot analysis [Fig.4]. Thereby the Q_{EC} value was determined to be 5.4±0.2 MeV. This value seems to be a natural trend in the β-decay energy systematics [Fig.5].

References

1) C.J. Gross, K.P. Lieb, D. Rudolph, M.A. Bentley, W. Gelletly, H.G. Price, J. Simpson, D.J. Blumenthal, P.J. Ennis, C.J. Lister, Ch. Winter, J.L. Durell, B.J. Varley, O. Skeppstedt and S. Rastikerdar, Nucl. Phys. **A535** 203 (1991)
2) K. Heiguchi, T. Maeda, H. Tomura, B.J. Min, Y. Haruta, S. Mitarai and T. Kuroyanagi, Kyushu Univ. Tandem Accelerator Lab. Report 33 (1985-1987)
3) B.J. Min, S. Suematsu, S. Mitarai, T. Kuroyanagi, K. Heiguchi and M. Matsuzaki, Nucl. Phys. **A530** 211 (1991)
4) K. Takahashi, M. Yamada and T. Kondoh, Atomic Data and Nucl. Data Tables, **12** 101 (1973)
5) A. Wapstra and G. Audi, Nucl. Phys. **A432** 1 (1985)

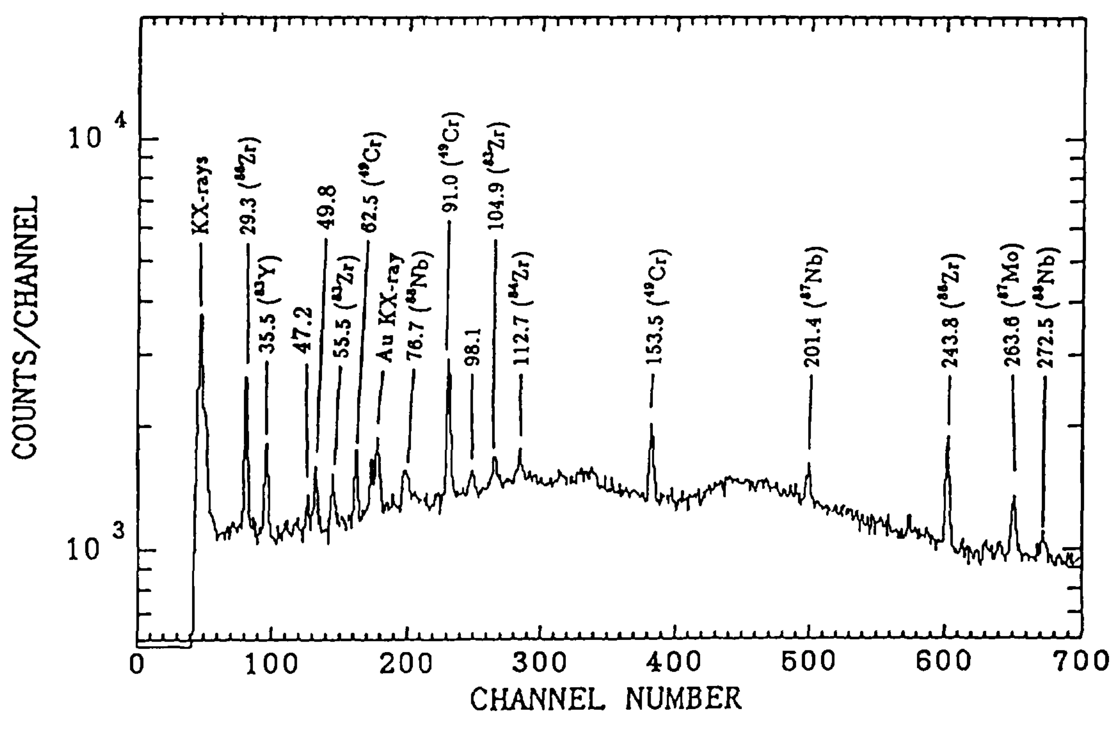

Fig.1. Projected spectrum of γ-rays obtained from $\beta\gamma$, $\gamma\gamma$-coincidence measurement in which activities were produced by ^{54}Fe + ^{35}Cl (103 MeV) reaction. Peaks are labelled by their energys in keV.

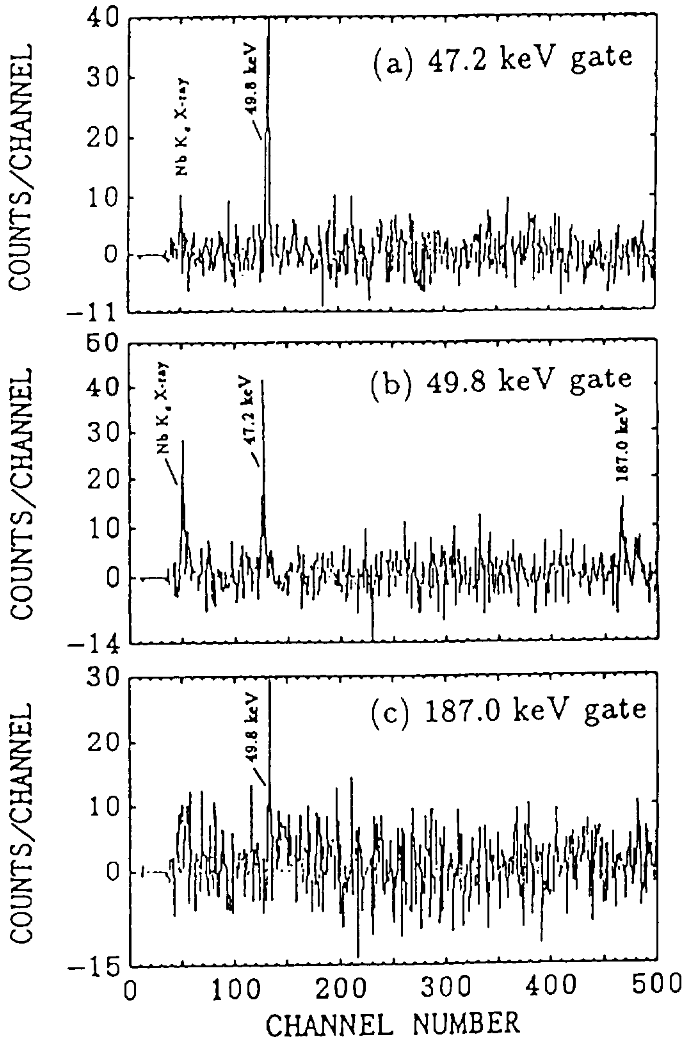

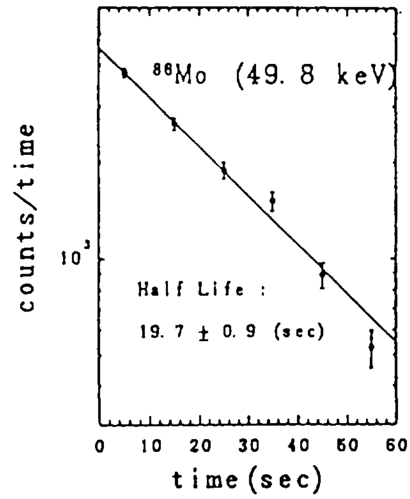

Fig.3. Decay curve of the 49.8 keV γ -ray in coincidence with the β-rays. The irradiation and measurment times were 17 and 60 sec.

Fig.2. Gamma-ray spectra obtained in coincidence with the 47.2 keV (a), 49.8 keV (b) and 187.0 keV (c) γ-rays. The background has been subtracted.

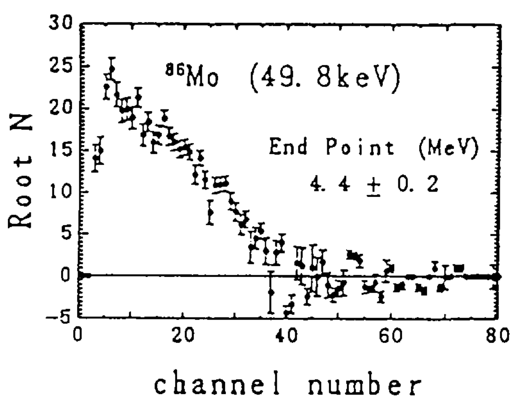

Fig.4. $\sqrt{N}$ plot of the β-ray spectrum in coincidence with the 49.8 keV γ-ray .

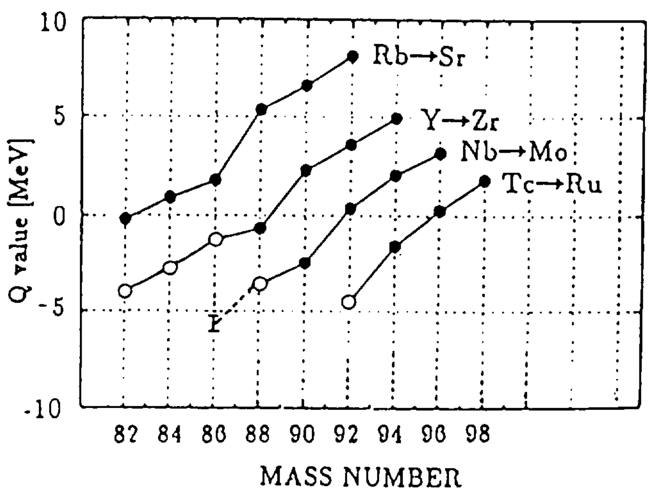

Fig.5. Systematics of Q values. A vertical bar shows the region given by present result. Closed and open circles show experimental and calculated data, respectively, from Ref.5.

V-A-5 Precise and Systematic Measurement on $\vec{p}$+d Scattering from 5 to 18 MeV

K. Sagara, H. Oguri, S. Shimizu, K. Maeda, H. Nakamura and T. Nakashima

The Faddeev calculations on N+d system have succeeded in reproducing without adjustable parameters many observables except for the vector analyzing power A_y for which the calculations predict 30% smaller values at the peak around 120°. Recently this discrepancy has been found to be solved if large charge independence breaking(CIB) and charge symmetry breaking(CSB) is assumed in the P-state NN interaction[1] or if the short range LS force in the NN interaction is modified[2]. To obtain from 3N system the information on the NN interaction which can never or hardly obtained from 2N system, however, the existing N+d expermental data are not enough in the accuracy.

Here we report precise and systematic measurement on the differential cross section and A_y for the D(p,p)D scattering at E_p =5, 6, 6.5, 7, 8, 8.5, 9, 10, 12, 14, 16 and 18 MeV. The typical statistical error in the A_y is ±0.0009 or less, and the the uncertainty in the absolute value of the A_y is estimated to be less than 0.8 %. The overall uncertainty in the differential cross section is 0.7 to 1 %.

For the A_y measurement, a high intensity polarized proton beam from the Lamb-shift type ion source was used. The beam polarization was measured always during the experiment by using the p-^{4}He scattering at the beam dump. the beam intensity was 0.2 t0 0.3 and the polarization was 75% and 53% in the spin up and down states, respectively. For the cross section measurement a proton beam from a direct extraction ion source was used.

The target D_2 gas of 0.3 to 0.8 atm was contained in a cell of 9 cm in diameter. To reduce the multiple scattering in the cell window, thin aluminum, havar and mylar foils were used. To reduce the false asymmetry in the measurement, the scattered particles were detected by the left and right counters placed symmetrically with respect to the beam axis. In the A_y measurement, more than 10^6 events were accumulated for each scattered proton and recoiled deuteron in each counter in each spin mode.

Special care was taken to obtain the absolute value of the cross section. Using the same set-up, the p+p cross section was measured and the results were consistent with the existing data within 0.5-1%.

The measured $\vec{p}$+d data were consistent with the other existing data, however the accuracy and smoothness of the data were by far improved as shown in Fig.1. These data were well reproduced by the Faddeev calculation[3] using the Paris NN potential whose short range of the LS force was modified, as shown in Figs 2 and 3. Some disagreement at forward angle may come from the approximate treatment of the Coulomb force in the calculation. It is very interesting whether the difference between the A_y peak heights for $\vec{n}$+d and $\vec{p}$+d can be reproduced when the Coulomb force is treated correctly in the Faddeev calculation. If not, it readily implies the breaking of the charge symmetry in the nuclear force.

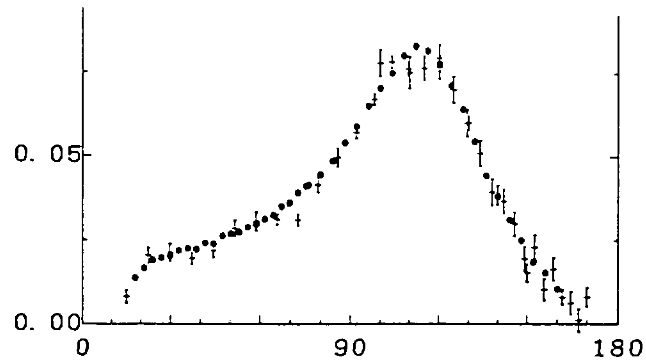

Fig. 1. Comparison of the present data (closed circle) and existing data[4] on A_y for D($\vec{p}$,p) scattering at 5 MeV.

References

1) H.Witala and W.Glöckle, Nucl. Phys. **A528** 48 (1991);
2) T. Takemiya, Prog. Theor. Phys. **86** 975 (1991).
3) T. Takemiya, private communication.
4) R. E. White, W. Grüebler, B. Jenny, V. König, P.A. Schmelzbach and H. R. Bürgi, Nucl. Phys. **A321** 1 (1979).
5) W. Tornow, C. R. Howell, M. Alohali, Z. P. Chen, P. D. Felsher, J. M. Hanly, R. L. Walter, G. Mertens, I. Slaus, H. Witala and W. Glöckle, Phys. Lett. **B257** 273 (1991); C. R. Howell, W. Tornow, K. Murphy, H. G. Pfützner, M. L. Roberts, Anli Li, P. D. Felsher, R. L. Walter, I. Slaus, P.A. Treado and Y. Koike, Few Body Systems **2** 19 (1987); W. Tornow, R. C. Byrd, C. R. Howell, R. S. Pedroni and R. L. Walter, Phys. Rev. **C27** 2439 (1983); W. Tornow, C. R. Howell, R. C. Byrd, R. S. Pedroni and R. L. Walter, Phys. Rev. Lett. **49** 312 (1982).

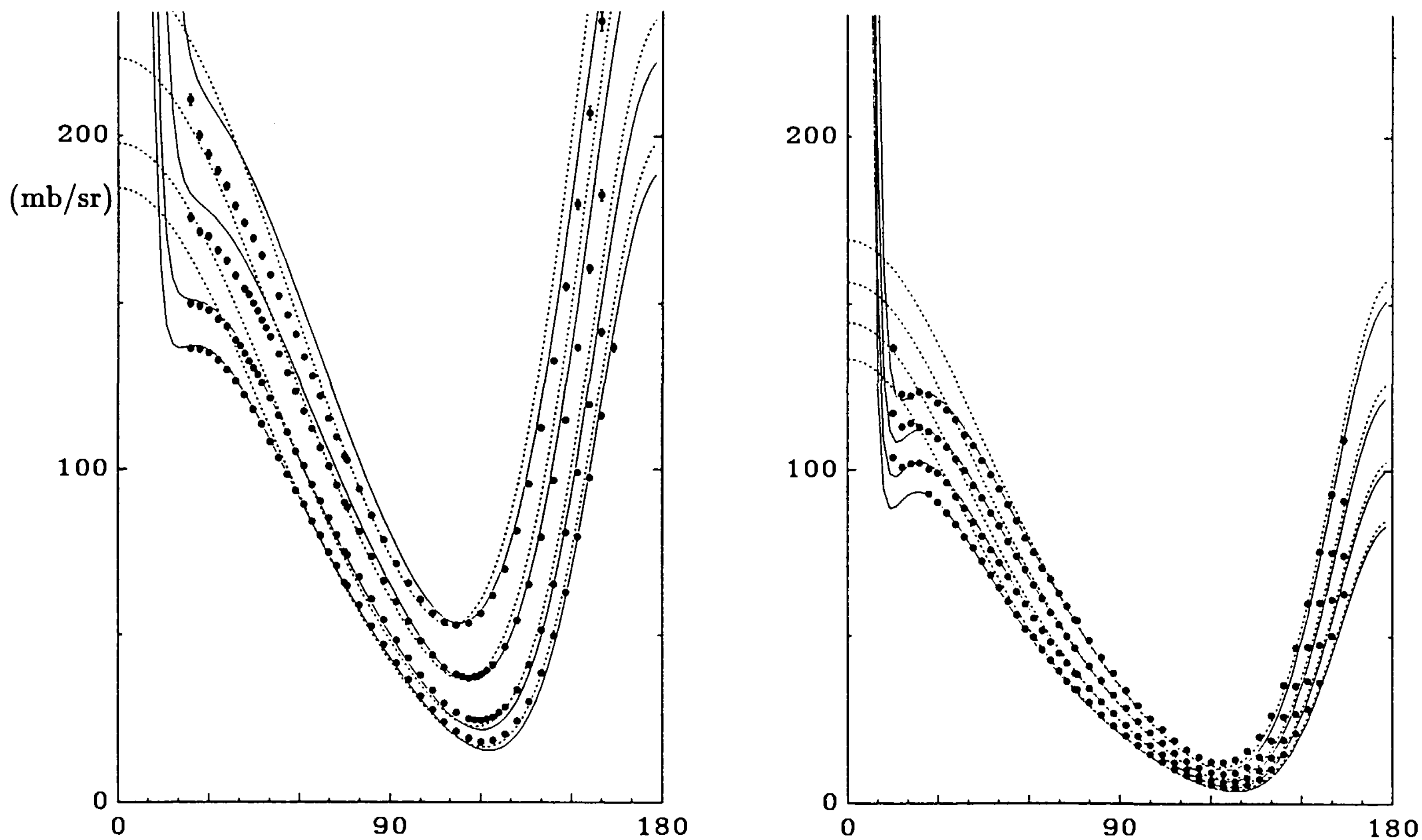

Fig. 2. Differential cross section for D(p,p) scattering at 5(top), 6.5, 8.5 and 10 MeV(bottom) on the left, and at 12(top), 14, 16 and 18 MeV(bottom) on the right. Curves are the Faddeev calculation for p+d(solid) and n+d(dotted).

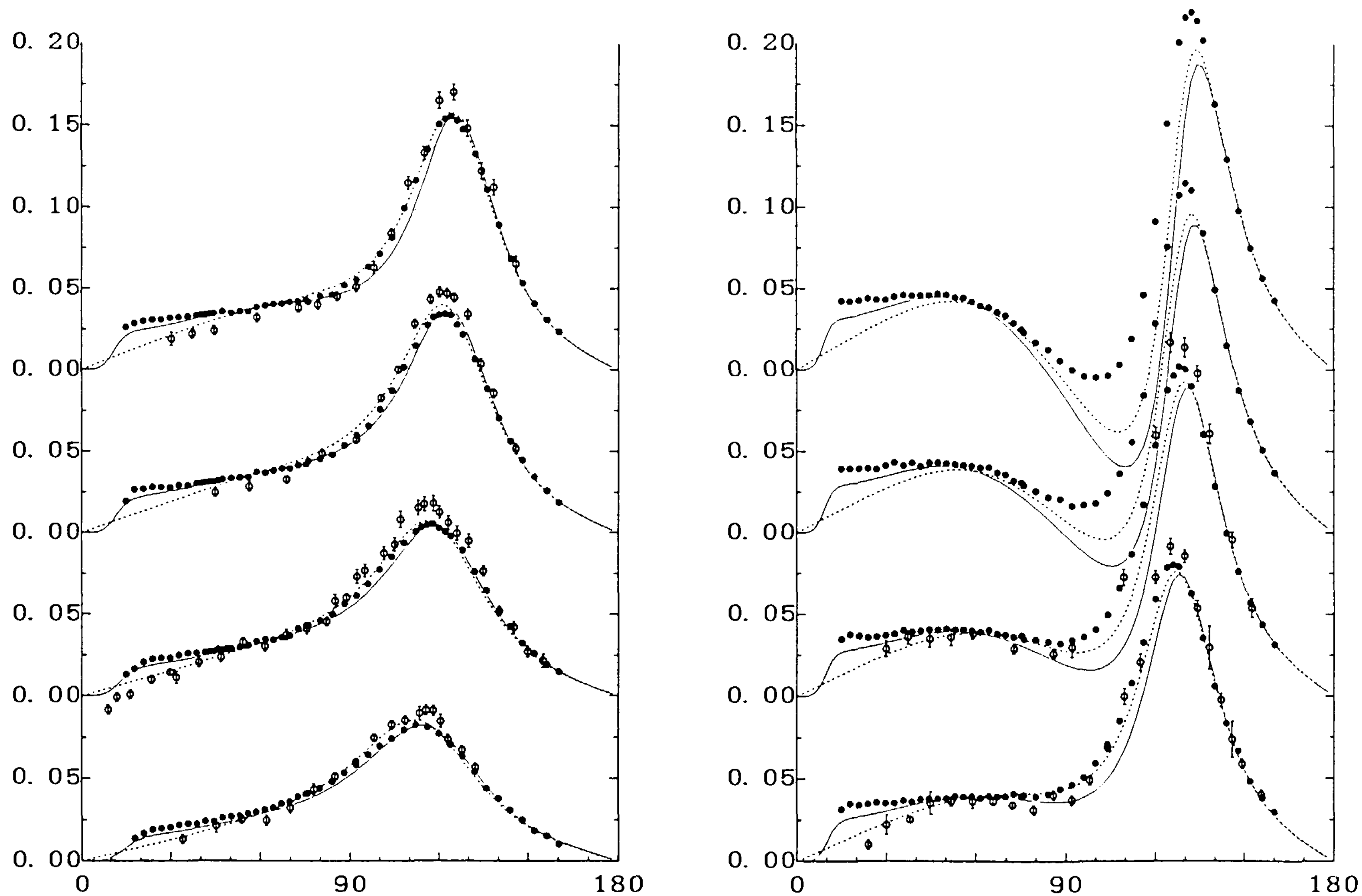

Fig. 3. A_y for $D(\vec{p},p)$ scattering at 5(bottom), 6.5, 8.5 and 10 MeV(top) on the left, and at 12(bottom), 14, 16 qnd 18 MeV(top) on the right. Open circles are A_y for$D(\vec{n},n)$ scattering[5]. Curves are the same as in Fig. 2.

V-A-6

Analyzing Powers of p+d Scattering Below Deuteron Breakup Threshold

S. Shimizu, K. Sagara, K. Maeda, H. Nakamura,
T. Miwa, N. Nishimori, S. Ueno and T. Nakashima

Inclusion of the "exact" Coulomb force in the Faddeev calculation for the p+d scattering has been performed recently at energies below the deuteron breakup threshold.[1] It is well expected that other groups will start the full Coulomb calculation first in this energy region. To compare with the calculation, highly accurate p+d experimental data have been desired.

A_y and $d\sigma/d\Omega$ for the $\vec{p}$+d scattering have been measured at E_p^{lab}= 2, 2.5, 3 and 4 MeV, below and just above the deuteron breakup threshold (E_p^{lab}= 3.3MeV). The typical statistical error of A_y is ±0.0005, and the error in the absolute A_y value is estimated to be less than 1 %. iT_{11}, T_{20}, T_{21}, T_{22} for the $\vec{d}$+p scattering have also been measured in the typical statistical accuracy of ±0.0006 and the absolute accuracy of 1% at E_d^{lab}= 5 and 6 MeV, which correspond to E_p^{lab}= 2.5 and 3 MeV, respectively. The errors shown in Figs. 1 ~ 3 are the statistical ones only. The present data are consistent with the preceding data[2,3], though the experimental errors become by 3 to 10 times smaller, as shown in Fig. 1.

Polarized proton or deuteron beam of 300 nA at most was incident on the D_2 or H_2 target gas of 0.28 atm enclosed in a gas cell of 90 mm in diameter. For forward angle measurement, a special shape gas cell was used. The beam entrance and exit windows were made of 2 and 4 μm aluminum foils, respectively, and the side windows of 1.5 μm mylar foils. Due to the usage of these thin and low atomic number foils, the multiple scattering effect in the windows was considerably reduced and scattering protons and deuterons down to 0.8 MeV could be detected. The statistical accurate data were obtained owing to the thick target realized by the gas cell and high beam intensity. The polarization of proton and deuteron was measured continuously during the experiment by using $^4He(\vec{p},p)$ scattering and $^3He(\vec{d},p)$ reaction, respectively, at the beam dump.

The experimental results at E_d^{lab}= 5 MeV are compared with the "exact" Coulomb calculation[1] using a separable expansion of the Paris nucleon-nucleon (NN) potential in Fig. 1 and left hand sides of Fig. 3. The large discrepancy at the A_y peak, which is known well at higher energies, is confirmed also at this low energy. Though the "exact" Coulomb treatment is essentially important to reproduce the cross section, a forward bump for iT_{11} predicted by the "exact" Coulomb calculation is not observed. There is an apparent discrepancy also at the minimum of T_{22}. Takemiya[4] has found that the A_y peak discrepancy can be solved by modifying the short range part of the LS force in the Paris potential, as shown in right hand sides of Fig. 3. The analyzing powers are compared with the calculation by Takemiya with the original and modified Paris potentials treating the Coulomb force approximately[5]. The modification is effective for the A_y and iT_{11}, but has no effects on the tensor analyzing powers. Obvious discrepancy is seen at the T_{22} minimum and at the backward parts of T_{20} and T_{21}.

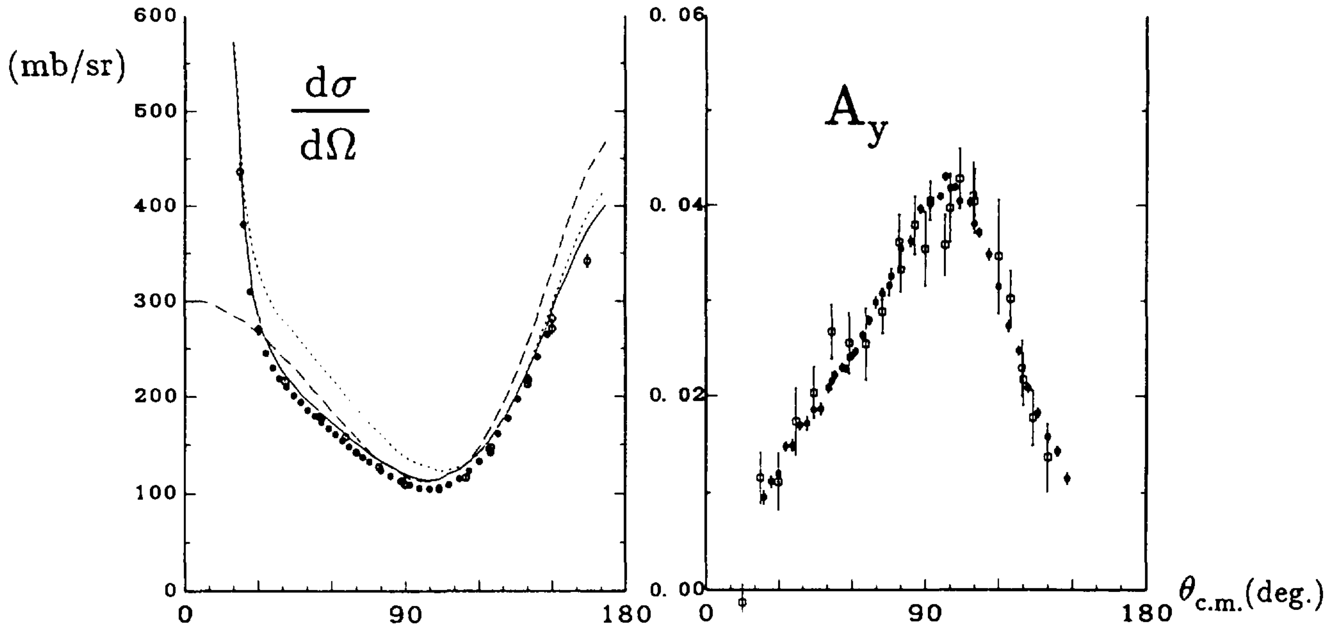

Fig. 1. Comparison of the present data at E_p^{lab}= 2.5 MeV with preceding ones for the cross section (open circles)[2] and A_y (open squares)[3]. Dashed curve is Faddeev calculation for n+d scattering using a separable expansion of the Paris potential. Dotted and solid curves are for p+d with approximate and "exact" Coulomb treatment, respectively.

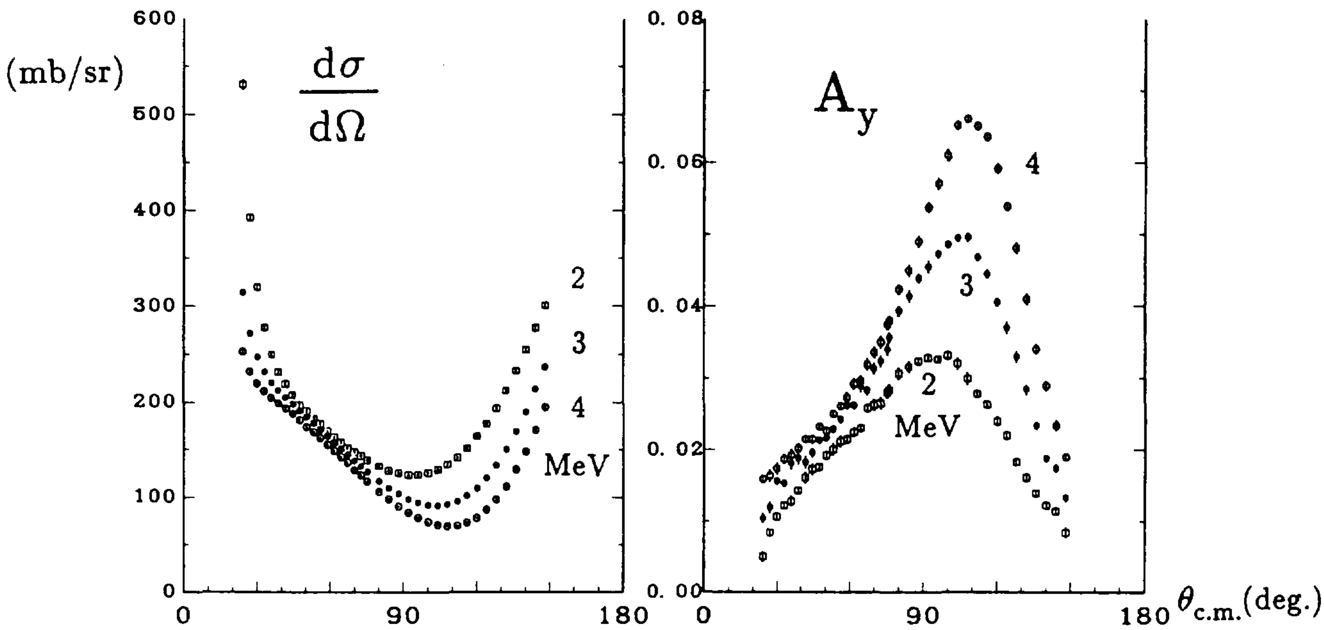

Fig. 2. Present data for $d\sigma/d\Omega$ and A_y for p+d scattering at E_p= 2, 3 and 4 MeV.

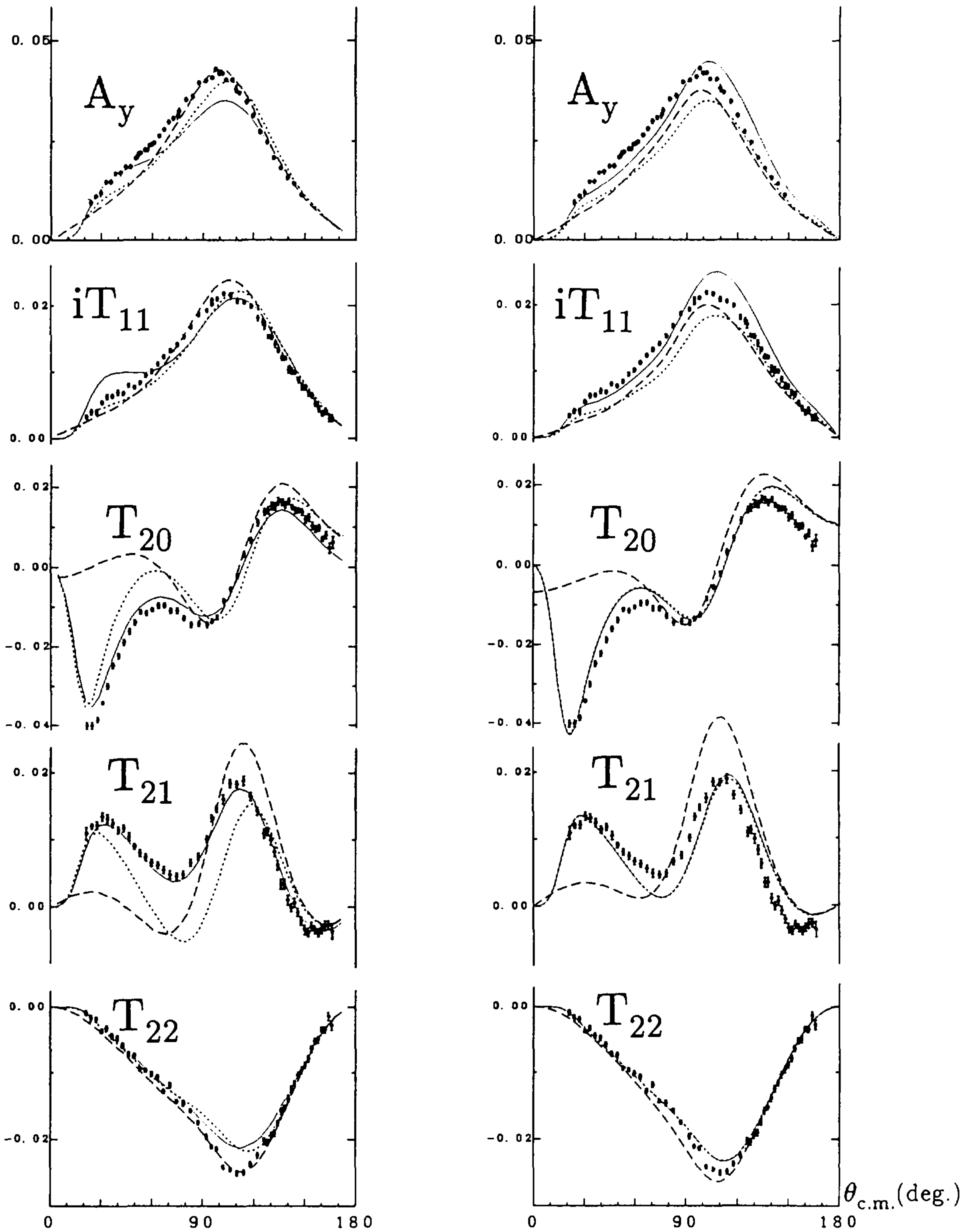

Fig. 3. Analyzing powers for p+d scattering at E_p^{lab}= 2.5 MeV. Curves in the left figures are the same as in Fig. 1. Dashed curves in the right figures stand for n+d calculation using original Paris potential, and dotted and solid ones stand for approximate Coulomb p+d calculation using original and modified Paris potentials, respectively.

The present data indicate that some refinements are necessary in the NN interaction not only in the spin vector part but also the spin tensor part and that the "exact" treatment of the Coulomb force still has some problems. The full Coulomb calculations with several realistic potentials are highly desired.

References:

1) G.H.Berthold, A.Stadler and H.Zankel, Phys.Rev. C41, 1365(1990).
2) R.Sherr et al., Phys.Rev. 72, 662(1947).
3) R.E.White et al., Nucl.Phys. A321, 1(1979).
4) T.Takemiya, Prog.Theor.Phys. 86, 975(1991).
5) P.Doleshall et al., Nucl.Phys. A380, 72(1982).

V-A-7 $^{52}Cr(d,p)^{53}Cr(3/2^-$, g.s.) reactions at 18MeV

K. Maeda, S. Shimizu, T.Matsuda, N. Nishida, H. Nakamura, K. Sagara
and T. Nakashima

Polarization transfer coefficients(PTC's) (K_y^y, K_{xz}^y, $K_{xx}^y-K_{zz}^y$) on $^{52}Cr(d,p_0)^{53}Cr(3/2^-$, g.s.) have been measured at 18 MeV by a double scattering method. A high intensity polarized deuteron beam produced from the Lamb shift type ion source, was accelerated by Kyushu University tandem accelerator and incident on a 99% enriched ^{52}Cr target of 10 mg/cm^2 in thickness. The beam intensity on the target was 0.5μA and the polarization was about 75%. The emitted protons were momentum analyzed and focused by a QDQ magnetic analyzer and lead to a high efficiency proton polarimeter using liquid helium target [1]. The horizontal and vertical angular spreads of Q-D-Q magnetic analyzer were $\pm 1°$ and $\pm 2°$, respectively.

The differential cross section and the whole analyzing powers, iT_{11}, T_{20}, T_{21} and T_{22} of the same $^{52}Cr(d,p)$ reaction have been also measured by the usual single scattering method. To reduce the false asymmetry the left and right ΔE-E counters were placed symmetrically with respect to the beam axis. The horizontal and vertical angular spreads of counters slits were $\pm 0.5°$ and $\pm 2°$, respectively, for the forward angle measurement (10° to 120°) and $\pm 1°$ and $\pm 2°$ for the backward measurement(125° to 150°). The target thickness was 2 mg/cm^2.

The experimental results for the $^{52}Cr(d,p_0)$ are shown in Fig. 1. The absolute cross section were estimated from the elastic scattering cross section measured at the same time.

The DWBA analysis has been made using a deuteron optical potential which reproduces the elastic scattering, and proton potential proposed by Bechetti & Greenles [2]. The form factor of the ^{53}Cr were determined by the neutron separation energy method. The form factor of the deuteron internal wave function and the interaction term V_{pn} were taken from the Reid soft core potential [3]. The finite range DWBA code DWUCK5 [4] was used. The results of the calculation are shown in Fig. 1, by the dotted curves.

To take into account the deuteron virtual break up effect, another approach has been done in the adiabatic approximation(so called Johnson and Soper approximation [5]), using Bechetti & Greenles potentials for nucleon-^{52}Cr nucleus. The other parameters are same as the DWBA calculation. The results are shown in Fig. 1 by the solid curves. The dashed curves show the calculation in which the deuteron D state is eliminated. Comparing the dashed curves with solid curves, it can be seen that the deuteron D state has no effect to A_y, but four observables X_2, T_{21}, K^y_{xz}, $K^y_{xx}-K^y_{zz}$ are mainly originated from this D state effect.

For the cross section, the solid curve(adiabatic approximation) is a little smaller, but the dashed curve(DWBA) is too larger at backward angle. For A_y, two curves are out of phase at forward angle. DWBA gives better fit at forward angle, but it predicts too large positive value at backward angle. For X_2, T_{20} and K^y_y, the adiabatic approximation gives remakable fits. For other observables, both curves give fairly good fits. Angular momentum(L) dependence of the reduced transition matrix β is shown in Fig.2. The DWBA amplitude has two maxima at the inside and the outside of the nucleus, L$\sim$3 and 8. But the adiabatic amplitude has only one maximum at L$\sim$8.

The difference of the two calculations can be seen also in the near/far analysis shown in Fig. 3. The far side component of the DWBA is by far larger than the near side component at backward angle, while in the adiabatic approximation near and far components are close at the backward angle.

It is concluded that the deuteron breakup effect is dominant in the ^{52}Cr(d,p_0) reaction, which means that the contribution from the interior of the nucleus and far-side component are suppressed in this reaction.

References:

1 K.Sagara, K.Maeda, H.Nakamura, K.Aita, M.Izumi, T.Yamaoka, Y.Nishida, M.Nakashima, T.Nakashima and A.Isoya, Nucl. Instrum. and Meth A270(1988)450

2 F. D. Becchetti, G. W. Greenlees, Phys. Rev. **182** (1969) 1190

3 R. V. Reid, Ann. of Phys. **50** (1968) 411

4 P.D. Kunz, program code DWUCK5, University of Colorado, U.S.A.

5 R. C. Johnson and P. J. R. Soper, Phys. Rev. **C1** (1970) 976

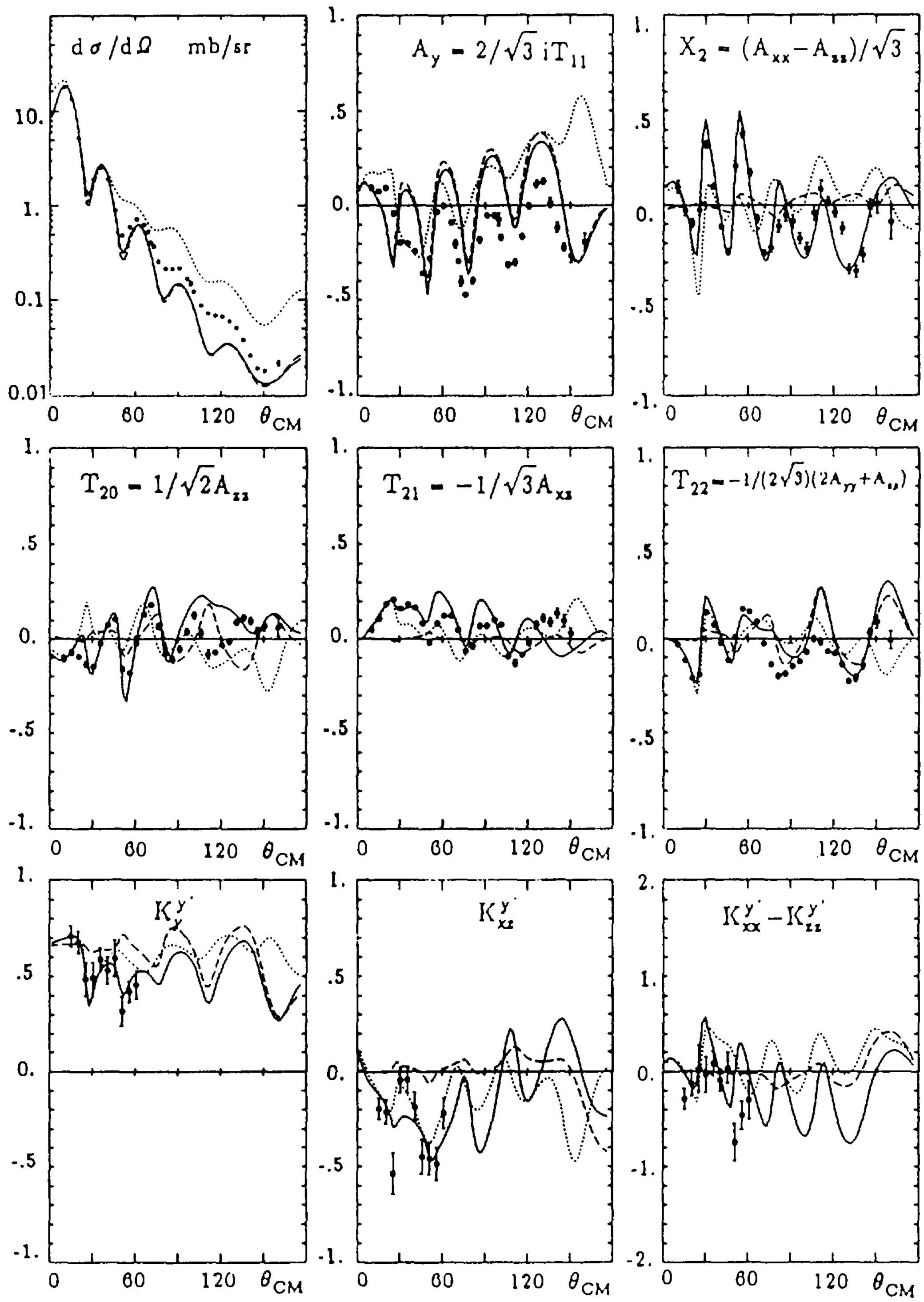

Fig. 1.

The cross section $d\sigma/d\Omega$, the vector analyzing power A_y, tensor analyzing powers T_{20}, T_{21}, T_{22} and aditional A_{yy}, X_2, the PTC's K_y^y, K_{xz}^y and K_{xx}^y - K_{zz}^y for the $^{52}Cr(d,p_0)^{53}Cr(3/2^-$, g.s.) transition at Ed = 18.0 MeV.

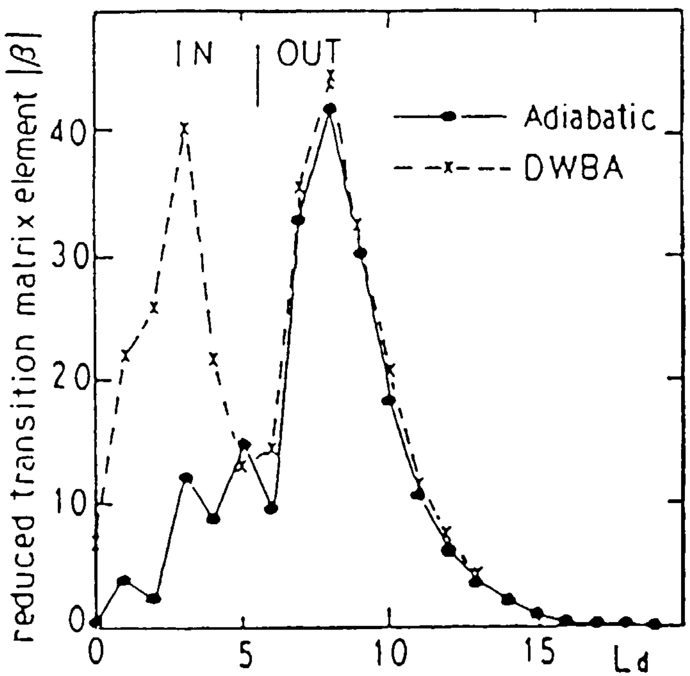

Fig. 2.

Dependence of the reduced transition matrix element on the angular momentum Ld in deuteron channel in the $^{52}Cr(d,p_0)$ reaction at 18Mev.

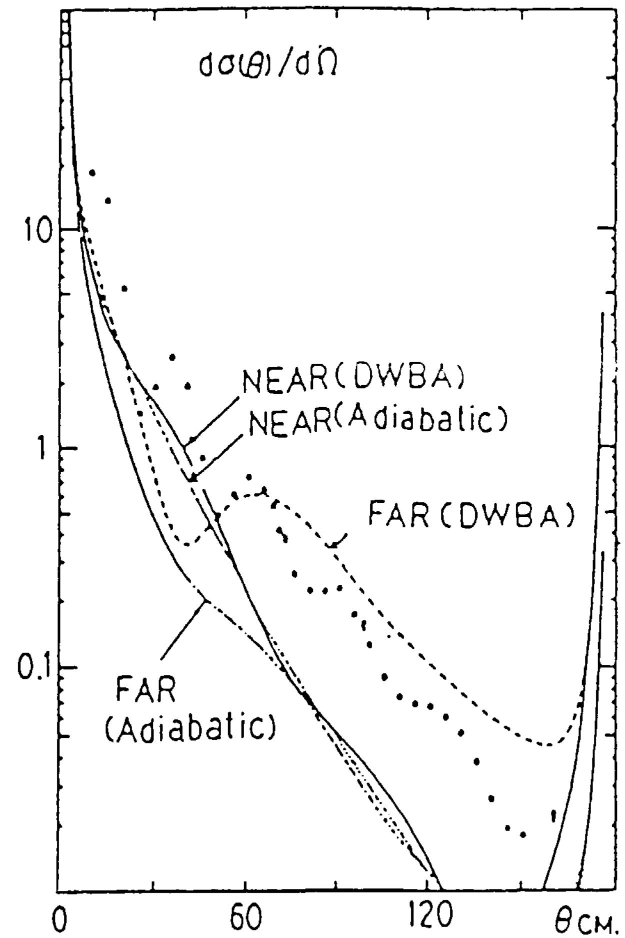

Fig. 3.

The near-far analysis of the $^{52}Cr(d,p_0)$ cross section at 18MeV.

V-A-8

Gamow-Teller Strength in the Beta-Decays of Proton Rich T_z = -3/2 Nuclei of ^{25}Si and ^{29}S

S. Morinobu, S. Hatori[1], H. Miyatake[2], T. Shimoda[2], N. Takahashi[2] and Y. Fujita[2]

A paper on a part of this subject has been submitted to Nuclear Physics.

1. Introduction

A large quenching of the Gamow-Teller(GT) strength compared to the sum rule limit has been claimed from the forward angle (p,n) reactions and a renormalization of the beta-decay axial coupling constant g_A has been presumed to occur in complex nuclei. For a correct understanding of the phenomena, it is especially important to accumulate the beta-decay data which will give detailed information on the strength distribution in the daughter nuclei without ambiguity.

Since the beta-decay probes only the strength within a 'window' set by the decay Q-value, the measured beta-decay strengths are to be compared with, in stead of the sum rule as used in the (p,n) reaction analysis, the best available theoretical expectations, to find the quenching of the GT-strength. Brown and Wildenthal[1]) have analyzed the measured low energy beta-decay rates of the nuclei around the stability line, with the aid of shell model calculations in the full (2s, 1d) basis, and reported an average quenching factor of 58 ± 5 % for nuclei with Tz $\geqq$ -1.

In order to extend this kind of analysis over such a wide range of excitation energies that may cover a substantial part of the GT-strength in the daughter nuclei, the beta-decay measurements were undertaken in the present work for the proton rich nuclei of ^{25}Si and ^{29}S in the sd-shell. The branching ratios of the beta-decays were were determined by incorporating the measurements of both the beta-rays and beta-delayed protons. For eliminating the beta-emitting contaminations, a recoil mass separator was used to collect the short-lived activities on a small detector.

2. Experiment and data analysis

The ^{25}Si and ^{29}S activities were produced by the $^{24}Mg(^{3}He,2n)$ and $^{28}Si(3He,2n)$ reactions at 35 MeV, respectively. The ^{3}He beams from the AVF cyclotron at the Research Center for Nuclear Physics, Osaka University were used. The reaction products recoiling out of the target were mass-analyzed by the recoil mass separator CARP[2]) placed at zero degrees to the beam direction.

The mass-separated ions were implanted in a Si surface barrier detector which was viewed by a beta-ray counter telescope at the focal plane of the

---

Present address:
[1] Research Center for Nuclear Science and Technology, The University of Tokyo, Tokyo 113, Japan
[2] College of General Education, Osaka University, Toyonaka, Osaka 560, Japan

CARP. The decay events in the detectors were recorded together with the time of occurrence in an event-by-event mode. The counter set-up as well as the details of the experimental procedure is given in ref. 3. We obtained (a) singles spectra of the delayed protons, (b) spectra of the protons in coincidence with beta-rays and (c) singles beta-ray time spectra. For ^{29}S case, gamma-ray-proton coincidences were also recorded.

3. Results and comparison with shell model calculation

The decay schemes were reconstructed for all the daughter nuclei taking into account of the energies of the proton transitions and, in the case of ^{29}S, gamma-proton coincidences. The procedure included relocations and eliminations of the previously reported proton transitions as well as the addition of a newly observed transition in the ^{25}Si case. The beta decay branching ratios were calculated for the individual daughter states from the measured spectra presented above and were in turn converted into the B(GT) values.

The obtained experimental GT-strength functions are shown in figs. 1 for the case of ^{25}Si. Marked changes from the previous data[4,5]), mainly caused by the reconstruction of the decay schemes, were present in both the cases of ^{25}Si and ^{29}S. Also noted was the fact that the strength to the IAS in the ^{25}Si case is such large as to compare the the single particle value of a $d_{5/2}$ proton transition into a $d_{5/2}$ neutron.

For comparison with the theoretical predictions, shell model calculations in the full (2s, 1d) space were carried out for the states having the possibility to be fed by the beta-decays. The computer code developed by Ogawa was used together with the Brown-Wildenthal effective interaction and the results for the ^{25}Si case are also included in the figure.

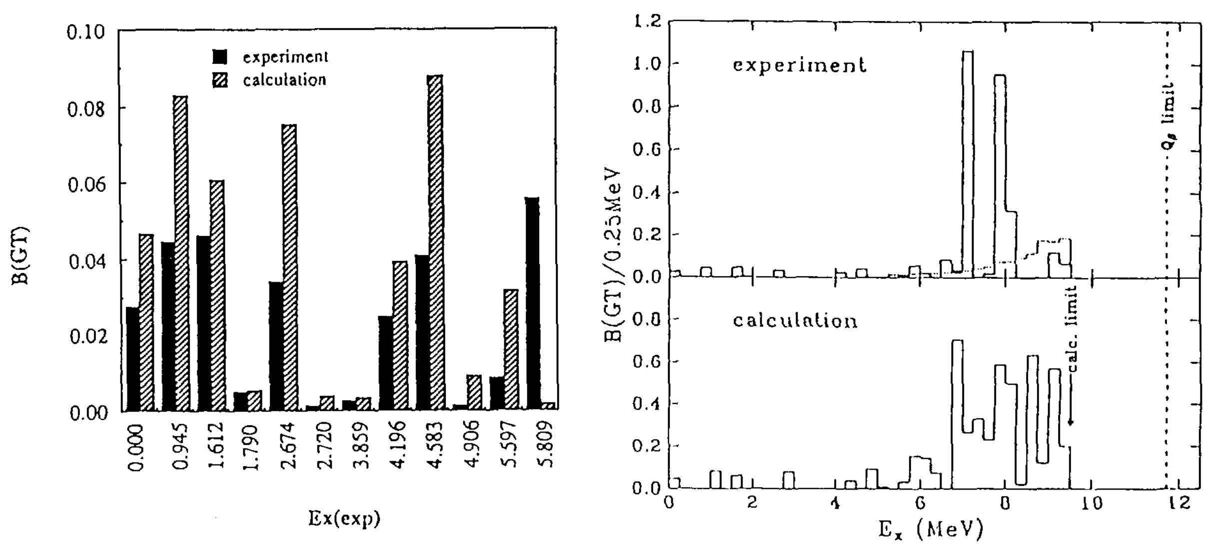

(a) (b)

Fig.1 Comparison of the experimental and calculated GT-strengths in the decay of ^{25}Si, displayed as a function of the excitation energy of the final state: (a) for the low-lying states and (b) in the form of gross distribution.

The comparison revealed a satisfactory reproducibility of the calculation for the level structures of the daughter nuclei below about 5 MeV in excitation energy. However, the state correspondence between experiment and calculation becomes ambiguous at higher energies in both the nuclei and the calculation generally tends to predict much more levels than the observed.

The GT-strengths for the seemingly well reproduced states below 6 MeV are compared in fig. 1(a). The calculation generally predicts roughly the correct behaviour of the relative variation of the strength with energy, while the absolute value is generally overestimated. The quenching factors in this energy region are 0.52 ± 0.02 and 0.50 ± 0.03 for ^{25}Al and ^{29}P, respectively, in agreement with the value deduced for $T_z \geqq -1$ nuclei. These observations are suggestive of a presence of common renormarization of the axial beta-decay coupling constant g_A.

The gross distribution patterns of the experimental and calculated GT-strengths are shown in fig. 1(b), as the histograms of summed strengths in 0.25 MeV wide energy bins. In the high energy region above 6 MeV, The difference in shape of the distribution between experiment and calculation is apparent. This was also the case for $^{29}S \rightarrow {}^{29}P$. Considering these facts, it seems rather difficult to say that a common quenching factor is calculable above 6 MeV by simply comparing the experiment with calculation.

4. Conclusion

The above comparison of the experimental GT-strengths in ^{25}Al and ^{29}P with shell model calculations shows a problem in the predictability of the shell model, especially in the high energy regions above 6 MeV. It should also be noticed, although not explicitly shown in fig. 1, that the concentration of the GT-strength in the IAS in 25Al cannot be explained by the theory. Further improvement is evidently necessary in the calculation before a definite conclusion on the common renormalization of the GT-coupling constant may be derived.

References:

1) B. A. Brown and B. H. Widenthal: At. Data and Nucl. Data Tables, 33, 347, (1968).
2) S. Morinobu, I. Katayama, M. Fujiwara, S. Hatori, N. Ikeda, H. Miyatake, H. Nakabushi, and K. Katori: to be published in Nucl. Instr. and Meth. B.
3) S. Hotori, H. Miyatake, S. Morinobu, K. Katori, M. Fujiwara, I. Katayama, N. Ikeda, T. Fukuda, T. Shinozuka and K. Ogawa: to be published in Nucl. Phys. A.
4) P. L. Reeder, A. M. Poskanzer, R. A. Esterlund and R. McPherson: Phys. Rev. 147, 781, (1966).
5) D. J. Vierra, R. A. Gough and J. Cerney: Phys. Rev. C19, 177 (1979).

V-A-9

MEASUREMENT FOR $^{12}C(2^+)$ SPIN ALIGNMENT FOLLOWING THE $^{12}C + ^{16}O$ COLLISION AROUND E_{cm}=32MeV

Takashi MUKAE, Hiroshi FUJITA*, Takumi OKAMOTO, Shunji NIIYA, Makoto MATSUO, Shinichi MITSUOKA, Kenji UTSUNOMIYA, Yasuharu SUGIYAMA**, Yoshiaki TOMITA**, Kazumi IDENO**, Hiroshi IKEZOE**, Yoshimaro YAMANOUCHI**, Tsuyoshi SUGIMITSU, Norihisa KATO and Shunpei MORINOBU

Previous observation[1)] of some resonance-like structure in the mutually excited $^{12}C(2^+)$ + $^{16}O(3^-)$ channel around E_{cm} = 32MeV in particular has stimulated us to study it in more detail by measuring the magnetic substate population of the outgoing $^{12}C(2^+)$ particles.

The present measurement is focussed on the $^{12}C(2^+)$ + $^{16}O(0^+gs)$ (single excitation) and $^{12}C(2^+)$ + $^{16}O(3^-)$ (mutual excitation) channels.

Excitation functions were taken at θ_{lab} = 7.0° from 72.2MeV to 79.0MeV in a step of 0.4MeV. Angular distributions were measured in the laboratory angle ranging from 4.0° to 15.0° in a step of 1° at the beam energies of 75.0MeV (on resonance) and 77.8MeV (off resonance).

The experiments were carried out at JAERI Tandem Van de Graaf accelerator by using the magnetic spectrograph ENMA. An $^{16}O^{6+}$ beam was used to bombard a ^{12}C target with 50 $\mu g/cm^2$thickness. After the outgoing ^{12}C particle were momentum analyzed by the spectrograph, they were identified with a hybrid focal plane detector which allowed measurements of position, energy and δE of each particle. Typical momentum spectra are shown in Fig. 1. The broadened line shape for the $^{12}C(2^+)$ channels due to recoil by γ-ray emission is clearly observed as well as some sharp peaks for the $^{12}C(0^+gs)$ ones.

The obtained excitation functions are shown in Fig. 2. In the single excitation a resonant structure seems to exist at E_{cm} = 32.06MeV. In the mutual excitation a weakly correlated structure is also seen at the same energy. Because of this, we measured the angular distribution at two energies noted above.

Department of Physics, Kyushu University, *Daiichi College of Pharmaceutical Sciences, **Department of Physics, JAERI

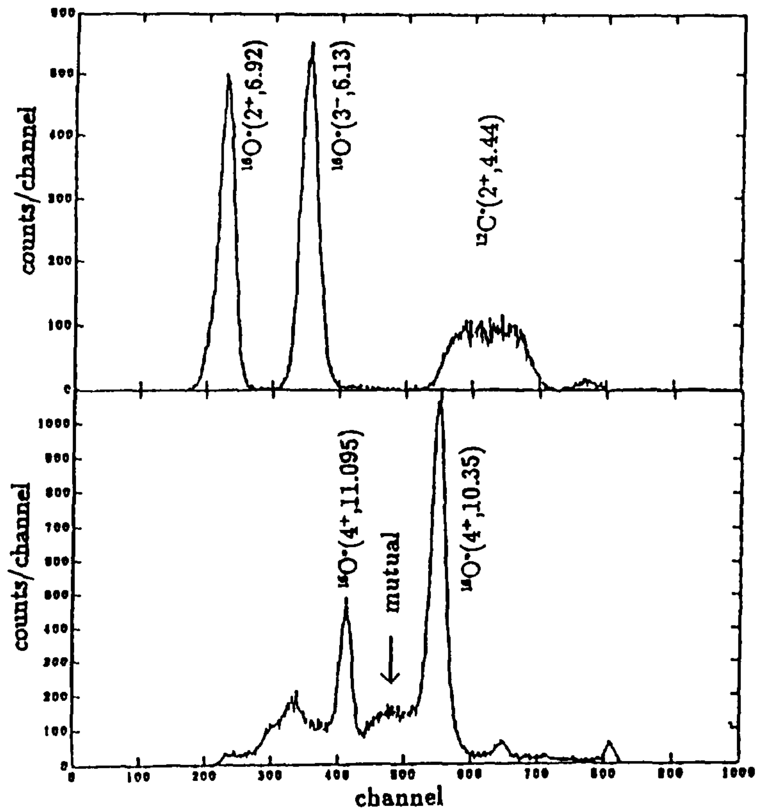

Fig. 1 Typical momentum spectra.

The relative differential cross sections are given in Fig. 3. In the single excitation an oscillatory amplitude for on resonance is smaller than the one for off resonance. In the mutual excitation the relative differential cross section for on resonance is out of phase with the one for off resonance.

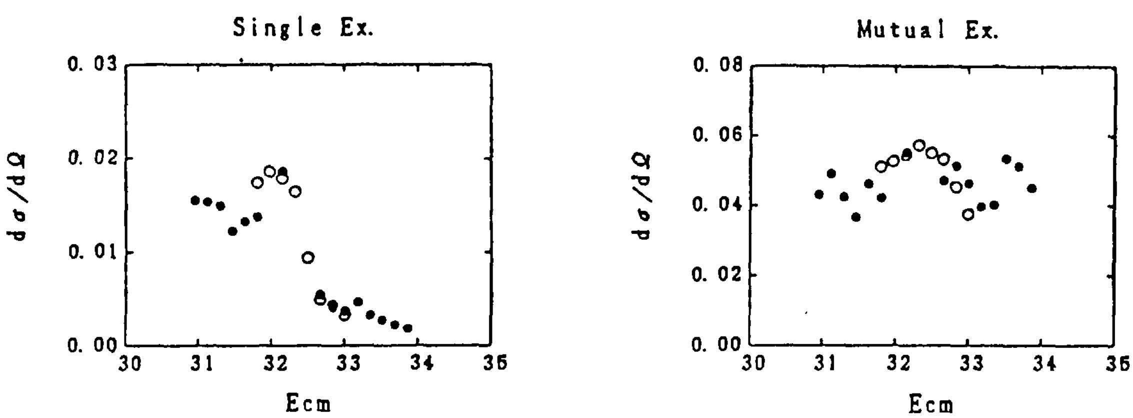

Fig. 2 Excitation function.

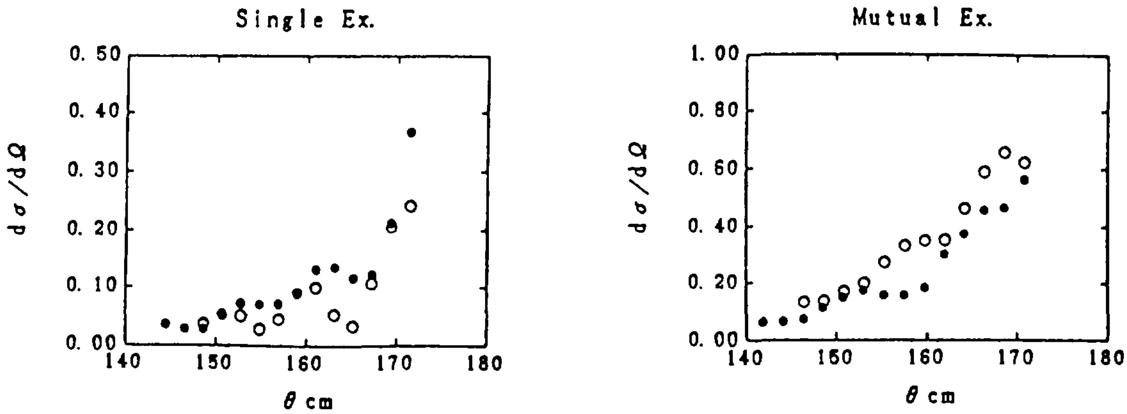

Fig. 3 Differential cross section.

The broadened line shape at each angle is analyzed in a similar procedure described in ref. 2. The magnetic substate population was determined through a least square fit to the measured line shape. Examples of the fitting are shown in Fig. 4 and the angular dependence of magnetic substate population is presented in Fig. 5.

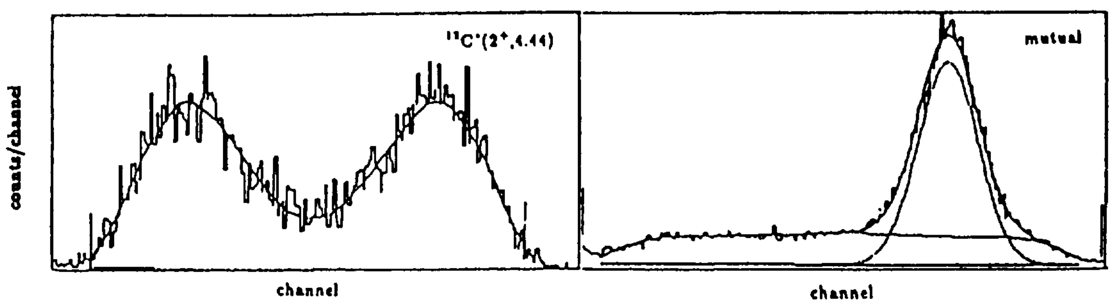

Fig. 4 Examples of line shape fitting.

Cross section for each magnetic substate[3)] is predicted theoretically by the following equations: in single excitation

$$d\sigma_m(\theta) = \Big|\sum_{\mu L'} a_{L'}(L'I-\mu\mu|L0)Y_{L'}^{-\mu}(\theta,0)d^{I}_{\mu m}(\theta)\Big|^2 \qquad (1)$$

and in mutual excitation

$$d\sigma_m(\theta) = \sum_{S\mu'}\Big|\sum_{L'} a_{L'}(II'\mu\mu'|SM)(L'S-MM|L0)Y_{L'}^{-M}(\theta,0)d^{I}_{\mu m}(\theta)\Big|^2. \qquad (2)$$

If only one partial wave contributes on resonance ,we can estimate the substate population parameters. In Fig. 5 comparison between calculation and experiment is made for a (L, L′) combination, where L and L′ denote the initial and final angular momentum, respectively. Solid curve is the result of calculation. In the single excitation calculation with L = J = 16, L′ = J − 2 = 14 or L = J = 17, L′ = J − 2 = 15 seem to be in better agreement with the experimental. Hence we conclude that the transition from L = J to L′ = J−2 is dominant and that spin of the resonance may be 16 or 17ħ. In the mutual excitation, however, the calculation any (L, L′) combination failed to reproduce the experiment and further consideration is necessary.

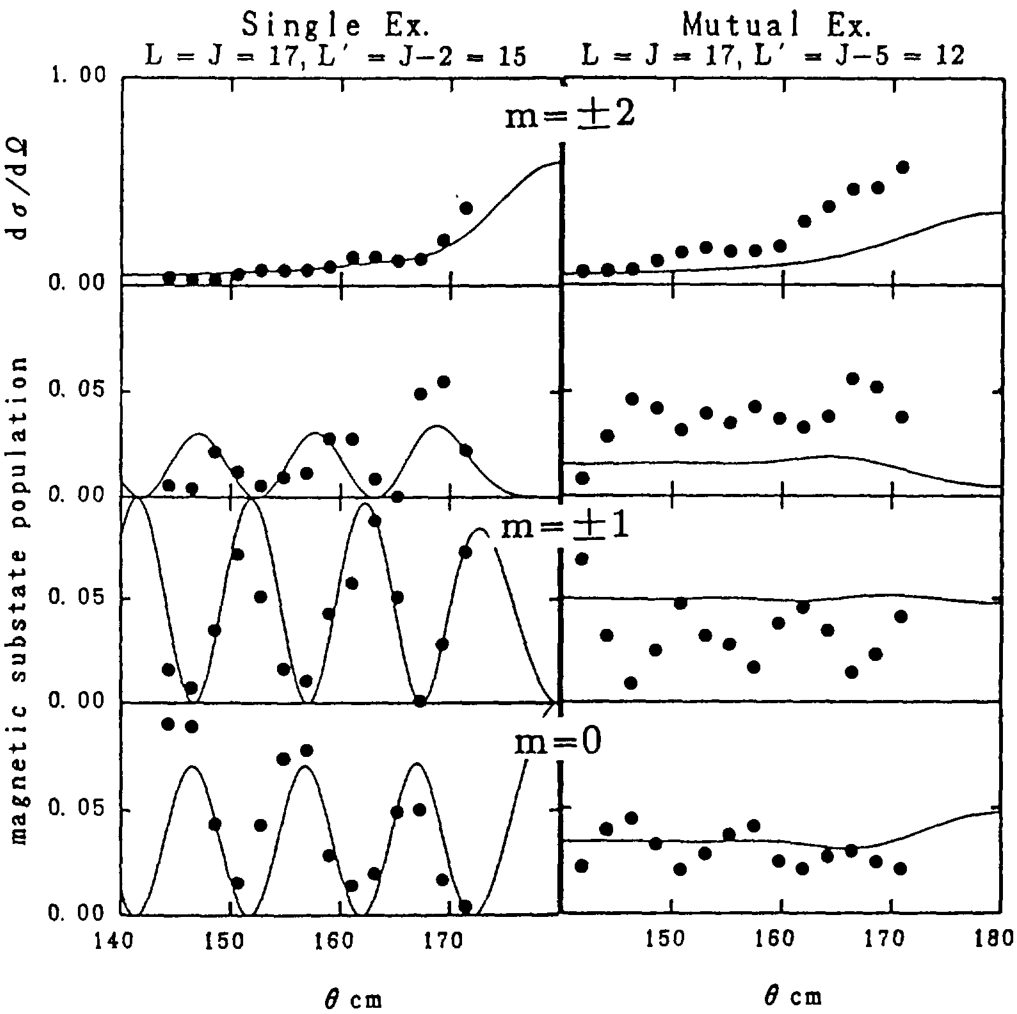

Fig. 5 Magnetic substate population.

References:

1) N. Kato et al., Kyushu University Tandem Accelerator Laboratory Report (1980−1984) p.106.
2) Y. Sugiyama, Y. Tomita, H. Ikezoe, and N. Shikazono, Z. Phys. A - Atoms and Nuclei 322 (1985) 579.
3) A. H. Wuosmaa, et al., Phys. Rev. C41 (1990) 2666.

V-A-10

Electron detector to identify the $^{16}O(0^{+},6.05\ MeV)$

T. Sugimitsu, K. Utsunomiya, T. Okamoto, S. Niiya, S. Mitsuoka,
T. Mukae, M. Hijiya, K. Nakamoto, H. Fujita and S. Morinobu

In the study of molecular resonances, recently much attension has been paid to the excitation of highly excited and/or mismatched channels. In particular when the ^{16}O nucleus is a reaction partner in these channels, it is vitally important to clearly identify the ^{16}O state at 6.05 MeV from the more strongly excited one at 6.13 MeV. Here is described our electron detector system which has been just tested with $^{16}O(p,p)^{16}O^{*}$ reaction and has begun to be successfully applied to the study of $^{12}C+^{16}O$ resonance reactions(fig. 1B). As shown in fig. 1A the detector is in principle similar with that of ref. 1. However, two such detectors are arranged in the reaction plane(fig. 1B) and one more would be added from the vertical port to increase the detection efficiency. A NE102A plastic scintillator(65 mm diameter and 0.5 mm thickness) is held at one end of a rolled aluminized myler and at the other end is equipped an photomultiplier(HAMAMATSU R329) 185 mm apart from the scintillator. The forward face of the scintillator is also protected against light with aluminized myler. This scintllator system is housed in an aluminum tube so that the photomultiplier may be operated in atmosphere. At the forward end of the tube is glued an 50 μm myler and at the rear end is welded a vacuum clamp connector, through which signal and bias cables can be wired out of the scattering chamber via a flexible bellow tube. A reasonable thickness of myler is inserted between scintillator and front myler window to stop light charged particles. A 96 μm myler strip which is 110 mm long and has a 10 mm diameter utilized as target holder in order to reduce the electrons ejected by high energy gamma-rays from materials surrounding the target. To see the performance of each system, a target of tungsten oxide evaporated on a thin carbon foil is bombarded with 8.9 MeV proton beam and SSD-scintillator coincidence events are accumulated under the same condition as in ref. 1. Efficiencies for electrons(or positrons) from internal pair processes and for 6.13 MeV gamma-rays are similarly estimated. Although the electron efficiency is a little smaller than that of ref. 1 probably due to smaller light yields in our case, the gamma-ray efficiency is also smaller by a factor of more than two. As a result the figure of merit(electron efficiency/gamma-ray efficiency) is estimated to be 107 and 167 in our two detectors, while it is reported to be 77 in ref. 1.

References:

1) W. K, Wells, D. Cebra and D. P. Balamuth: Nucl. Instr. and Meth. A223, 103, (1984)

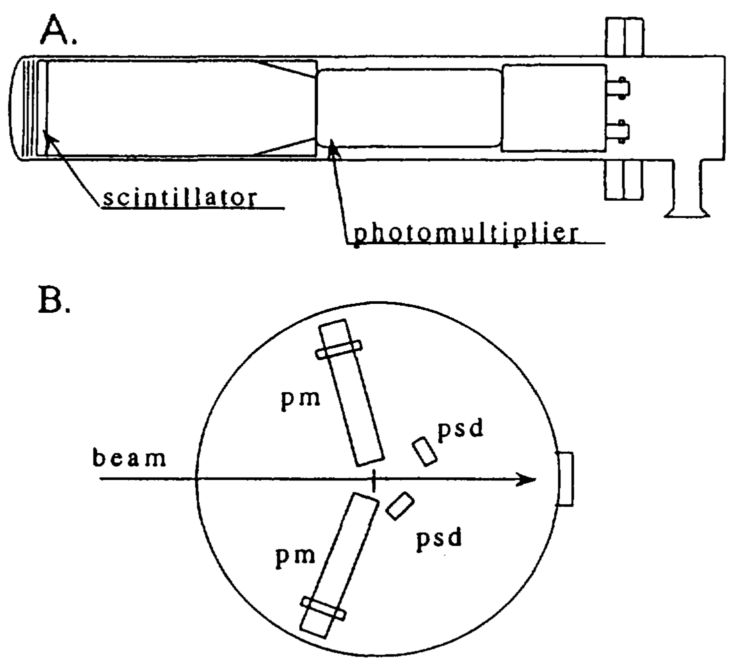

Fig. 1. (A) Structure of the detector. (B) Set up for the $^{12}C+^{16}O$ reaction.

B. Department of Energy Conversion Engineering

V-B-1 Luo-Kawai model and its application to nuclear data evaluation

Yukinobu Watanabe

A paper on this subject was presented at the Specialists' Meeting on High Energy Nuclear Data (Oct. 3-4, 1991, JAERI) and published in JAERI-M 92-039, p.143, with the following abstract:

A semiclassical distorted wave model proposed by Luo and Kawai is briefly reviewed. The model calculations are compared with several experimental angular distributions and proton energy spectra of (p,p') scattering at 20- 200 MeV. Some problems relating to the application to high energy nuclear data evaluation are discussed.

V-B-2 Measurements of continuum spectra of charged particles emitted from reactions induced by protons of 10 to 40 MeV

Y. Watanabe, A. Aoto, H. Hane, H. Kashimoto, and N. Koori*

A paper on this subject was published in GENSHIKAKU KENKYU Vol. 36, No.4, p.137 (1992) with the following abstract:

We introduce a measuring system for continuum spectra of emitted charged particle which has been utilized in the measurement of charged particle nuclear data using the tandem Van de Graaf accelerators at Kyushu University and Japan Atomic Energy Research Institute. A problem of background component due to slit scattering is discussed in the data processing of (p,xp) spectra. Several experimental results and theoretical analyses are briefly reported.

* College of General Education, The University of Tokushima, Tokushima 770

V-B-3 <u>Measurements of double differential charged-particle emission cross sections for reactions on ^{98}Mo and ^{nat}Si induced by 25.6 MeV proton</u>

Y. Watanabe, A. Aoto, H. Hane, H. Kashimoto, Y. Koyama, H. Sakaki, N. Koori*, Y. Yamanouchi** , M. Sugimoto** , and S. Chiba**

This paper on this subject was submitted to Tandem ANNUL REPORT 1991, Japan Atomic Energy Research Institute, with the following abstract:

Double differential cross sections of charged particles emitted from proton-induced reactions on ^{98}Mo and ^{nat}Si have been measured at 25.6 MeV to investigate preequilibrium process. The exciton model calculation using the same parameters as those obtained from the previous analysis in 10-20 MeV region shows good agreement with the measured proton spectra for ^{98}Mo. Preliminary calculations based on the SMD-SMC model are also compared with the experimental (p,xp) and (p,xn) spectra.

---

* College of General Education, The University of Tokushima, Tokushima 770
** Japan Atomic Energy Research Institute

V-B-4 <u>Calculations of Kerma Factors for ^{12}C at Neutron Energies of 10 - 20 MeV</u>

H. Shinohara, H. Kashimoto, and Y. Watanabe

A paper on this subject will be published in Engineering Sciences Reports, Kyushu University, Vol. 14, No.2 (1992) with the following abstract:

Kerma factors of ^{12}C in the neutron energy region from 10 to 20 MeV are calculated using the latest evaluated nuclear data library JENDL-3. The partial kerma factor for (n,n')3α reaction process shows the most important contribution to the total kerma factor at energies more than 14 MeV. The phase space model is applied to the modelling of the (n,n')3α process. The calculated result by the phase space model provides rather better agreement with experimental values than that by the evaporation model at high neutron energies.

V-B-5

Parameters of Reaction Cross Section Calculation for Medium Nuclei

T. Kawano, H. Tanaka, K. Kamitsubo and Y. Kanda

A paper on this subject was presented at the 1991 Symposium on Nuclear Data, and published in JAERI-M 92-027, p.225, with the following abstruct:

Cross sections for neutron induced reactions of ^{58,60}Ni, ^{59}Co, and ^{54,56}Fe are calculated employing optical, Hauser-Feshbach, and pre-equilibrium models.

Neutron optical model parameters (OMP's) of target nuclei were estimated previously from experimental total cross sections and differential elastic scattering cross sections.. These parameters are adopted for the Hauser-Feshbach calculation, and reaction cross sections are compared with ones when some global OMP's and the other published OMP's are employed. The comparisons of proton OMP's are also performed.

The reaction cross sections are calculated with some combinations of neutron and proton OMP, and the level density parameters are adjusted so as to reproduce available experimental data. Some of these combinations show that it is difficult to reproduce the experimental data by means of adjustment of level density parameters only.

VI. Nagoya University

VI-A-1

Measurement of β^{+}-activity by detecting 511 keV annihilation γ-rays

K. Kawade, K. Katou, A. Osa, M. Shibata, H. Yamamoto, T. Katoh, T. Iida* and A. Takahashi*

A paper on this subject was published in Nuclear Instruments and Methods in Physics Research A 301 (1991) pp. 594-595 with the following abstract.

A method was proposed to measure β^{+}-activities of radionuclides emitting almost no γ-rays by detecting 511 keV annihilation γ-rays with a Ge detector. The β^{+}-sources with maximum energies up to about 3.4 MeV can be regarded as 511 keV point γ-sources, if the sources are set between two 10 mm thick acrylic plates. The effect of diffused annihilation positions of β^{+}-particles in the absorber on detection efficiencies was observed to be negligible with an accuracy of 1.0 %.

* Department of Nuclear Engineering, Osaka University

VI-A-2

Measurement of formation cross sections of short-lived nuclei by 14 MeV neutrons

Toshio Katoh, Kiyoshi Kawade, Hiiroshi Yamamoto,
Akito Takahashi* and Toshiyuki Iida*

Measurement of formation cross sections of short-lived nuclei produced by 14 MeV neutron were made using the Intense Neutron Source(OKTAVIAN) at Osaka University. Cross sections of (n, 2n), (n, p), (n, n'p) and (n, α) reactions for Ru, Pd, Cd and Sn were obtained by the activation method. Pneumatic tubes were used for the transportation of samples between the irradiation points and the detector. Gamma-rays from irradiated samples were measured by a Ge detector, and cross sections were obtained from the amount of induced activities.

Measured cross sections are shown in following figures.

* Department of Nuclear Engineering, Osaka University

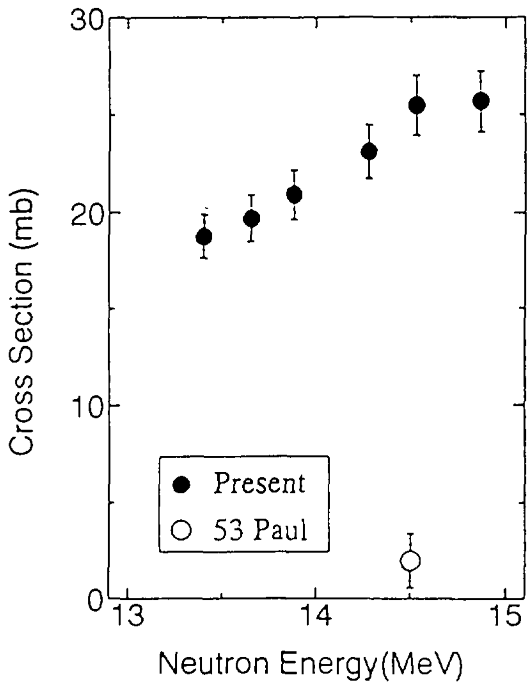

Fig. 1 $^{101}Ru(n,p)^{101}Tc$

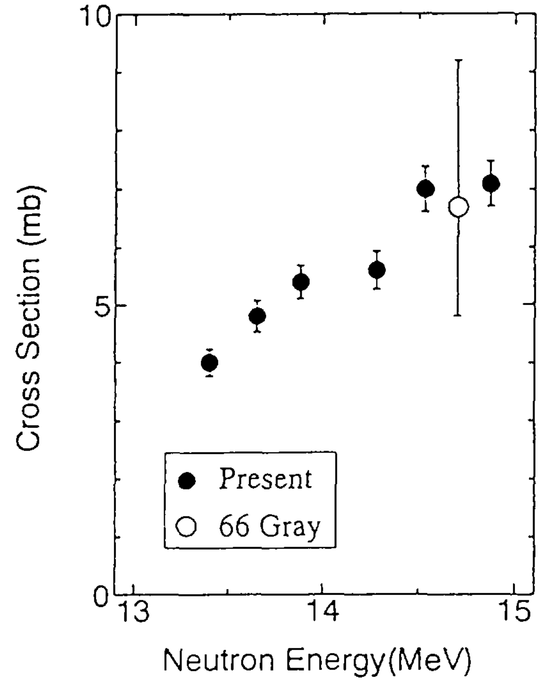

Fig. 2 $^{102}Ru(n,p)^{102m}Tc$

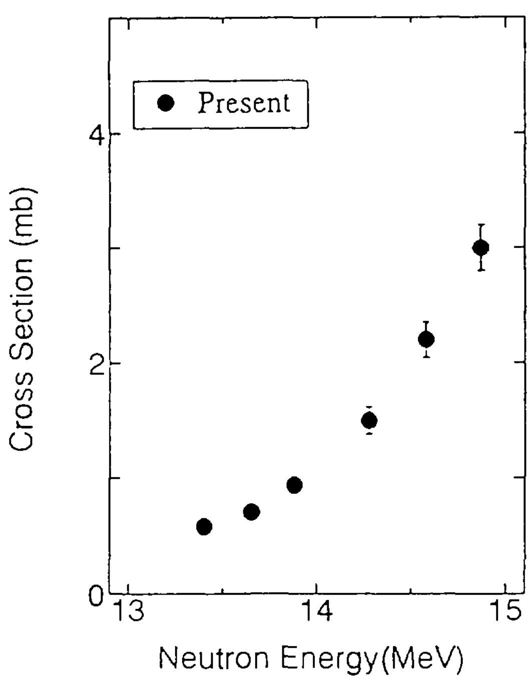

Fig. 3 $^{102}Ru(n,np)^{101}Tc$

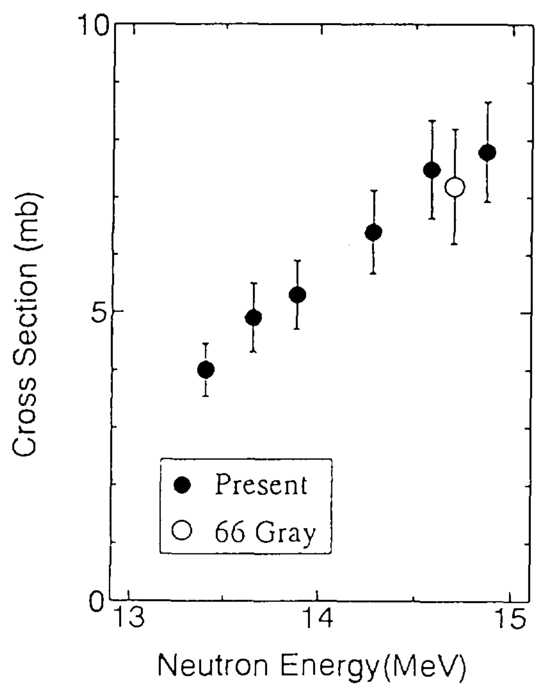

Fig. 4 $^{104}Ru(n,p)^{104}Tc$

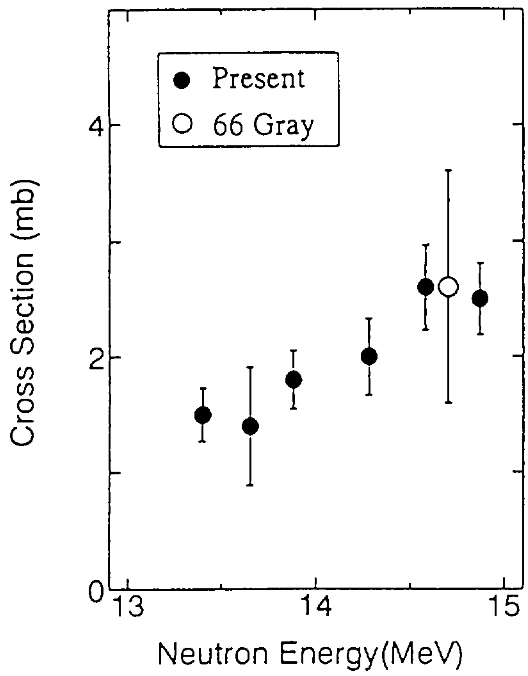

Fig. 5 $^{104}Ru(n,\alpha)^{101}Mo$

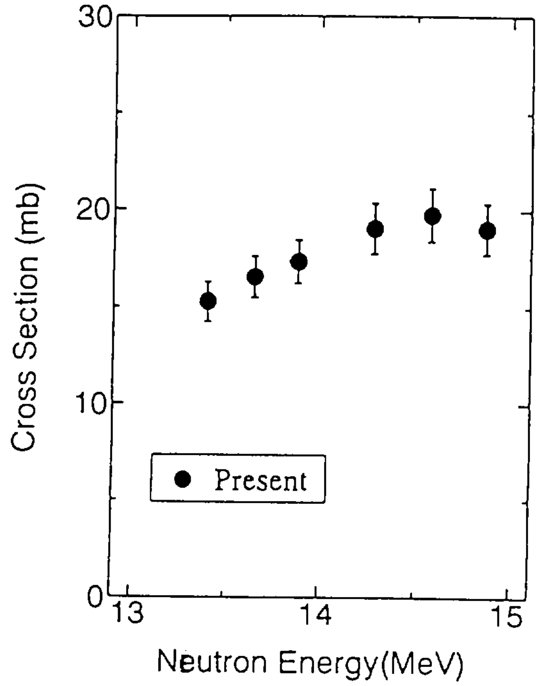

Fig. 6 $^{104}Pd(n,p)^{104m}Rh$

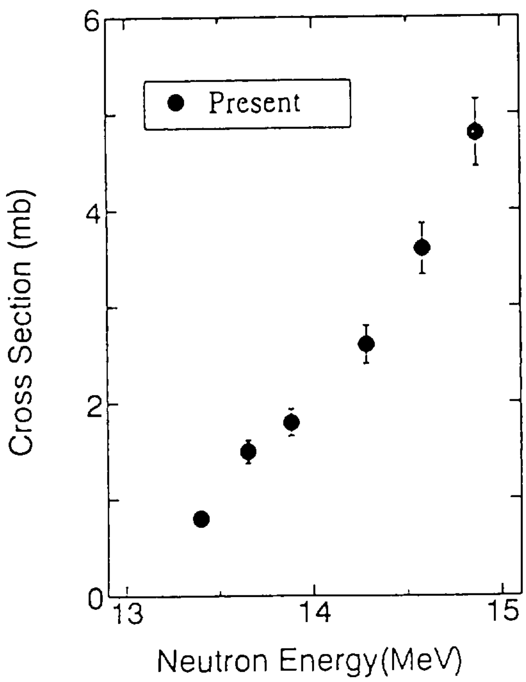

Fig. 7 $^{105}Pd(n,np)^{104m}Rh$

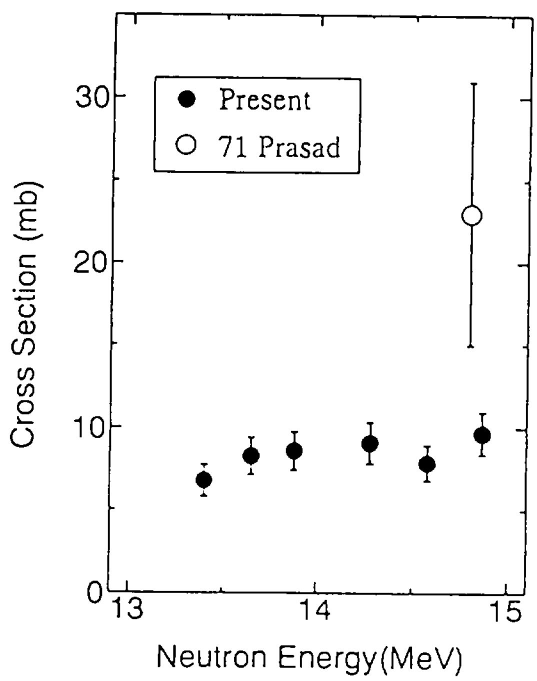

Fig. 8 $^{105}Pd(n,p)^{105m}Rh$

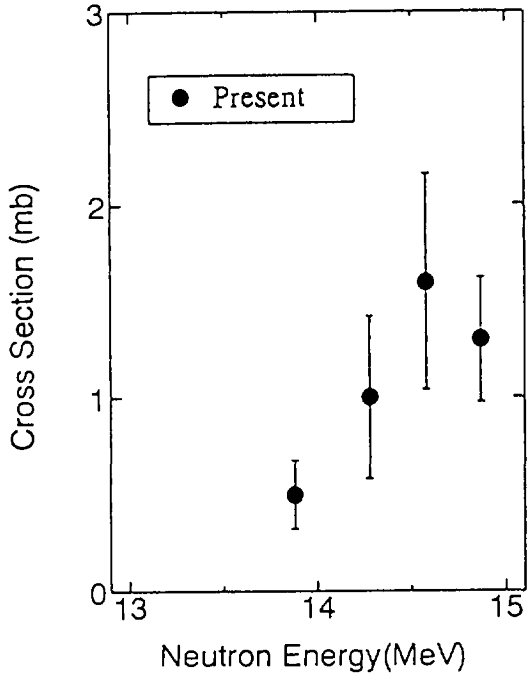

Fig. 9 $^{106}Pd(n,np)^{105m}Rh$

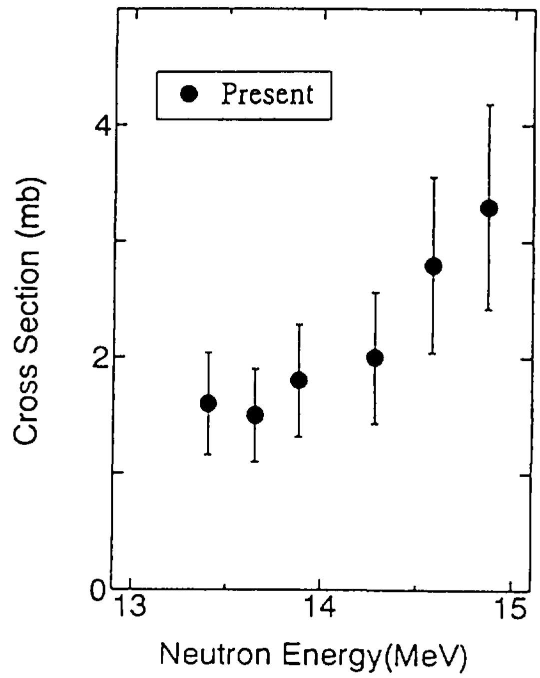

Fig. 10 $^{108}Pd(n,p)^{108g}Rh$

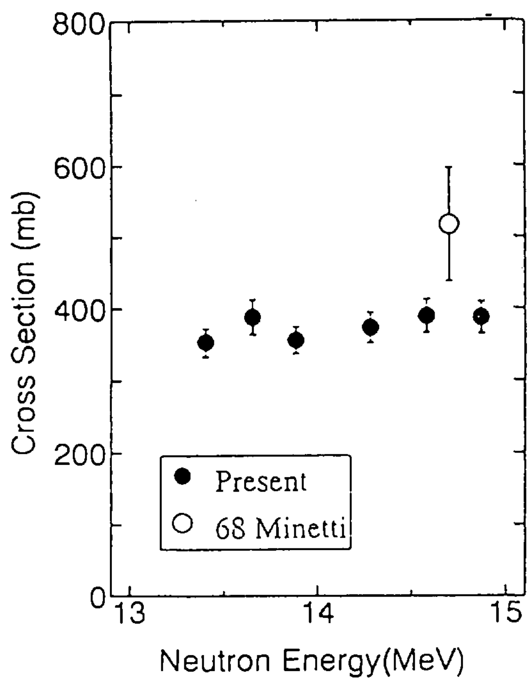

Fig. 11 $^{108}Pd(n,2n)^{107m}Pd$

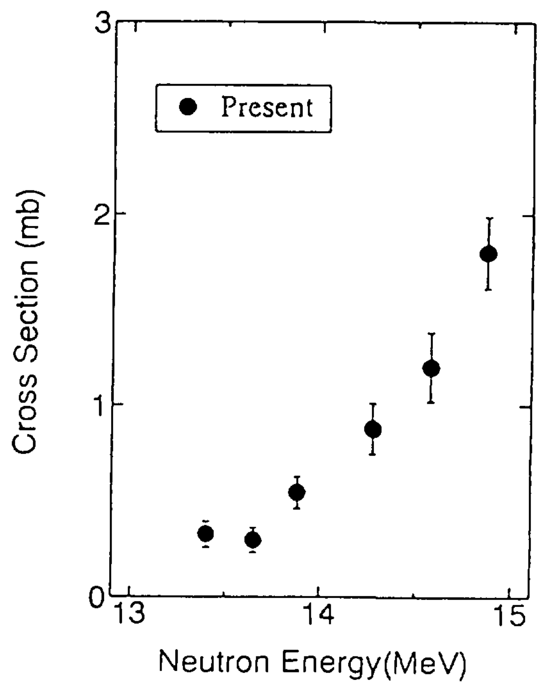

Fig. 12 $^{108}Pd(n,np)^{107}Rh$

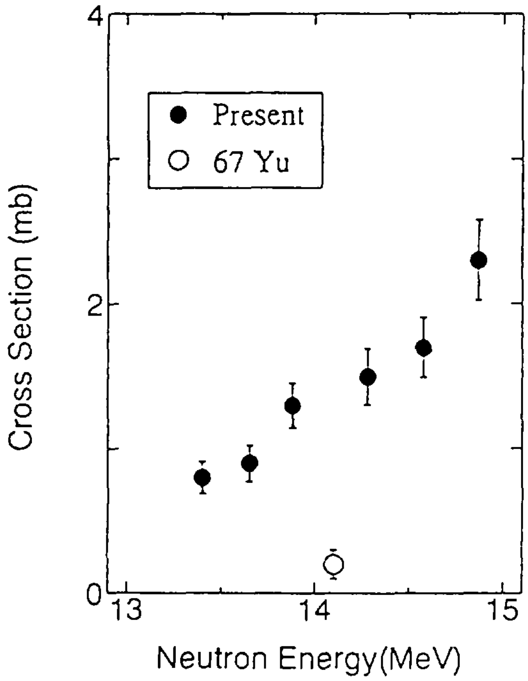

Fig. 13 $^{116}Cd(n,p)^{116g}Ag$

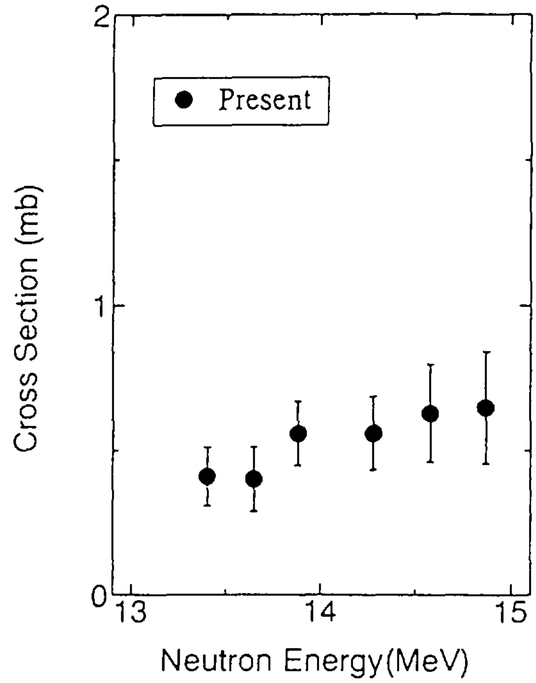

Fig. 14 $^{112}Cd(n,a)^{109m}Pd$

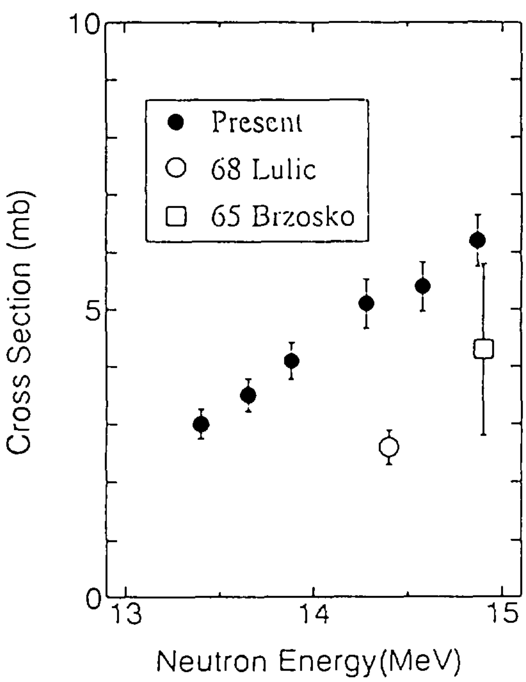

Fig. 15 $^{119}Sn(n,p)^{119g}In$

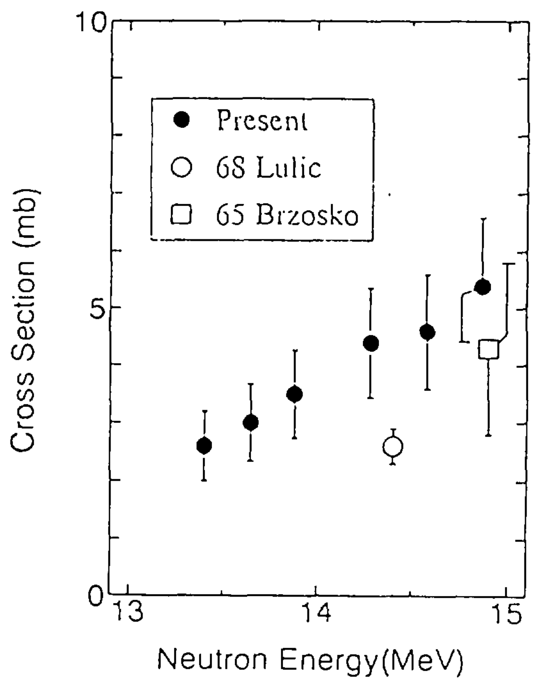

Fig. 16 $^{119}Sn(n,p)^{119m}In$

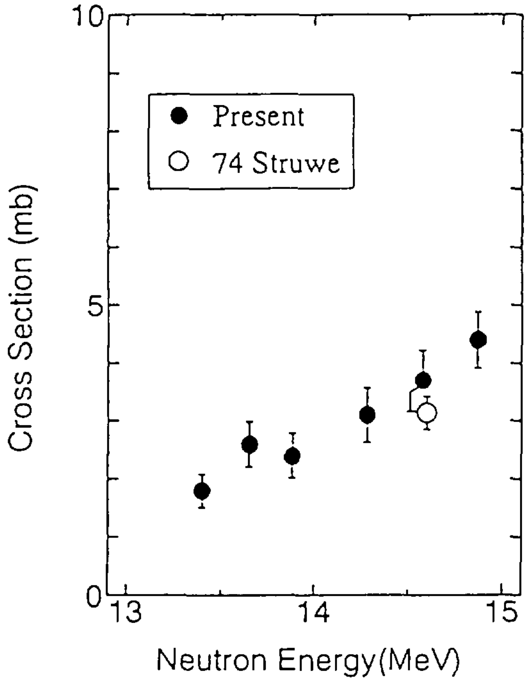

Fig. 17 $^{120}Sn(n,p)^{120m}In$

VII. Nuclear Energy Data Center

VII-A-1

Evaluation of Photoreaction Nuclear Data on ^{209}Bi

Sin-iti Igarasi

As one of the evaluations for photoreaction nuclear data projected in JNDC, nuclear data on ^{209}Bi has been taken. Since there were very scarce experimental data, most of the reaction data have been obtained using nuclear model calculations.

Photo-absorption cross sections were calculated using the giant dipole resonance with two peaks and quasi-deuteron models. Resonance parameters for the former were adopted as follows so that the experimental data[1] might be reproduced:

$$\sigma_a^{GD}(\varepsilon) = \Sigma\sigma_m / \{ 1 + [(\varepsilon^2 - E_m^2)^2 / \varepsilon^2 \Gamma_m^2] \},$$

$$E_1 = 13.45 \text{ MeV},$$
$$\sigma_1 = 521 \text{ mb},$$
$$\Gamma_1 = 3.97 \text{ MeV},$$
$$E_2 = 20.0 \text{ MeV},$$
$$\sigma_2 = 20.0 \text{ mb},$$
$$\Gamma_2 = 5.0 \text{ MeV},$$

The parameters for the first peak were selected from the compilation by Dietrich and Berman[2], and for the second peak were taken so as to fit the experimental data around 20 MeV.

The quasi-deuteron model was used above about 15 MeV where the (γ,np) reaction is effective. It was taken as

$$\sigma_a^{QD}(\varepsilon) = L\ (NZ/A)\ \sigma_D(\varepsilon)\ f(\varepsilon),$$

where $\sigma_D(\varepsilon)$ is the deuteron photo-disintegration cross section[3],

$$\sigma_D(\varepsilon) = 61.2(\varepsilon - B_D)^{3/2} / \varepsilon^3, \quad \text{(mb)}$$

and $f(\varepsilon)$ is the Pauli blocking factor given by Chadwick et al.[4],

$$f(\varepsilon) = 8.3714\times10^{-2} - 9.8343\times10^{-3}\times\varepsilon + 4.1222\times10^{-4}\times\varepsilon^2 - 3.4762\times10^{-6}\times\varepsilon^3 + 9.3537\times10^{-9}\times\varepsilon^4.$$

The Levinger parameter L and the deuteron binding energy B_D are taken as 6.5 and 2.225 MeV, respectively. Branching ratios for the reactions were calculated using a computer code ALICE–F[5] which is a modified version from the original one by Blann[6].

Figures 1 to 3 show good agreement between the present results and the experimental data. Photo–absorption and some reaction cross sections are given in Fig. 4. Whole results of the evaluation are compiled in ENDF/B format on magnetic disk.

References

1)R.R.Harvey, J.T.Caldwell, R.L.Bramblett and S.C.Flutz: Phys. Rev. 12, B126 (1964).
2)S.S.Dietrich and B.L.Berman: Atomic Data and Nucl. Data Tables 38, 199 (1988).
3)J.R.Wu and C.C.Chang: Phys. Rev. C16, 1812 (1977).
4)M.B.Chadwick, P.Oblozinsky, P.E.Hodgson and G.Reffo: Phys. Rev. C44, 814 (1991)
5)T.Fukahori: private communication.
6)M.Blann: Ann. Rev. Nucl. Sci. 25, 123 (1975).

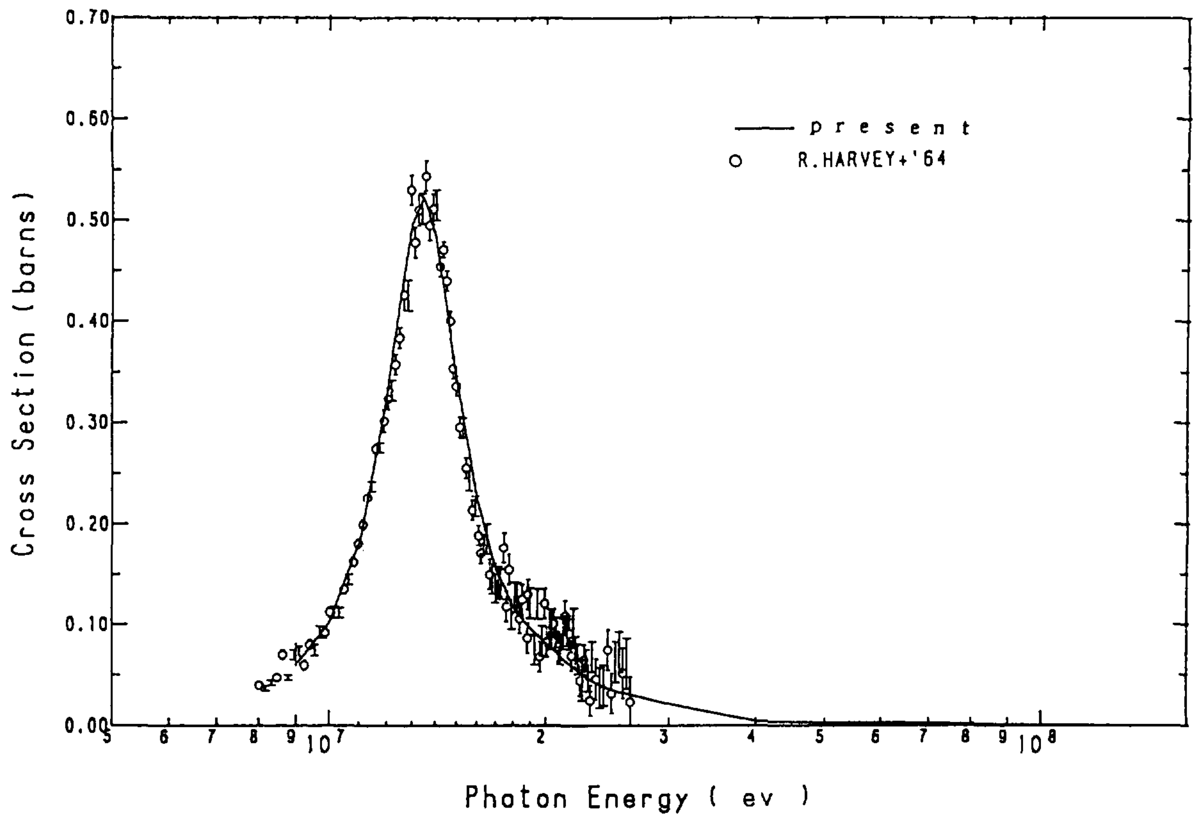

Fig. 1 ^{209}Bi(γ,xn) Cross Section

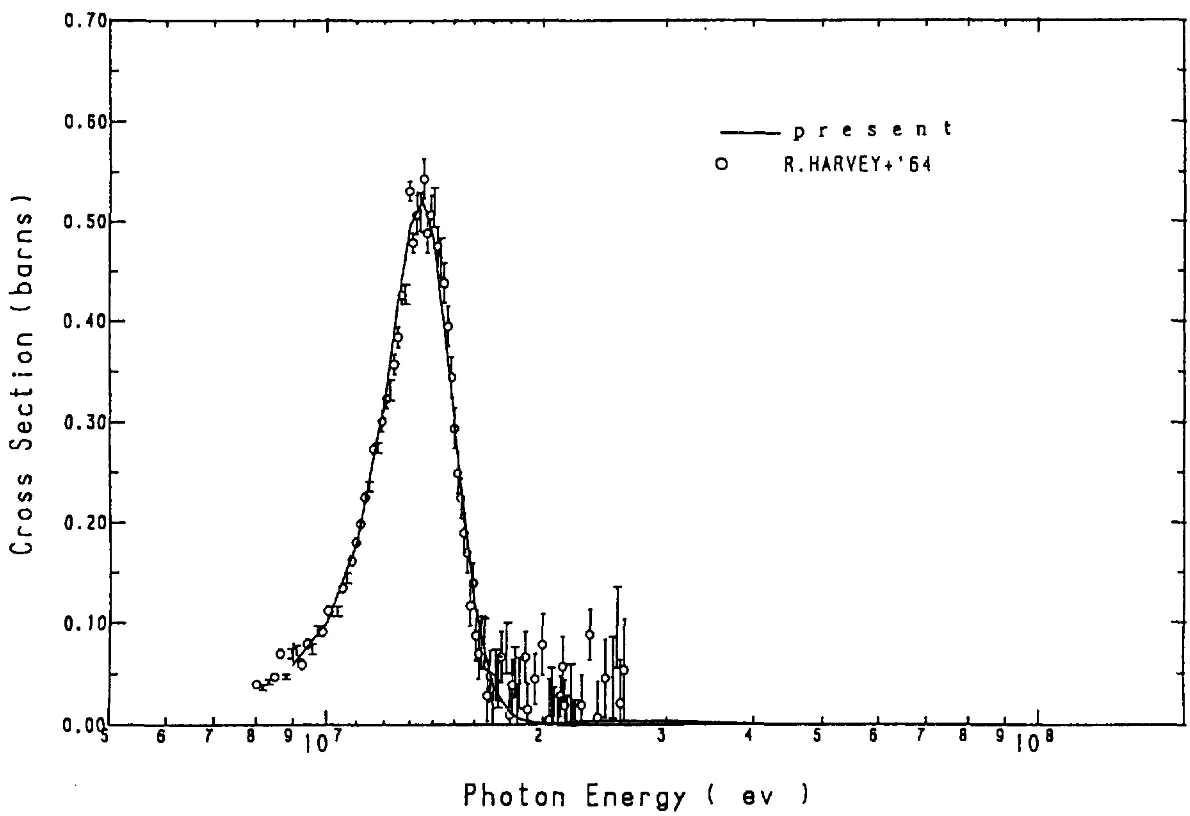

Fig. 2 ^{209}Bi(γ,n+np) Cross Section

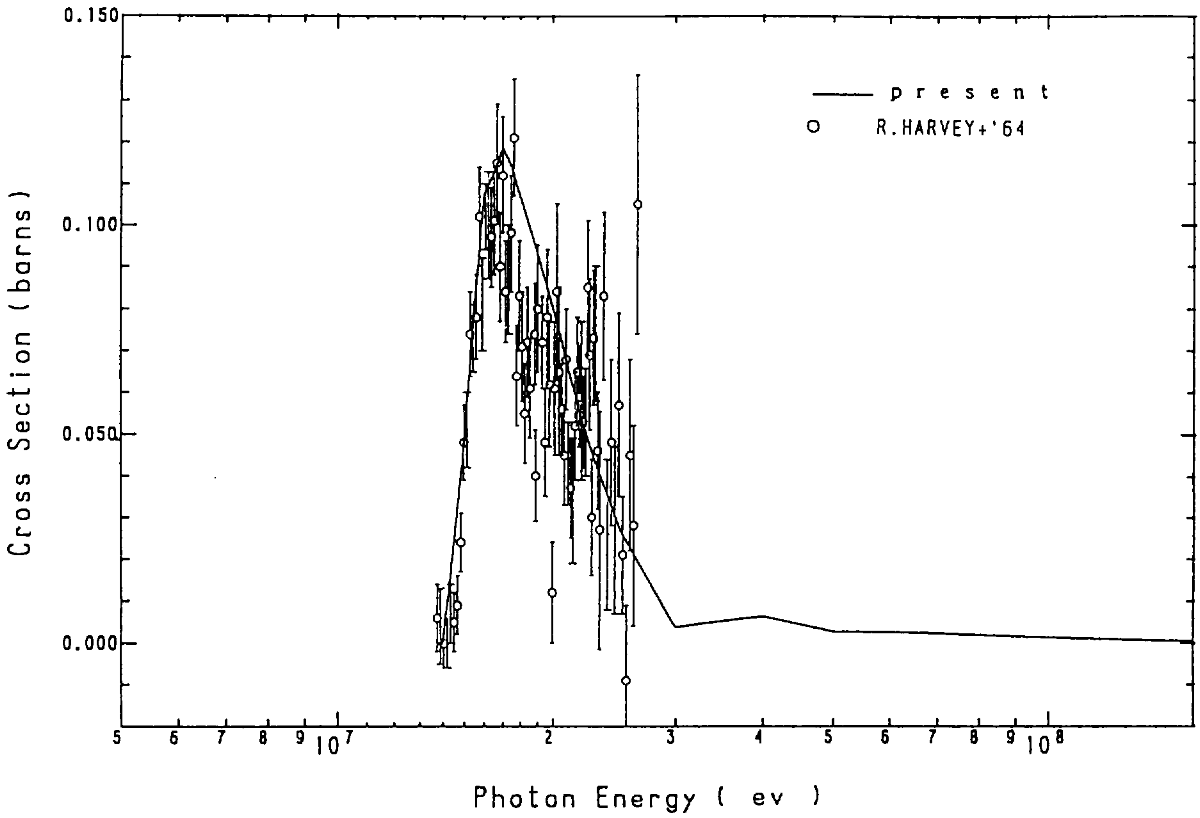

Fig. 3 ^{209}Bi(γ,2n+2np) Cross Section

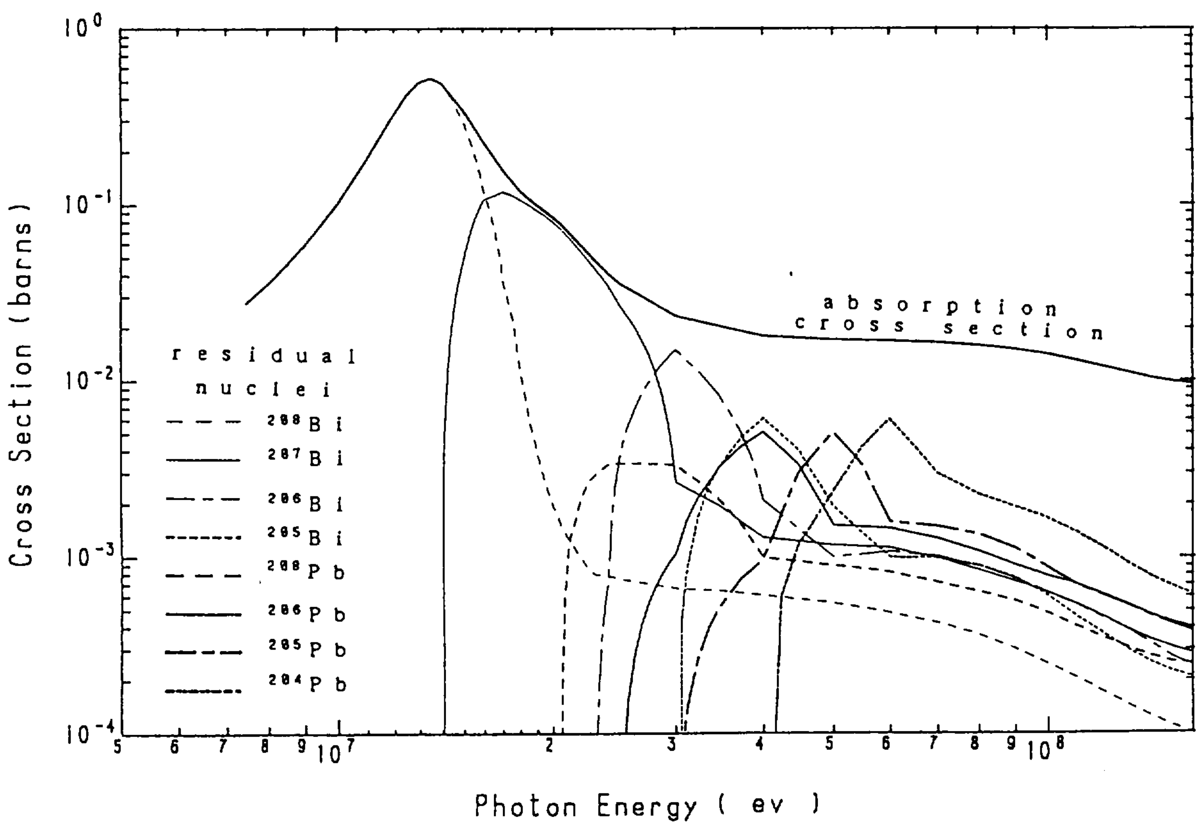

Fig. 4 ^{209}Bi Photo-absorption Cross Section and Some Isotope Production Cross Sections

VIII. Osaka University

A. Department of Nuclear Engineering

VIII-A-1

Measurements of Secondary Particle Spectra with 14 MeV Incident Neutrons

Akito Takahashi

Double differential neutron emission cross sections at 14 MeV incident neutron energy have been measured using the TOF spectrometer of OKTAVIAN[1]. A book of data tables and graphs for Li-6, Li-7, B-10, B-11, O-16, Ca, Ti, Mn, Fe, Ni, Co, Zr, Nb, Mo, Sn, Sb, Ta, W and Bi has been published[2]. In addition, data have been measured for Ge and As[3]. We have terminated this series of measurements in March 1992. However, a new series of measurements for mass number 100-150 is under planning to investigate the level density behavior in this mass region.

Current effort of measurements is concentrated on double differential charged particle emission cross sections by 14 MeV incident neutrons. A E-TOF spectrometer was developed[4]. Using this technique, we can measure double differential proton and alpha-particle emission cross sections, with comparable accuracies to Grimes' data. We have taken data for Fe, Ni and Co[5]. To investigate the direct breakup processes of

C(n,n'3alpha) and Be(n,2n2alpha) reactions, we are measuring angle-dependent alpha-particle spectra using thin foils of Be and carbon.

References:

1) A. Takahashi, "Measurement of double differential neutron emission cross sections at 14 MeV", Proc. Beijing Symp. Fast Neutron Physics, Sept. 1991, pp.3, World Scientific publ.

2) A. Takahashi, et al., "Double and Single Differential Neutron Emission Cross Sections at En = 14.1 MeV: Vol.2", OKTAVIAN Report A-92-01, Osaka University, (1992)

3) M. Gotoh, A. Takahashi, "Measurement of Double Differential Neutron Emission Cross Sectiona at En = 14.1 MeV for Ge and As", JAERI-M 92-027, pp.301, (1992)

4) S. Ogino, et al., "Development of Neutron-induced Secondary Charged Particle Spectrometer Based on Two-dimensional E-TOF Analysis", OKTAVIAN Report A-91-01, Osaka University, (1991)

5) S. Ogino, A. Takahashi, "Secondary Charged Particle Spectrometer Based on E-TOF Two-dimensional Analysis (II)", JAERI-M 91-032, pp.293, (1991)

IX. The University of Tokushima

IX-A-1

Elastic and Inelastic Proton Scattering from ^{12}C and ^{16}O Nuclei

N. Koori, Y. Watanabe+, H. Hane+, A. Aoto+, H. Kashimoto+, H. Sakaki+,
Y. Koyama+, H. Shinohara+, H. Ijiri+, K. Sagara++, H. Nakamura++,
K. Maeda++ , S. Shimizu++, and T. Nakashima++

We have been studying experimentally and theoretically the mechanism of proton-induced reactions on light and medium-heavy nuclei, paying special attention to the continuum in the energy spectra of emitted particles[1-4]. In our program of polarized proton experiments covering the energy range 12-16 MeV, several data on elastic and inelastic proton scattering have also been accumulated for the 1p-shell nuclei. These data are analyzed on the basis of the optical model and the coupled channel (CC) method and are compared with available neutron data. Among these results, the analyses of elastic proton scattering from ^{12}C and ^{16}O with the spherical optical model (SOM) are described in this report.

The two sets of parameters derived by Nodvik et al.[5] and Woye et al.[6] were found to be inadequate for consistent description for its differential cross sections and analyzing powers for ^{12}C. The SOM fitting by means of the ECIS79 code was carried out to our data for

+ Department of Energy Conversion Engineering, Kyushu University.
++ Department of Physics, Kyushu University.

^{12}C in order to obtain improved parameter sets; the results are shown in Table I. As found in the table, the depth of imaginary part becomes much larger than the result by Woye et al. and the diffuseness of spin-orbit term becomes smaller than their result. The effect of resonance structure and coupling of the excited states($2^+{}_1$, $0^+{}_2$ $3^-{}_3$ etc.) should be investigated because such effect is known to be important for ^{12}C.

Recently we have measured differential cross sections and analyzing powers for elastic and inelastic scattering of ^{16}O nuclei. Figure 1 show the measured experimental data of the elastic scattering at 14 and 16 MeV. The results of SOM fits are also shown by solid lines in the figure; the derived parameters are given in Table II. The experimental results for ^{16}O show more remarkable variation with incident energy than those for ^{12}C, especially for the analyzing powers. This may be due to strong resonance in the compound nucleus ^{17}F; it has been reported that there is a broad $f_{7/2}$ single particle level in ^{17}F around 17.5 MeV and appreciably sharp resonance at 14.7 MeV in the excitation function of the elastic scattering. As seen in Fig.1, agreement of the SOM prediction with the experimental data is not so good with respect to the analyzing powers. Further analyses will be necessary to investigate the effect in detail.

References

[1] N. Koori et al., JAERI-M 89-167 (1989).
N. Koori et al., JAERI-M 91-009 (1991).
N. Koori et al., JAERI-M 92-029 (1992)

[2] Y. Watanabe et al: Proc. 1990 Symp. on Nuclear Data, JAERI-M 91-032 (1991) p.336.

[3] Y. Watanabe et al., Proc. Int. Conf. on Nuclear Data for Science and Technology

[4] Y. Watanabe et al., Proc. XXth Int. Symp. on Nuclear Physics, Nuclear Reaction Mechanism, p.151 (1990).

[5] J.S. Nodvik et al., Phys. Rev. **125**, 975 (1962).

[6] E. Woye et al. Nucl. Phys. **A394**, 139 (1983).

Table I. Optical potential parameters for ^{12}C at 14 and 16 MeV.

Spherical optical model (ECIS79)

	V_0 (MeV)	R_0 (fm)	a_0 (fm)	W_s (MeV)	r_i (fm)	a_i (fm)	V_{so} (MeV)	r_{so} (fm)	a_{so} (fm)
14MeV	64.668	1.000	0.679	26.143	1.476	0.101	6.510	0.962	0.040
16MeV	62.422	1.023	0.667	22.210	1.479	0.095	6.177	0.969	0.059

Table II. Optical potential parameters for ^{16}O at 14 and 16 MeV.

Spherical optical model (ECIS79)

	V_0 (MeV)	R_0 (fm)	a_0 (fm)	W_s (MeV)	r_i (fm)	a_i (fm)	V_{so} (MeV)	r_{so} (fm)	a_{so} (fm)
14MeV	51.067	1.244	0.528	11.673	1.354	0.120	5.406	1.052	0.493
16MeV	53.034	1.216	0.680	19.203	1.455	0.127	3.430	1.289	0.032

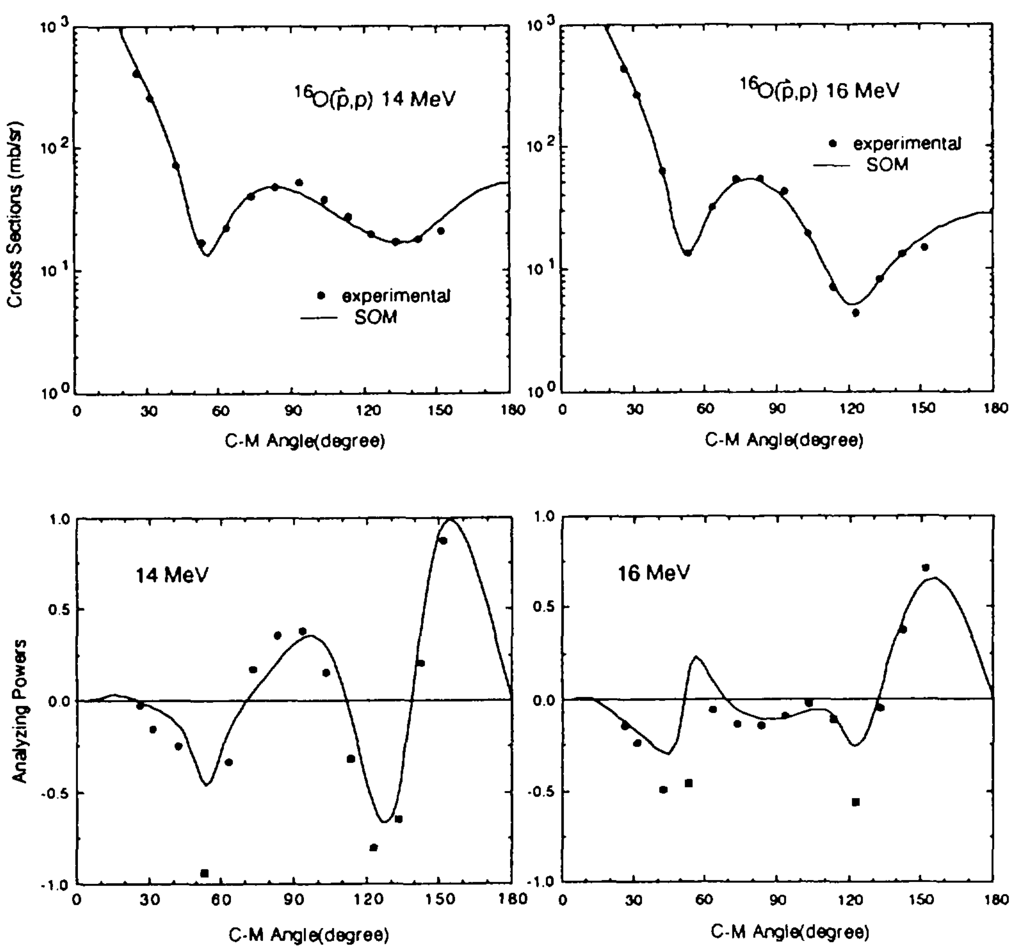

Fig.1. Comparison of experimental differential cross sections and analyzing powers of $^{16}O(p,p)$ elastic scattering at 14 and 16 MeV with the SOM fits.

IX-A-2

Polarized Proton Induced Breakup of ^{12}C at 16 MeV

N. Koori, Y. Watanabe[+], Kashimoto[+], H. Hane[+], A. Aoto[+], A. Nohtomi[++],

S. Widodo[++], O. Iwamoto[++], R. Yamaguchi[++], K. Sagara[+++],

H. Nakamura[+++], K. Maeda[+++] and T. Nakashima[+++]

A paper on this subject was published as JAERI-M 92-029 (1992) with the following abstract:

Double differential cross sections and analyzing powers were measured of protons and α particles emitted from the bombardment of ^{12}C with 16 MeV polarized protons. The measured energy spectra of protons and α particles were analyzed on the basis of the reaction model in which three- or four-body simultaneous breakup process is taken into account. The calculated proton and α particle spectra show good agreement with the continuous spectra observed in the low outgoing energy range.

[+] Department of Energy Conversion Engineering, Kyushu University.

[++] Department of Nuclear Engineering, Kyushu University.

[+++] Department of Physics, Kyushu University.

X. TOHOKU UNIVERSITY

A. Department of Nuclear Engineering

X-A-1 Double-differential Neutron Emission Cross Sections of Fe, Nb, Mo, Ta and Bi

M.Baba, S.Matsuyama, T.Ito, T.Okubo, H.Ide, F.Huang* and N.Hirakawa

Double-differential neutron emission cross sections (DDXs) have been measured for Fe, Nb, Mo, Ta, and Bi at 14.1 MeV incident energy, and for Nb, Bi at 18 MeV using Tohoku University Dynamitron TOF spectrometer. The scattering samples were right cylinders, 3-cm diam and 5-cm long, of natural elements. The method of experiment and data reduction was almost identical with that in our previous studies[1,2].

The experimental results were compared with the current evaluated file, JENDL-3 and ENDF/B-VI; the experimental data show marked disagreement with the evaluations both in shapes and angular dependence of emission spectrum especially in backward emission angles.

Angle-integrated neutron emission spectra and secondary neutron angular distributions were analyzed, respectively, using the statistical multistep reaction code EXIFON[3], and systematics by Kalbach[4] and by Kalbach-Mann[5].

---

*)Institute of Heavy Ion Physics, Peking University, PRC

The EXIFON calculations reproduce the experiments excellently both in shape and magnitude even in the energy region of collective levels except for the systematic underestimation of the Bi data at 14.1 MeV. These calculations indicated that the direct inelastic-scattering to collective states plays an important role for production of high energy secondary neutrons.

It proved that the experimental angular distributions are reproduced consistently by both the systematics if we adopt the MSD (multi-step direct) to MSC (multi-step compound) ratio calculated by the EXIFON code. In our previous analyses[1,2] where MSD to MSC ratio was approximated by the exciton to evaporation ratio, both systematics in particular Kalbach-Mann's one tended to overemphasize the forward rise and discrepancy became more pronounced with decreasing target mass.

Therefore, for quantitative comparison of secondary neutron anisotropy, we compared the experimental angular distribution with the calculations for Kalbach-Mann systematics in terms of the 1-st order reduced Legendre coefficient $b_1 = a_1/a_0$, where a_0 and a_1 are, respectively, the 0-th and 1-st order Legendre coefficients representing the angular distribution. The b_1 values were compared as a function of target mass including the experimental data for lighter mass target by our previous measurements[2]. The experimental b_1 tends to decrease with target mass and this trend is followed better by the calculation based on EXIFON than that by previous exciton/evaporation treatment.

Details of the study was presented at the IAEA Coordinated Research Meeting held at Chiang Mai, March-31 to April-2 , 1992, and to be published from IAEA.

References:

1) M.Baba et al.: J.Nucl.Sci.Technol., 27(7) 601(1990)

2) M.Baba et al.: Proc.Conf. Nuclear Data for Science and Technology (Mito 1988) p.291

3) H.Kalka: Z.Phys., A341 298(1992) and private communication

4) C.Kalbach and F.M.Mann, Phys. Rev., C23(1) 112 (1981)

5) C.Kalbach: ibid., C23(1) 124(1981)

X-A-2 Double-differential (n,α) Cross Sections of Ni and Fe

M.Baba, N.Ito, S.Matsuyama, I.Matsuyama, F.Huang*, N.Hirakawa
S.Chiba**, T.Fukahori**, M.Mizumoto**, K.Hasegawa** and S.Meigo**

Double-differential (n,α) cross sections of Ni and Fe have been measured for incident neutrons between 4.2 and 14 MeV using a specially-designed gridded-ionization chamber (GIC)[1,2] as a high efficiency α-particle spectrometer.

A schematic view of the GIC is shown in Fig.1. The sample foils of elemental Ni and Fe, about 3-μm thick, are placed in the center of the twin GIC and secondary α-particles are detected in 4π geometry. The energy and emission-angle of α-particles are determined by processing the two-dimensional data for anode versus cathode signal[1,2]. α-particles are selected by adjusting the pressure of the counting gas of Kr-CO_2 or Kr-CH_4.

Mono-energetic neutron beam was produced by Tohoku University 4.5 MV Dynamitron accelerator and JAERI 20MV tandem accelerator; neutrons between 7 and 11 MeV were obtained by the JAERI tandem via the d-D reaction using a gas target. A copper collimator was employed to define the neutron beam within a sample diameter (2.3-cm) for reduction of backgrounds from the counter gas and structural materials. Backgrounds were measured by replacing the sample-foils with a Au foil. The effects of contaminant neutrons from the beam stop and the d-D breakup reaction were also measured, respectively, with empty and ^{3}He targets, and proved to be less than several % in the

---

* Heavy Ion Physics Institute, Peking University, PRC
** Japan Atomic Energy Research Institute, Tokai Research Establishment

energy region below 11 MeV. Absolute cross sections were determined relative to H(n,p) cross sections by measuring recoil-proton yields with the GIC or a recoil-proton telescope.

In these experiments, a care was taken to reduce backgrounds and to improve the GIC pulse-height stability[1,2]. For measurements between 4 and 11 MeV, we employed Kr-CH_4 gas to reduce large backgrounds from the O(n,α) reaction. For 14 MeV measurements, Kr-CO_2 was used with reduced CO_2 content ($\sim$2.5 %). The instability of GIC could be eliminated by a few days evacuation of GIC with a turbo-molecular pump. By these improvements, it became possible to obtain reliable α-particle data with sufficient signal to background ratio up to 14 MeV incident energy.

Signals from cathode and two anodes were unti-gated by corresponding ring signals and accumulated in a three-parameter list mode. Figure 2 illustrates an example of the two-dimensional map for anode versus cathode signal. Data were corrected for energy loss of α-particles within the sample using an iteration technique.

Figures 3 and 4 illustrate, respectively, the examples of α-particle energy spectrum and angular distributions for Ni together with ENDF/B-VI. The energy distributions show angle dependence attributable to kinematical effect while the angular distributions are almost isotropic. It is noted that the present results are significantly lower than ENDF/B-VI. Data analyses are in progress.

References:

1) M.Baba et al.: Proc.Int.Conf."Nucl.Data for Sci.& Technol." (Jeulich 1991) p.477

2) N.Ito et al.: JAERI-M 92-027 (JAERI 1992) p.257

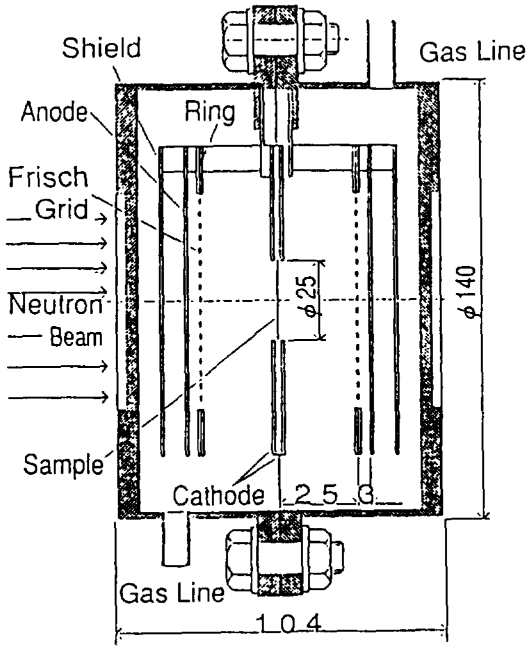

Fig.1: Schematic view of GIC

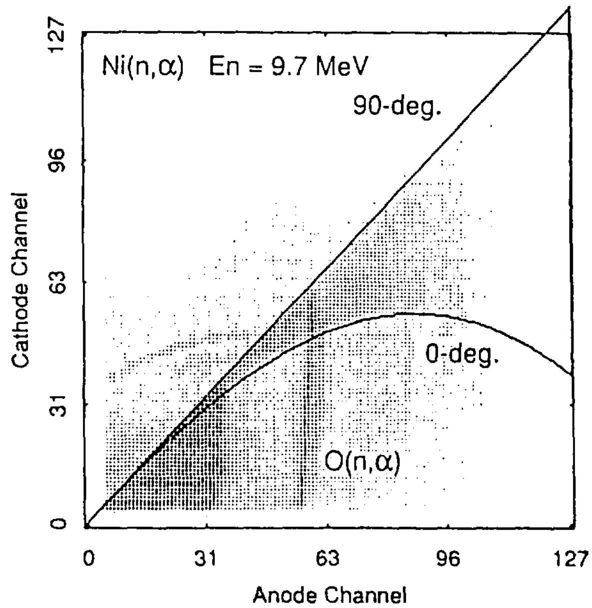

Fig.2: Two-dimensional spectrum anode versus cathode signal

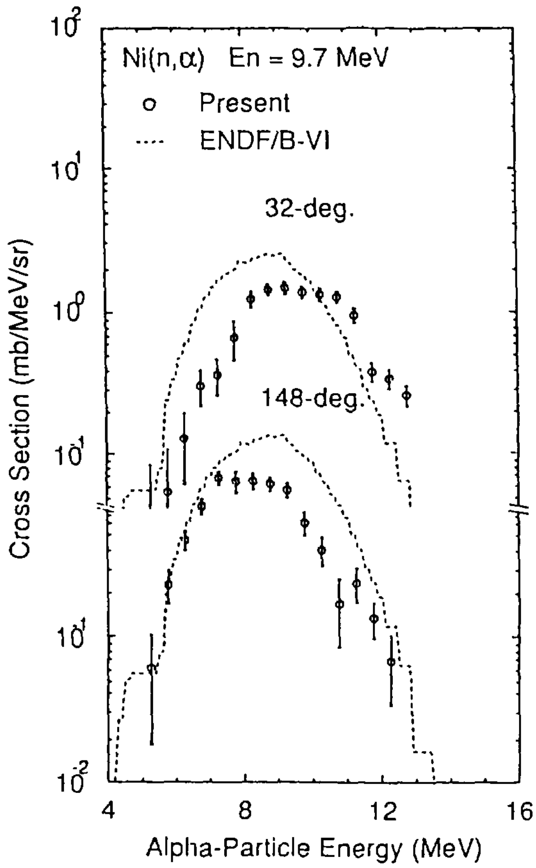

Fig.3: DDX for Ni(n,α) reaction

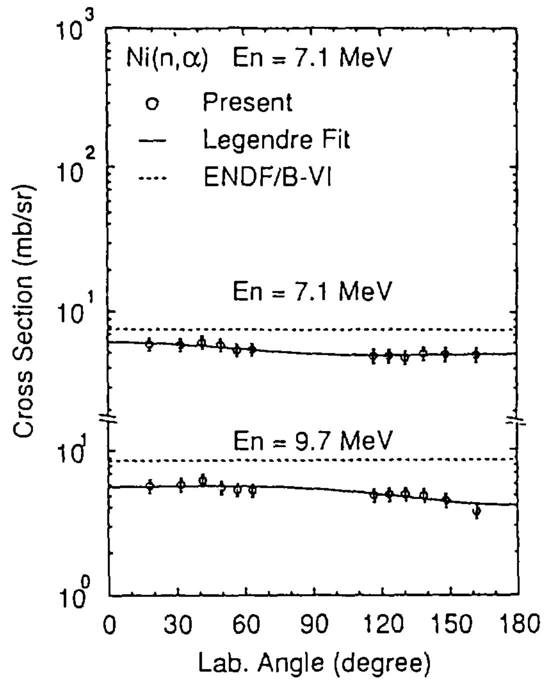

Fig.4: Angular distributions for Ni(n,α) reaction

B. Laboratory of Nuclear Science

X-B-1

The reactions ^{6}Li(e,e′p) and ^{6}Li(e,e′t)

M. Hotta, T. Tamae, H. Miyase* and T. Suda*, M. Sugawara, T. Tadokoro,
A. Takahashi and E. Tanaka

In order to investigate the cluster structure and the mechanism of the electro disintegration in ^{6}Li, coincidence ^{6}Li(e,e′p) and ^{6}Li(e,e′t) experiments have been performed at the energy transfer from 28 to 37 MeV and momentum transfer of 61 MeV on an average. An enriched ^{6}Li target of 95.5 % purity and 6 mg/cm^2 thickness was bombarded with a 134 MeV continuous electron beam from a pulse stretcher ring.

Scattered electrons were measured at 26° with a double-focused magnetic spectrometer. Charged particles emitted from the target were detected with detector telescopes out of the scattering plane. Each telescope consists of three layers of Si-diode detectors. Groups of proton, deuteron, triton, helium-3 and alpha are identified in ΔE-E two dimensional plot. A typical missing energy spectrum for the ^{6}Li(e,e′p) reaction is shown in Fig. 1. There are two narrow peaks in low and high missing-energy regions corresponding to the proton-knockout reaction of p- and s-shells. Events with a three-body α-n-p final state are also seen between the two peaks.

In the missing-energy spectrum for the ^{6}Li(e,e′t) reaction, the events corresponding to two-body t-^{3}He breakup can be clearly identified (Fig. 2). In the angular distributions for the ^{6}Li(e,e′p) reaction in the missing-energy region below t+d threshold, one can see a peak in forward angles and existence of a large longitudinal-transverse interference term as shown in Fig. 3. The angular distributions for the ^{6}Li(e,e′t)^{3}He reaction show distorted sine curves (Fig. 3). More careful analysis in under way about the difference of shapes between the two energy regions.

*College of General Education, Tohoku University

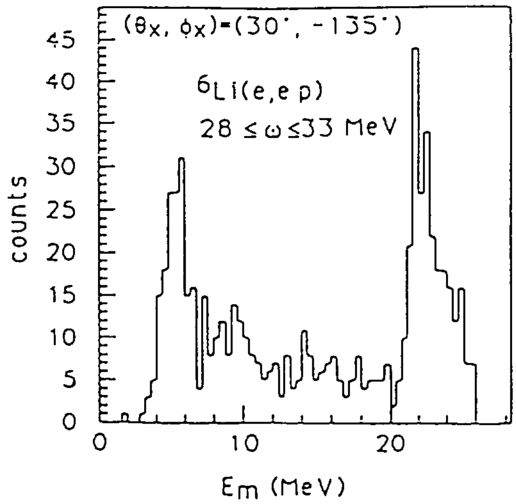

Fig. 1. Missing-energy spectrum for the ^{6}Li(e,e'p) reaction.

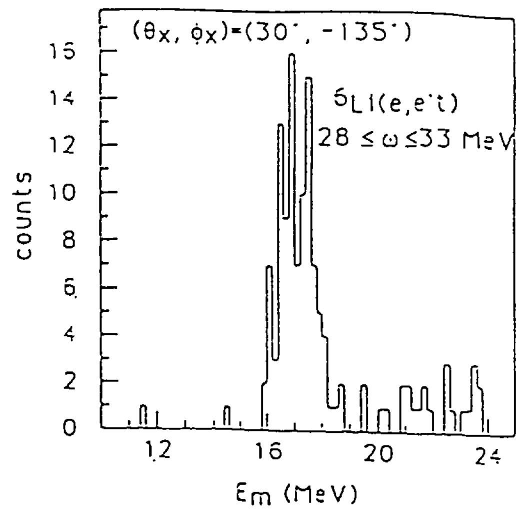

Fig.2. Missing-energy spectrum for the ^{6}Li(e,e't) reaction.

preliminary

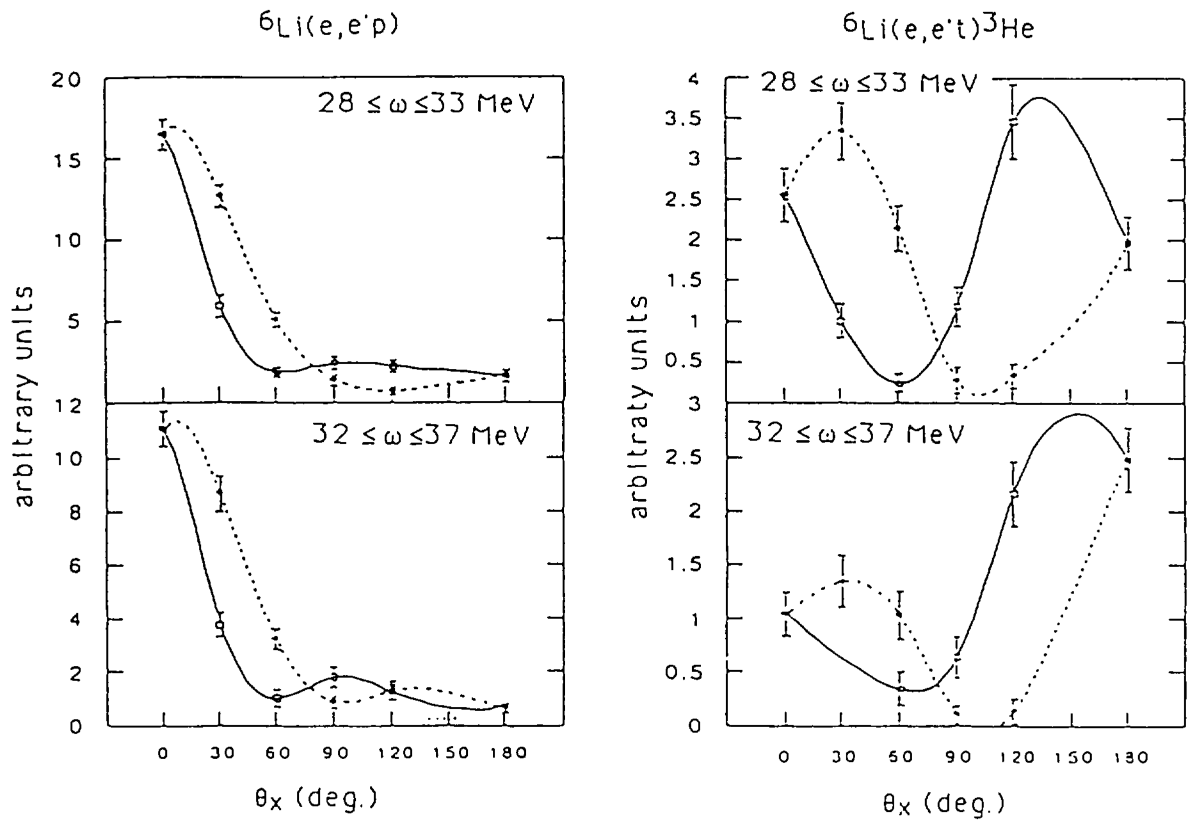

Fig.3 Angular distributions for the 6Li(e,e'p) and ^{6}Li(e,e't)^{3}He reactions. Solid circles and open squares represent the cross sections at ϕ_x=-135^0 and -45^0 respectively. The solid and dotted lines are connected smoothly by eye.

X-B-2

Out of Plane Measurement for the $^{12}C(e,e'n)^{11}C$ reaction at $\omega = 45$ MeV

K. Takahisa, T. Saito, S. Suzuki, C. Takakuwa, M. Oikawa, T. Tohei*, T. Nakagawa* and K. Abe†

Out of plane measurement for the $^{12}C(e,e'n)^{11}C$ have been carried out at an excitation energy of 45 MeV. The neutron detectors were set at following combinations of scattering angle θ and reaction-plane angle ϕ; (30°, 180°), (60°, 180°), (90°, 180°), (180°, 180°), (210°, 180°), (30°, 135°), (60°, 135°), (90°, 135°) and (30°, 90°). Fig. 1 shows a missing energy spectrum. Fig. 2 shows angular distributions for the $^{12}C(e,e'n_{0,1})$ reaction on plane ($\phi = 180°$) and out of plane ($\phi = 135°$, 90°). This distribution was very different from the giant dipole resonance region[1]. The ratio of cross sections on plane and out of plane is compared with three processes which are giant dipole resonance (GDR), quasi free knock-out (QFK) process and charge exchange process (CEP). The cross section ratio of $\sigma(\phi = 90°)/\sigma(\phi = 180°)$ is compared with these three processes as shown in Fig. 3. It is clear that the QFK contribution is not main. So the angular distribution was tried to reproduce with the GDR and CEP processes as shown in Fig. 4. It seems that the reaction mechanism for the $^{12}C(e,e'n_{0,1})^{11}C$ is understood as the mixing process of giant dipole resonance and charge exchangeprocess at the energy transfer of 45 MeV.

References

1) K. Takahisa et al., Res. Rep. Lab. Nucl. Sci. 22 (1989) 1.

*Department of Physics, Tohoku University
†College of General Education, Tohoku University

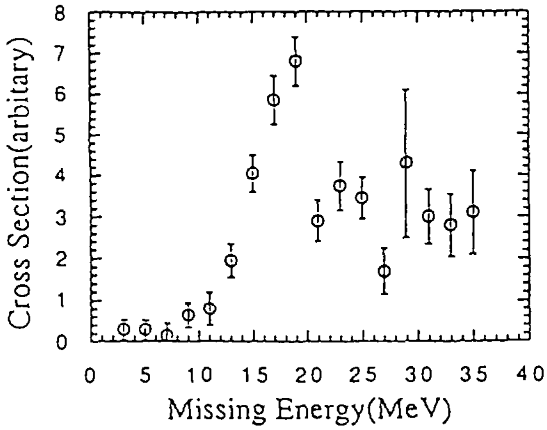

Fig. 1. Missing energy spectrum.

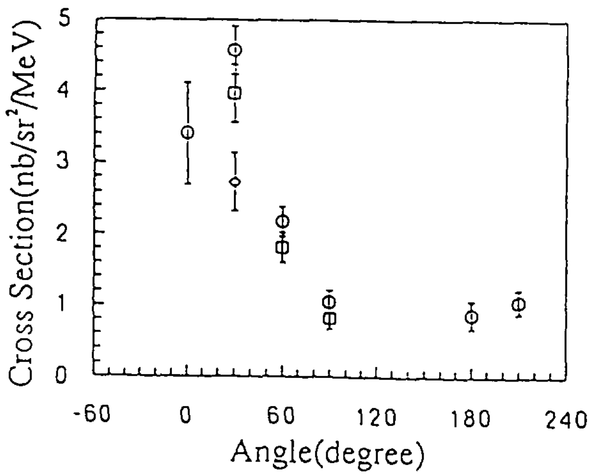

Fig. 2. Angular distribution of the diffrential cross section for the ^{12}C(e,e$\acute{n}_{0,1}$) reaction at 129MeV. The open circles, squares and diamonds show the cross section on plane, at ϕ = 135° and at ϕ = 90 °.

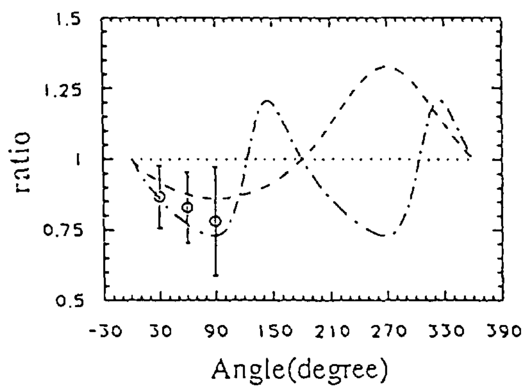

Fig. 3. Angular dependence of the cross section ratio $\sigma(\phi = 135°)/\sigma(\phi = 180°)$. The open circle shows the present data. The dotted, dashed and dash-dotted lines represent the results of the QFK, CEP and GDR calculations.

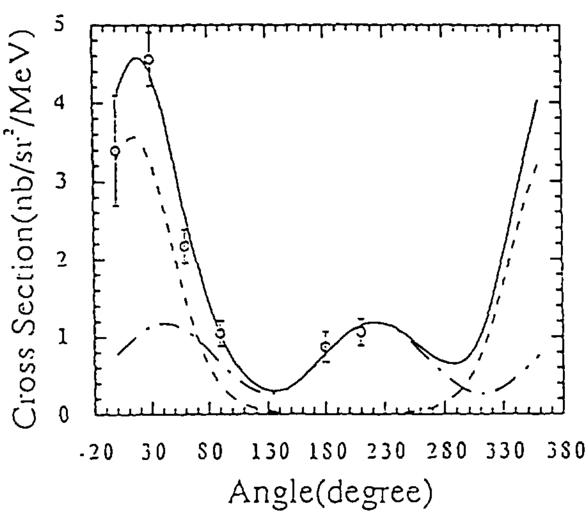

Fig. 4 The experimenal and theoretical angular distributions for the ^{12}C(e,e$\acute{n}_{0,1}$) reaction. The dashed and dash-dotted lines indicate the predections from the CEP and GDR processes. The soid line shows the sum of them.

X-B-3

Photonuclear Reaction with Tagged Photons

H. Ito, S. Ito, O. Konno, K. Maeda*, H. Matsuyama, T. Sasaki, T. Suda*, M. Takeya and T. Terasawa

○ ^{13}C, $^{56}Fe(\gamma,n)$

(collaborated with T. Murakami, Kyoto University)

Experiments of (γ,n) reactions on $^{13}C$and ^{56}Fe have been carried out by using a newly developed neutron detection system in an energy region of 20 MeV $\leq E_\gamma \leq$ 70 MeV. The (γ,n) reactions have been regarded as a suitable method to observe the nuclear isospin structure. One can expect to get the strength of the isovector quadrupole resonance from the photoneutron angular distribution. An unified study of the reaction mechanism of photoreactions, especially single-nucleon emission process, in the energy region above the giant resonance is also able to be studied. Differential cross sections of $\theta_n \sim 55°$, 90° and 125° were mainly measured at the flight path of 2.5 m, and that of $30° \leq \theta_n \leq 90°$ were also observed at five points. The typical time resolution of the present measurement was $\Delta t \sim 0.9$ nsec (FWHM).

○ $^{31}P(\gamma,p)$

The $^{31}P(\gamma,p)$ experiment has been carried out to study the contribution of two nucleons process. It has been found that one of low-lying states excited in$^{12}C(\gamma,p)$ reaction has a large strength which is not observed in the (e,e′p) reaction in the quasi-elastic region. It is suggested that multi-nucleon process has an importance in the photonuclear process in contrast with the (e,e′p) reaction.

The photoproton energy spectra were measured with tagged photons in an energy region of 50 MeV $\leq E_\gamma \leq$ 80 MeV at proton emission angles of 45° and 60° with NaI scintillators. The data of this experiment is under the analysis.

○ Improvement of the Tagged Photon Resolution

A high resolution electron counter (HR) system for the tagged photon experiment has been developed. The HR system (see Fig. 1) consists of forty plastic scintillators, four optical fiber bundles with ten branches and four photomultiplier tubes and the existing

*College of General Education, Tohoku University tagging counters (2.6 MeV energy resolution). Each HR scintillator is aligned with one-third overlap. The special resolution of 3 mm was obtained by analyzing the hitting electron patterns of the HR system. The global position of the electron is decided in coincidence with the tagging counter which is placed behind of the HR system. We achieved the photon energy resolution of 430 keV at E_γ = 42.2 MeV and 650 keV at E_γ = 65.6 MeV.

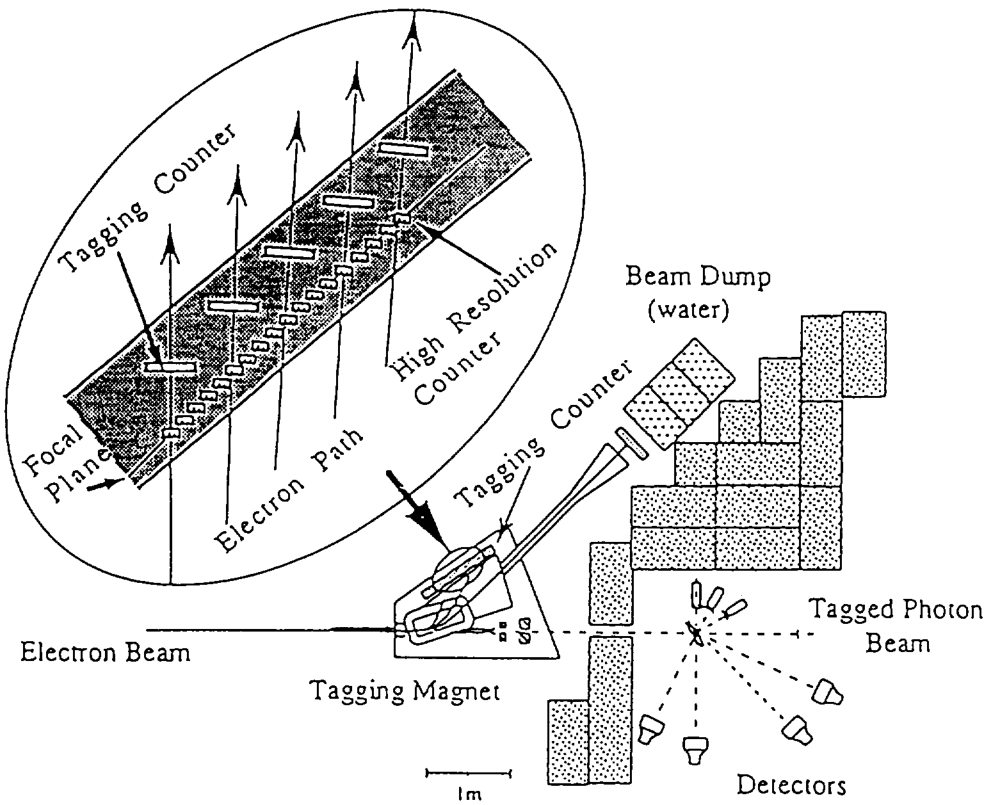

Fig. 1. Setup of the high resolution tagging counter system.

○ Development of the large size neutron counter system

(collaborated with T. Fukuda, INS, University of Tokyo)

We have developed the LArge Neutron Detector (LAND) in order to perform the (γ,n) measurements with enough statistics and resolutions.

NE213 liquid scintillator makes possible to separate neutron events from γ-ray events by pulse shape discrimination (PSD) method. To get large detection efficiency, we decided to make the large volume detector with the aluminum container. One of the most difficult problem was to choose the reflector materials for getting good light collection. We finally decided to use the material of mirror reflection with more than 90 % reflection rate, and which does not fuse into xylene based liquid scintillator. The final design is shown in Fig 2. Dimensions of the detector are 130 mm in diameter and 1000 mm in length.

We measured n-γ separation at several parts of detector, by moving the collimated ^{241}Am – Be source. Good separations of neutrons from γ-ray were obtained for whole position along the detector. The neutron detection efficiency were measured by using the quasi-monoenegetic neutron obtained through ^{7}Li(p,n) reactions at E_p = 35 MeV. The preliminary neutron detection efficiency is about 12 %. The data analysis of the (γ,n) reactions and the neutron response of the LAND are in progress.

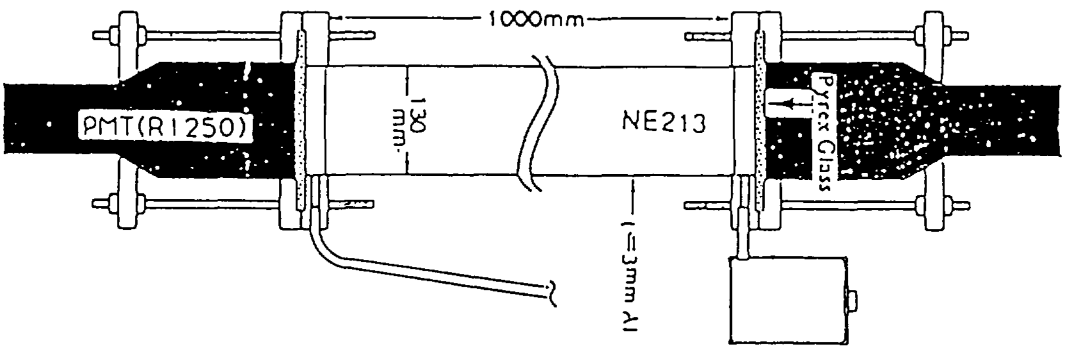

Fig. 2. Schematic drawing of the LAND.

○ New Beam Transport System

Tow experimental halls have been separately used for electron scattering and pion photoproduction experiments using higher energy electrons (2nd experimental hall), and for photoreaction experiments using lower energy electron (1st experimental hall). Since the 150 MeV Pulsed Beam Stretcher Ring (SSTR) has completed in the 2nd experimental hall, the coincidence experiments such as (e,e'p), (e,e'n) and photon tagging have been concentrated in the 2nd hall. A new beam transport system has been designed to do two experiments in parallel by introducing continuous beam from the 2nd hall to the 1st hall. It takes about 90 m with two sets of symmetrical bending magnets each of which is achromatic. Parts of the system have been completed. Construction and alignment start in July. Beam test is scheduled in the end of this year.

XI. Tokyo Institute of Technology

A. Research Laboratory for Nuclear Reactors

XI-A-1 Electric and Magnetic Dipole Transitions from Broad s-Wave Neutron Resonance in Even-Even sd-Shell Nuclei

H. Kitazawa, M. Igashira, M. Shimizu, K. Muto, T. Oda, Y. Achiha, Y. -H. Lee and N. Mukai

Observations have been performed for electromagnetic transitions from the broad s-wave neutron resonances at 658 keV in ^{24}Mg, at 180 keV in ^{28}Si, and at 103 keV in ^{32}S. Capture gamma rays were measured with an anti-Compton NaI(Tl) detector, using a neutron time-of-flight technique. E1 and M1 transitions from those resonances to low-lying states with a strong single-particle character were found. The deduced partial radiative widths for E1 transition are in excellent agreement with the Lane-Mughabghab valence-capture model calculations taking the neutron effective charge, -Ze/A. Moreover, it is shown that essential features of the observed E1 and M1 transitions can be well explained by assuming a configuration-mixing wave function, $\Psi_i(1/2^+)=a(0^+\otimes 1/2^+)+b(1^+\otimes 1/2^+)+c(1^+\otimes 3/2^+)$, for each resonance. The M1 transition strengths are compared also with more detailed shell model calculations in the model space of a full $(sd)^n$ configurations, using the Wildenthal effective interaction.

This paper was submitted to the Physical Review C for publication.

XI-A-2 Retardation of Single-Particle E1 Transitions from the 622 keV d-Wave Neutron Resonance in ^{9}Be

H. Kitazawa, M. Igashira, S. Shibata, K. Tanaka,
K. Masuda and H. Takakuwa

Capture gamma rays from the 622 keV d-wave neutron resonance in ^{9}Be with large reduced neutron width have been observed by means of a time-of-flight method, employing an anti-Compton NaI(Tl) detector. Partial radiative widths have been derived for the strong primary E1 transition to the 3368 keV(2^{+}) state and also for the weak one to the 5958 keV(2^{+}) state in ^{10}Be. Those widths were compared with predictions of the Lane-Mughabghab valence-capture model. As a consequence we found certain evidence to show that the 3368 keV state transition is appreciably hindered. This E1 retardation may be explained as caused by a coupling between the neutron single-particle transition and the E1 giant resonance excitation of the target nucleus.

XI-A-3 Measurement of Neutron Capture Cross Section of ^{9}Be in the keV Region

M. Igashira, S. Shibata, K. Tanaka, K. Masuda,
H. Kitazawa and Y. Nagai

Neutron capture cross section of ^{9}Be was measured in the energy region of 10-90 keV, using a time-of-flight method and an anti-Compton NaI(Tl) detector. The primary gamma-ray transitions to the ground state(0^{+}), the 3.368 MeV state(2^{+}), and the 5.958 MeV state(2^{+}) in ^{10}Be were observed, and the partial capture cross sections were derived for those transitions.

XI-A-4 Measurement of keV-Neutron Capture Cross Section of ^{7}Li

M. Igashira, K. Masuda, K. Tanaka, H. Kitazawa and Y. Nagai

Neutron capture cross section of ^{7}Li was measured in the energy region of 10-80 keV, using an enriched $^{7}Li_2O$ sample. Capture gamma rays from the sample were measured with an anti-Compton NaI(Tl) detector, employing a time-of-flight method. The primary gamma-ray transition to the ground state of ^{8}Li was observed, and the corresponding partial capture cross section was derived. Moreover, the total capture cross section was extracted on the assumption that the branching ratios of the captured state are constant from the thermal region to the keV region.

XI-A-5 Measurement of keV-Neutron Capture Cross Section of Deuteron

M. Igashira, K. Tanaka, K. Masuda, H. Kitazawa and Y. Nagai

Neutron capture cross section of deuteron was measured in the energy region of 10-90 keV, using a time-of-flight technique and an anti-Compton NaI(Tl) detector. The capture gamma ray of deuteron was clearly observed around 6.3 MeV, and the capture cross section was derived.

Anomaly in the ^{15}N, ^{16}O, ^{19}F + $^{54,56}Fe$ fusion cross sections around the Coulomb barrier energy†

H. Funaki* and E. Arai

Tokyo Institute of Technology, Tokyo-Meguroku

Fusion cross sections have been determined by detecting evaporation residues from six systems formed by projectiles of ^{15}N, ^{16}O and ^{19}F and target nuclei of ^{54}Fe and ^{56}Fe at incident energies around the Coulomb barrier. The comparison of the experimental results with the prediction from the one-dimension barrier penetration model revealed that the ^{16}O reactions were only slightly enhanced, whereas the ^{19}F fusion reactions are more than ten times higher than the model calculation at sub-barrier energies. The fusion cross sections for ^{15}N projectiles showed a medium enhancement. The one-dimension model has reproduced to some extent the experimental data of the ^{15}N + ^{54}Fe and ^{16}O + $^{54,56}Fe$ systems by making corrections for the quadrupole deformation of the reacting nuclei. However, the ^{19}F data have not been predicted by this model calculation.

In order to improve the accuracy of the theoretical prediction we have introduced a correction term into the one dimensional model according to Wong [1]:

$$\sigma(E) = \frac{R_b^2\hbar\omega_b}{2E}\left[\ln(1+e^x) - \frac{2\pi e^x}{5\hbar\omega_b(1+e^x)}\sum_{i=1}^{2}\beta_2^{(i)^2} g_i(R_b) + \frac{\pi^2 e^x}{5(\hbar\omega_b)^2(1+e^x)^2}\sum_{i=1}^{2}\beta_2^{(i)^2} f_i(R_b)^2\right], \tag{1}$$

where

$$x = \frac{2\pi}{\hbar\omega_b}\left[E - V_b + \sum_{i=1}^{2} g_i(R_b)\beta_2^{(i)^2}/5\right]. \tag{2}$$

The functions $f_i(R_b)$ and $g_i(R_b)$ are defined as follows:

$$f_i(R_b) = (20\pi)^{-1/2}(Z_1Z_2e^2\mathcal{R}_i/R_b^2)(-5+3\mathcal{R}_i/R_b), \tag{3}$$

$$g_i(R_b) = -\mathcal{R}_i^2\left[46Z_1Z_2e^2/7R_b^3 + 5\mu(\hbar\omega_b)^2/\hbar^2\right]/8\pi, \tag{4}$$

where $\mathcal{R}_i = 1.2A_i^{1/3}$, and μ, Z_1 and Z_2 denote reduced mass, atomic number of the projectile and target nuclei, respectively.

Table 1 lists the parameters such as V_b, R_b, $\hbar\omega_b$ which have been determined from the CCFUS [2] calculation of fusion cross sections. The quadrupole deformation parameters β_2 have been calculated by equation (5) using $B(E2)$ data compiled by Endt [3]:

† This work was financially supported by a Grant-in-Aid for Scientific Research (B) of Monbusho under the contract No. 62460013.

*Present Address: R&D Center of Toshiba Co., Kawasaki J-210.

$$\beta_\lambda = \frac{[4\pi\,(2\lambda+1)\,B(E_\lambda)]^{1/2}}{Z(\lambda+3)}. \tag{5}$$

The experimental values of the ^{15}N + ^{54}Fe and ^{16}O + $^{54,56}Fe$ fusion cross sections agree with the predicted values within the statistical uncertainty. The value of $\hbar\omega_b$ ranges from 3.63 to 3.80 MeV, which are in accordance with $\hbar\omega_b$ values of 3.1 and 3.5 MeV determined by Liguori et al. [4] for the ^{16}O + $^{46,50}Ti$, respectively and with 3.15 MeV by Penna et al. [5] for the ^{14}N + ^{59}Co fusion reaction. However, the ^{15}N + ^{56}Fe data still show some deviation, and the ^{19}F reaction cross sections cannot be reproduced by this model calculation at sub-barrier energies (Details are reported elsewhere [6]).

Table 1: The parameters of V_b, R_b, $\hbar\omega_b$, β_2

System	V_b (MeV)	R_b (fm)	$\hbar\omega_b$ (MeV)	β_2 (projectile)	β_2 (target)
$^{15}N+^{54}Fe$	25.9	9.41	3.63	0.37	0.18
$^{15}N+^{56}Fe$	25.7	9.48	3.64	0.37	0.24
$^{16}O+^{54}Fe$	30.3	9.15	3.80	0.37	0.18
$^{16}O+^{56}Fe$	30.0	9.27	3.76	0.37	0.24
$^{19}F+^{54}Fe$	33.2	9.43	3.70	0.47	0.18
$^{19}F+^{56}Fe$	33.0	9.48	3.66	0.47	0.24

It was, however, possible to reproduce the experiment by augmentation of the $\hbar\omega_b$ values to 6 MeV for the ^{15}N + ^{56}Fe and 7 MeV for the ^{19}F + $^{54,56}Fe$ reactions. In the present report we discuss the physical meaning of these big values of $\hbar\omega_b$.

Stelson et al. [7] have introduced the idea of barrier distribution $D(V_b)$, where a fusion cross section is the sum of contributions from many coupled channels with a barrier height of V_b:

$$\sigma(E) = \int_0^\infty \sigma_c(E, V_b) D(V_b) \mathrm{d}V_b, \tag{6}$$

$$\int_0^\infty D(V_b) \mathrm{d}V_b = 1. \tag{7}$$

Starting from the asymptotic function (8) we can derive a equation of $D(E)$ as follows:

$$\sigma_c(E, V_b) = \pi R_b^2 \left(1 - \frac{V_b}{E}\right), \tag{8}$$

$$\frac{1}{\pi R_b^2} \frac{\mathrm{d}^2(\sigma E)}{\mathrm{d}E^2} = D(E), \tag{9}$$

which means that the value $(\sigma E)^{1/2}$ is a linear function of E in the energy region where $D(E)$ is constant.

We have displayed in Fig. 1 the experimental values of $(\sigma E)^{1/2}$ as a function of CM energy of incident particles for all six systems. The arrows show the barrier height. It is interesting to note that the slop of the data points holds constant in the region where $(\sigma E)^{1/2} = 20 - 150$ (mb$\cdot$MeV)$^{1/2}$ for the ^{15}N + ^{54}Fe reaction in Fig. (a) and the ^{16}O + $^{54,56}Fe$ reactions in Figs. (c) and (d), respectively. That means the barrier has no large energy dependency in these energy regions.

The $^{15}N + ^{56}Fe$ in Fig. (b) and ^{19}F reaction data in Figs. (e) and (f) show, however, a break around the barrier energy. This means that the assumption of constant barrier distribution is broken for these three reactions.

Rowley et al. [8] started from the equation (10) for the fusion cross section and introduced a distribution function $G(x)$:

$$\sigma_c(E, V_b) = \frac{\hbar\omega_b R_b^2}{2E} \ln\left\{1 + \exp\left[\frac{2\pi}{\hbar\omega_b}(E - V_b)\right]\right\}, \tag{10}$$

$$\frac{1}{\pi R_b^2}\frac{\mathrm{d}^2(\sigma E)}{\mathrm{d}E^2} = \frac{2\pi}{\hbar\omega_b}\frac{e^x}{(1+e^x)^2} \equiv G(x), \tag{11}$$

where

$$x = \frac{2\pi}{\hbar\omega_b}(E - V_b). \tag{12}$$

This means that the energy dependency of $G(x)$ becomes intermediate around the barrier energies with increase of the $\hbar\omega_b$ value.

We draw from this experiment the conclusion that the $^{15}N + ^{56}Fe$ and ^{19}F reactions have coupling channels distributed over a wide energy region, whereas the energy region of channel coupling is rather restricted for the $^{15}N + ^{54}Fe$ and $^{16}O + ^{54,56}Fe$ reactions.

References:

[1] C.Y. Wong, *Phys. Rev. Lett.*, **31** (1973) 766.

[2] C.H. Dasso and S. Landowne, *Comput. Phys. Commun.*, **46** (1987) 187.

[3] P.M. Endt, *Atomic data and Nucl. Data Tables*, **23** (1979) 3.

[4] R. Liguori Neto, J.C. Acquadro, P.R.S. Gomes, A. Szanto de Toledo, C.F. Tenreiro, E. Crema, N. Carlin Filho, and M.M. Coimbra, *Nucl. Phys.*, **A512** (1990) 333.

[5] T.J.P. Penna, P.R.S. Gomes, E.F. Chagas, R. Liguori Neto, J.C. Acquadro, E. Crema, N. Carlim F., and M.M. Coimbra, eds. C. Signorini, S. Skorka, P. Spolaore and A. Vitturi, in *Heavy Ion Interactions Around the Coulomb Barrier*, Lecture Notes in Physics **317** p.73, Springer-Verlag, 1988.

[6] H. Funaki, Dissertation, Tokyo Institute of Technology, 1992; H. Funaki, M. Shimizu, and E. Arai, *Progress Report* p.125, JAERI, 1991.

[7] P.H. Stelson, *Phys. Lett. B*, **205** (1988) 190; P.H. Stelson, H.J. Kim, M. Beckerman, D. Shapira, and R.L. Robinson, *Phys. Rev. C*, **41** (1990) 1584.

[8] N. Rowley, G.R. Satchler, and P.H. Stelson, *Phys. Lett. B*, **254** (1991) 25.

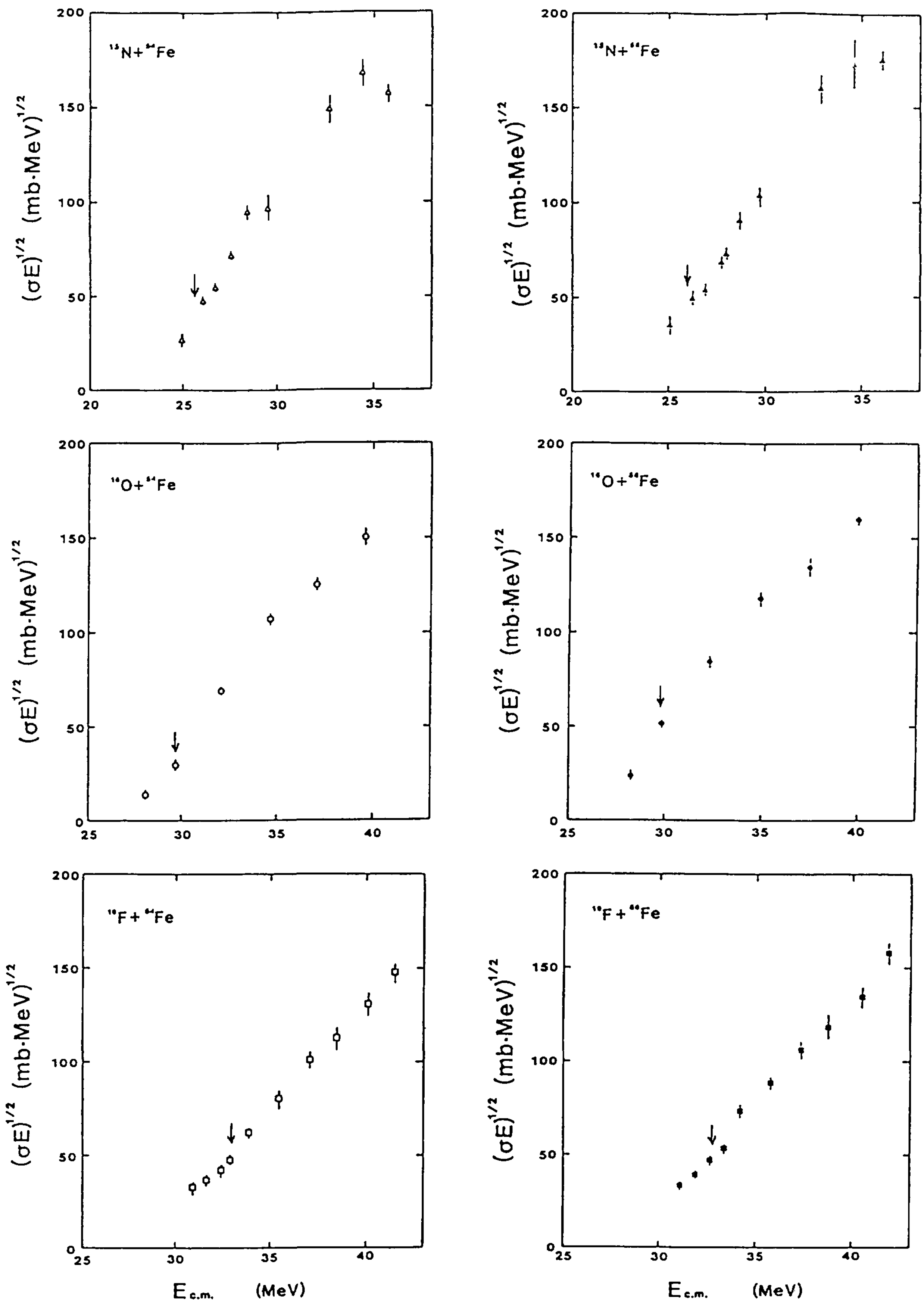

Figure 1: $(\sigma E)^{1/2}$ as a function of $E_{\rm c.m.}$ (a) ^{15}N+^{54}Fe (b) ^{15}N+^{56}Fe (c) ^{16}O+^{54}Fe (d) ^{16}O+^{56}Fe (e) ^{19}F+^{54}+Fe (f) ^{19}F+^{56}Fe.